The removal of selected personal care products from a municipal membrane bioreactor secondary effluent with reverse osmosis membranes

By

Zilungile Mqoqi

A thesis submitted in fulfilment of the requirements for the degree

Master of Engineering: Chemical Engineering

In the

Faculty of Engineering and the Built Environment

at the

Cape Peninsula University of Technology

Supervisor: **Prof Mujahid Aziz**

February 2023

Declaration

I, Zilungile Mqoqi, declare that the contents of this dissertation/thesis represent my own unaided work and that the dissertation/thesis has not previously been submitted for academic examination towards any qualification. Furthermore, it represents my own opinions and not necessarily those of the Cape Peninsula University of Technology

Signed: Zilungile Mqoqi Date: February 2023

Abstract

Recent studies have observed an abundance of chemicals of emerging concern (CEC) in various water sources. As a result of their presence, there is a significant concern regarding their negative impact on humans and the environment. Personal care products (PCPs) form part of CECs and are commonly used for health and hygiene. The trace amounts of PCPs found in the environment, and surrounding water sources are evidence of the non-uniform removal efficiency of conventional wastewater treatment systems. Reverse Osmosis (RO) systems are recommended for PCP removal as they have been reported to be successful in removing trace organic material, and they produce quality effluent

In this study, the focus was on the removal of Triclosan (TCS), methylparaben (MeP), and Ethylhexyl methoxycinnamate (EHMC) from a synthetic municipal secondary membrane bioreactor effluent. The research investigated the influence of membrane characteristics, physicochemical properties of the products, and water quality on the removal of selected PCPs. It was achieved by determining the effect of feed pH (3, 6, 10) and temperature (15°C, 25°C, 35°C) on the removal of chemical oxygen demand (COD), total dissolved solids (TDS) measured as turbidity and selected Inorganics ammonia and phosphate ions. A bench-scale reverse osmosis system was used to evaluate the efficiency of reverse osmosis (XLE) efficiency and nanofiltration (NF270) aromatic polyamide thin film composite membranes' removal of the selected PCPs.

The synthetic feed consisted of organic and inorganic substances spiked with the commercial model PCPs with concentrations ranging from 450-480 µg/L blended with deionized water. Experimental runs were operated over approximately 8 hours with 45-minute intervals. Grab samples were analyzed for Electric Conductivity (EC), Total Dissolved solids (TDS), and feed, brine and permeate temperature to monitor the system operation. After treatment, the composite permeate samples were prepared for quantitative analysis through solid phase extraction (SPE) before being analyzed using gas chromatography-mass spectrometry (GC-MS).

Chemical analysis of various inorganics was conducted to calculate the percentage removal. Results uncovered considerable effects of pH control on eliminating the inorganics of interest and the carbon-oxygen demand (COD). Upon thorough analysis, results showed that both membranes had high overall efficiency at feed pH 6 and temperature at 35°C. The recorded percentage removal for COD, TDS, salt rejection, ammonia, and phosphorus was 92,59%, 87,53%, 91,68%, 96,46%, and 99,6%, respectively, for XLE. At the same time, XLE outperformed the NF270 under the same conditions.

Adjustment of feed pH for the XLE membrane was shown to be a factor of consideration for improving inorganic removal in the advanced treatment of domestic secondary MBR effluent. It was shown that water quality obtained with reverse osmosis and nanofiltration membranes could meet quality requirements for reuse applications in cooling systems and irrigation.

The membranes were characterized before and after treatment using Scanning Electron Microscopy (SEM), Energy Dispersive X-Ray Spectroscopy (EDX), and Attenuated Total Reflection-Fourier Transform Infrared Spectroscopy (ATR-FTIR). The results showed that pH and temperature had more effect on membrane structure for NF270 than XLE. Even though XLE outperformed NF270, NF could still produce quality effluent that met the criteria for reuse application. The SEM-EDX results show that the virgin XLE and NF270 membranes contained 78,08% and 76,14% of C, indicative of the aromatic functional group and 5,51% and 6,3% of S, respectively, representing polysulfone, the mechanical layer supporting filtration. After treatment, the analysis showed that the change in pH resulted in compromised membrane layers. The S content was relatively low for both membranes after each treatment, especially at pH 3 and 10. The lack of C for all pH conditions showed that the aromatic functional group was removed due to changing pH.

The effect of feed pH and temperature after treatment was nicely demonstrated by the ATR-FTIR spectra before and after treatment. The spectra for virgin membranes showed pronounced peaks, while the fouled membranes demonstrated deformed peaks at the same wave numbers due to temperature change. XLE spectra included a C-C and C-O stretch, C-O antisymmetric stretch, C-O-C asymmetric stretch vibration of the polysulfone layer, and aliphatic C-H deformation. The functional groups observed for NF270 were the carbonyl functional group (C=O), C-O and C-C stretching and an indication of the polysulfone support layer. When comparing NF270 to XLE, the spectrum of NF270 suggested a most significant effect of pH on the membrane than it did for XLE.

At pH 6 and 35°C, the overall PCP removal favoured NF270, with EHMC, MeP, and TCS reporting rejection of 99,92%, 99,67%, and 99,9%, respectively, making it a viable option for PCP removal even though considered a loose membrane. The target compounds were removed due to size exclusion, electrostatic repulsion, and hydrophobic interactions. The rejection for XLE resulted from size exclusion, while NF270 rejections were dominated by electrostatic repulsion due to the change in pH and varying ionization constants. The temperature had no significant difference in PCP rejection, and that rejection increased with pH for all membranes**.**

Consequently, municipal MBR secondary wastewater effluent treated by a bench-scale RO unit with RO and NF membranes is acceptable for effectively removing selected personal care products (EHMC, MeP and TCS). The temperature does not affect the removal of target analytes by both RO or NF membranes. However, increasing the feed pH has proven to be more effective in its removal. Ultimately, using a hybrid system could assist in further abatement for reuse applications.

Research outputs

Mqoqi Z & Aziz M; 2022, The removal of selected personal care products from municipal secondary membrane bioreactor effluent using reverse osmosis membranes, Inter-institutional Postgraduate Symposium, STIAS, Stellenbosch University, Stellenbosch, South Africa, 30 September 2022

Mqoqi, Z & Aziz, M; 2023, The Exclusion of Personal Care Products from Domestic MBR Secondary Effluent using Aromatic Polyamide Thin-film Composite NF/RO Membranes, Membranes. Submitted XX February 2023 [Paper ID.: XX-XX-XX]

Acknowledgements

I'm most grateful to the Almighty for giving me the strength to persevere and succeed with this project and blessing me with an unbeatable support system, my parents, friends, and family.

This research project was conducted within the Chemical Engineering Department at the Cape Peninsula University of Technology between January 2020 and February 2023

I want to express my gratitude to the following people for their contributions towards the completion of this thesis:

My Supervisor, Prof Mujahid Aziz, for his incomparable supervision, persistent guidance, motivation, encouragement and technical expertise in this research field. I am thankful for his sustained academic, moral and benevolent assistance throughout my educational journey

My Co-supervisor, Prof Ahmed Mohammaed, for his assistance

Department of Chemical Engineering, and the Research Directorate of the Cape Peninsula University of Technology (CPUT) for their support and South Africa's National Research Foundation (NRF-RSA) for the student scholarship.

The technical and administrative staff in the Chemical Engineering Department, especially Ms Hannelene Small, Ms Elizma Alberts and Mr Alwyn Bester, who was always more than willing to assist

Mrs Miranda Waldron at the Electron Microscope Unit and Ms Pei-Yin Liebrich at the University of Cape Town Molecular Biology Department.

The Environmental Engineering Research Group (EnvERG) for their support

Special thanks to my dearest friends, Kareema Smith, Nurah Jacobs, Zanelisiwe Ntombela, Winile Sindane, and Sharon Chakawa, for their love, moral support, motivation, and assistance during the early hours of the morning.

My siblings, Thembela, Zethu, Zizipho, and Mzubongile, for their unwavering love, encouragement, guidance, patience, and support.

Finally, my amazing mom, Mrs Nonceba Mqoqi, for always believing in and trusting me; her unconditional love and support

Dedication

This thesis is dedicated to my late sister, Nothemba Mqoqi, for believing in my abilities, encouraging me to do my master's, and being my constant source of strength and motivation.

Table of Contents

List of tables

List of figures

List of photos

List of Symbols

J_i	Water Flux
ΔP	Pressure difference
$\Delta \pi$	Osmotic pressure difference
A	Permeability Constant
B	Permeability Constant
C_{JO}	Feed salt concentration
C_{JL}	Permeate salt concentration
R	Rejection/ membrane selectivity

Abbreviations

Al	Aluminium
BOD	Biochemical Oxygen Demand
C	Carbon
CAS	Conventional Activated Sludge
COD	Chemical Oxygen Demand
EHMC	Ethylhexyl methoxycinnamate
GC-MS	Gas Chromatography-Mass Spectroscopy
K	Potassium
LC-MS	Liquid Chromatography-Mass Spectroscopy
MBR	Membrane Bioreactor
MeP	Methyl Paraben
Mg	Magnesium
Mn	Manganese
MWWTP	Municipal Wastewater Treatment Plants
MX	Musk Xylene
N	Nitrogen
Na	Sodium
NF	Nanofiltration
O	Oxygen
P	Phosphorus
PCP	Personal Care Products
PFAS	Polyfluoroalkyls
RO	Reverse Osmosis
SEM	Scanning Electronic Microscopy
Si	Silicon
TCS	Triclosan
TDS	Total Dissolved Solids
WWTP	Wastewater treatment plant

Chapter 1

Introduction

1.1. Background

Several studies have detected the presence of contaminants of emerging concern (CEC), such as natural steroidal hormones, industrial chemicals, pharmaceuticals and personal care products in wastewater (Ternes et al., 2015; Kim et al., 2018; Aziz & Ojumu, 2020). Personal care products (PCP) are various compounds used for health and cosmetics. The frequent use of PCPs is associated with large volumes of water. Claudia and Magrini (2017) reported that these products are released into the environment, whether the use is for household, body, or ingestion. Regularly using PCPs has been identified as a threat to the environment as they are sometimes environmentally persistent, bioactive, and potentially able to bioaccumulate (Juliano & Magrini, 2017).

PCPs can enter surface water by direct discharge from various industries, including households, wastewater treatment plants, and hospitals (Wang & Wang, 2016). Also, irrigation can result in traces of PCPs found in the soil with treated or untreated wastewater containing these products. The advent of more precise analytical methods has helped raise concerns regarding PCPs (Krogh et al., 2017). Among the several PCPs that have been found in previous studies include triclosan (TCS), methylparaben (MeP), Ethylhexyl methoxycinnamate (EHMC), etc. (Andrii et al., 2013; Silva et al., 2013; Guo et al., 2017; Heath et al., 2018; Najmi et al., 2020).

According to Wang et al. (2017), municipal wastewater is considered the primary source of PCPs humans use. Municipal wastewater consists of various waste runoffs, making its treatment complex. Unfortunately, not all treatments are effective in removing all compounds. Advanced technologies such as physical adsorption, biological degradation, chemical, advanced oxidation, etc., have shown promising results; however, the use of these technologies is limited due to the high cost of large-scale applications (Wang & Wang, 2016; Freyria et al., 2018; Rienzie et al., 2019). Thus the need for cost-effective and sustainable treatment methods.

With traces of PCPs still found in sources of water and aquatic animals, there is a need for effective treatments to eliminate the potential risk to public health. It has been reported that during the dry season, areas like the City of Cape Town (CCT) use a mixture of treated sewage wastewater effluent and natural water surface water for agricultural uses (Aziz & Ojumu, 2020). It further supports this research since these products may negatively affect the occupants around the area. Successfully removing these compounds substitutes freshwater sources for household and industrial needs (Acero et al., 2010).

This study aims at evaluating the use of reverse osmosis (RO) and nanofiltration (NF) to successfully remove selected PCPs from municipal secondary membrane bioreactor (MBR) effluent, thus eliminating the health concerns associated with these compounds. According to Acero et al.

(2010), compared to other physical-chemical treatments, using membranes has advantages such as low costs, low capital investments, requiring little use of chemicals, relatively uncritical scale-up, and high throughput while successfully maintaining product quality. NF and RO treat CECs as beneficial, resulting in a possible high-quality wastewater treatment plant (WWTP) effluent that can be reused (Lin et al., 2014; Kim et al., 2018; Lopera et al., 2019).

1.2. Effect of effluent with micropollutants on the surroundings environment

An inflow of contaminants of emerging concerns (CEC) persists for extended periods in surface waters, sludge, sewage, soil, aquatic bodies, treatment plants, wildlife, and humans resulting in a threat to the environment and human health (Kalia, 2019). The non-uniform removal efficiency of tertiary treatments results in these contaminants being detected in various water sources. Evaluating the impact of micropollutants such as PCPs is difficult as they dilute in water bodies. Xu et al. (2020) reported that they could potentially cause adverse effects on humans and the ecosystem, even at trace levels, due to their bioaccumulation ability, toxicity, and resistance to biodegradation.

The advancement of analytical methods has helped paint a picture of how the accumulation of PCPs in wastewater has a potential health effect on the ecosystem and human health. Dhodapkar & Gandhi (2019) reported that the ecotoxicological profile, impact of most CEC, and removal strategies are not fully understood and studied. Some sub-classes of PCPs, such as ultraviolet filters (UVFs) and synthetic musk compounds (SMCs), mainly used in cosmetics and household products, have been poorly studied. Still, they are known to have carcinogenic and endocrine-disrupting activity, are human respiratory toxicants and can cause dermal irritation due to their physicochemical properties (Ramos et al., 2020). Thus, it further encourages more studies in treatments that will effectively remove trace amounts of these compounds and study the negative effects of all classes of CECs.

1.3. Research problem

Personal care products form part of the chemical contaminants of emerging concern (CEC) class. These products are used daily and released to the environment through various sources. Recent studies have highlighted the frequent detection of these chemicals in aquatic organisms, municipal wastewater treatment plant effluent, and human beings creating a public health concern. The personal care products (PCPs) released by municipal secondary MBR effluent into the environment threaten water ecology and human health. While conventional treatment methods effectively remove micropollutants, traces of these products exist in water bodies at low concentrations, highlighting the need for additional treatment. Enhanced, innovative and susceptible analytical technologies are needed to detect their low concentration in complex matrices such as secondary wastewater. Under these circumstances, reverse osmosis with thin-film composite membranes is a possible solution for removing personal care products. However, during wastewater, operating conditions, physicochemical properties of the target PCPs, and membrane characteristics should be studied to ensure

1.4. Research topic

Researchers commented that reverse osmosis had shown promising results and thus could be a suitable tertiary treatment for secondary municipal wastewater to remove CECs, specifically personal care products. It was previously suggested that NF/RO is an ideal treatment process for removing trace organic contaminants; however, the complexity of the separation process and the physiochemical properties play a significant role in the effluent quality. Therefore, parameters such as feed pH, temperature and the type of membrane investigated can be controlled further to examine the behaviour of the selected personal care products and their removal due to the changing variables.

1.5. Research questions

- Using a bench-scale RO system, how effective is the use of RO removal of inorganics from municipal secondary MBR effluent at varying feed pH and temperature?

- How will the feed pH and temperature affect the removal of personal care products (PCPs)?

1.6. Research aim and objectives

This study investigates the removal of inorganics and selected personal care products (PCPs) in municipal secondary membrane bioreactor (MBR) effluent with low-pressure and low energy-intensive membranes using a reverse osmosis (RO) bench-scale unit for yielding effluent discharge or recycling application.

1.6.1. Objectives:

- Evaluate two types of thin-film composite (TFC) polyamide (PA) membranes (NF and RO) based on their different characteristic properties to measure the best quality of effluent with the removal of total dissolved solids (TDS), targeted inorganics, and COD.

- Investigate the removal efficiencies of selected personal care products (PCPs): triclosan (TCS), methylparaben (MeP) and Ethylhexyl methoxycinnamate (EHMC) using solid-phase extraction (SPE) and gas chromatography-mass spectrometry (GCMS) for quantification in the water.

1.7. Delineation of the study

This study focused on removing TDS, selected Inorganics, COD and PCPs, TCS, MeP, and EHMC from municipal secondary MBR wastewater effluent using a bench-scale RO system as a tertiary treatment process. A bench-scale RO system was used as a tertiary treatment process, SPE and GCMS for sample preparation and to analyse and quantify the PCP removed. This research focused on the effects of feed pH and temperature on evaluating the membrane's removal efficiencies and performance. Scanning Electron Microscopy (SEM), Attenuated Total Reflection-Fourier Transform Infrared Spectroscopy (ATR-FTIR), and Energy Dispersive X-Ray Spectroscopy (EDX) were used for membrane surface characterization. All other factors were out of the scope of the study.

1.8. Thesis outline

Chapter 1:
The chapter introduces the reader to the background of the project and the problem statement that the project addresses. The aims and objectives are included for addressing the issues stated and the delineation.

Chapter 2:
The literature review looks at all the studies other researchers conducted within the same or similar field. It may also identify gaps within research and highlight the literature on this study's focus points.

Chapter 3:
The chapter contains the materials and methods used for executing the project from the aims and objectives of the project. Also included are the instruments and equipment used.

Chapter 4:
This section contains the results and the discussion. The section is separated into …four sections, membrane characterization, RO system performance, inorganic removal, and PCP removal.

Chapter 5:
This section concludes the overall project collected from the experiments conducted in chapter 4. This chapter also includes recommendations observed during this study for further research.

Appendix:
This section includes tables, graphs and calculations that formed part of the methods and discussions in Chapters 3 and 4.

Chapter 2

Literature review

2. Literature review

2.1. Water treatment

Water is a valuable resource as it supports life on earth. Even though it covers most of the earth's surface, the available portable water is limited. The rapid increase in global water demand for agricultural, industrial, and domestic use, correlating with the increasing human population, results in the continuous release of pollutants into the aquatic environment (Díaz-Cruz, 2015; Aziz & Kasongo, 2019). Due to the severity of water pollution, many places worldwide are going through droughts and groundwater pollution (Lakhouit, 2019).

Water is needed to sustain life on earth; therefore, air, soil, and water quality are of immediate concern due to human interaction and the environment (Díaz-Cruz, 2015). As a result of the increasing production and use of chemicals, organic micropollutants in the environment are also increasing and, consequently, in drinking water too (Brunner et al., 2020). These pollutants form part of the CECs. CECs are new substances released into the surrounding environment in past years due to society's socio-economic structure (Díaz-Cruz 2015). Personal care products (PCPs) form a diverse organic group called pharmaceuticals and personal care products (PPCP). The presence of these contaminants within natural water has been known for a long time, but their impacts on the environment are only emerging in recent literature (Krogh et al., 2017). Traces of micropollutants (MP) are usually ranging from ng/L to µg/L. Still, due to the increasing population and high reliance on MPs' modern cultures, the increase in concentration is foreseeable (Khanzada et al., 2019).

PCPs are known for their potential risk to the aquatic ecosystem and human health due to the high quantities consistently released and their generally low biodegradability (Díaz-Cruz, 2015; Fu et al., 2019). Removing and assessing these contaminants is challenging because of their complexity and transformation in natural and drinking water(Lakhouit, 2019). They have very low concentrations, ranging from a few ng L^{-1} to µg L^{-1}, making it difficult to detect, analyze, and degrade in wastewater treatment plants. Some of these PCPs can resist degradation in secondary treatment plants, while some can be decreased by degradation or sorption to settle into particulate matter (Krogh et al., 2017).

2.2. Personal Care Products

The presence of substances or compounds in water may not necessarily mean they pose a risk or may be of concern. Still, it has been evident from investigations that detecting Pharmaceuticals and personal care products (PPCP) in water harms the health of the surroundings. The following list by Ebele et al. (2017) summarises the significant concerns about the detection of PPCPs in water:

- Partial removal from water treatment plants
- Evidence of the presence in the aquatic environment
- Extensive use and constant manufacture of new products contribute to their presence in the environment
- The continuous application and release to the environment may result in some being persistent compounds
- The metabolite of substances such as perfluoroalkyl (PFASs) are biologically active and can, therefore, affect non-target organisms raising the risk of ecotoxicological effects
- Their interference with the endocrine system may result in undesired impact or disruption of homeostasis.
- At low concentrations, a mixture of these compounds can lead to synergistic interaction

WWTPs are usually not designed and built to treat low concentrations, mainly due to a lack of discharge guidelines and environmental quality standards. Therefore, traces of PPCPs can still be detected in WWTP effluent (Freyria et al., 2018). Most WWTPs are designed to remove organic nutrients such as carbonaceous, nitrogenous, and phosphorous organic substances (Lopera et al., 2019).

Humans use these products daily, reaching the sewages or WWTPs when disposed of through domestic used water leaving households or during production. Figure 1 shows the transport of PPCPs to the environment, whether as a WWTP effluent or directly to water bodies(Morone et al., 2019). MPs enter the environment by discharging treated and untreated effluent from treatment plants and processing industries, agriculture and farmyard runoff mixing with fresh/surface water, manure/biomass sludge applications, wastewaters from hospitals, domestic residences, and other manufacturing industries (Lopera et al., 2019). The discharged effluent enters freshwater bodies, then is used for non-potable resulting in MPs' occurrence in soil, surface water, and groundwater in parts per billion (ppb). The selected compounds, shown in Table 2-1 and Table 2-2, were chosen because their presence presents a high risk to the environment and human health.

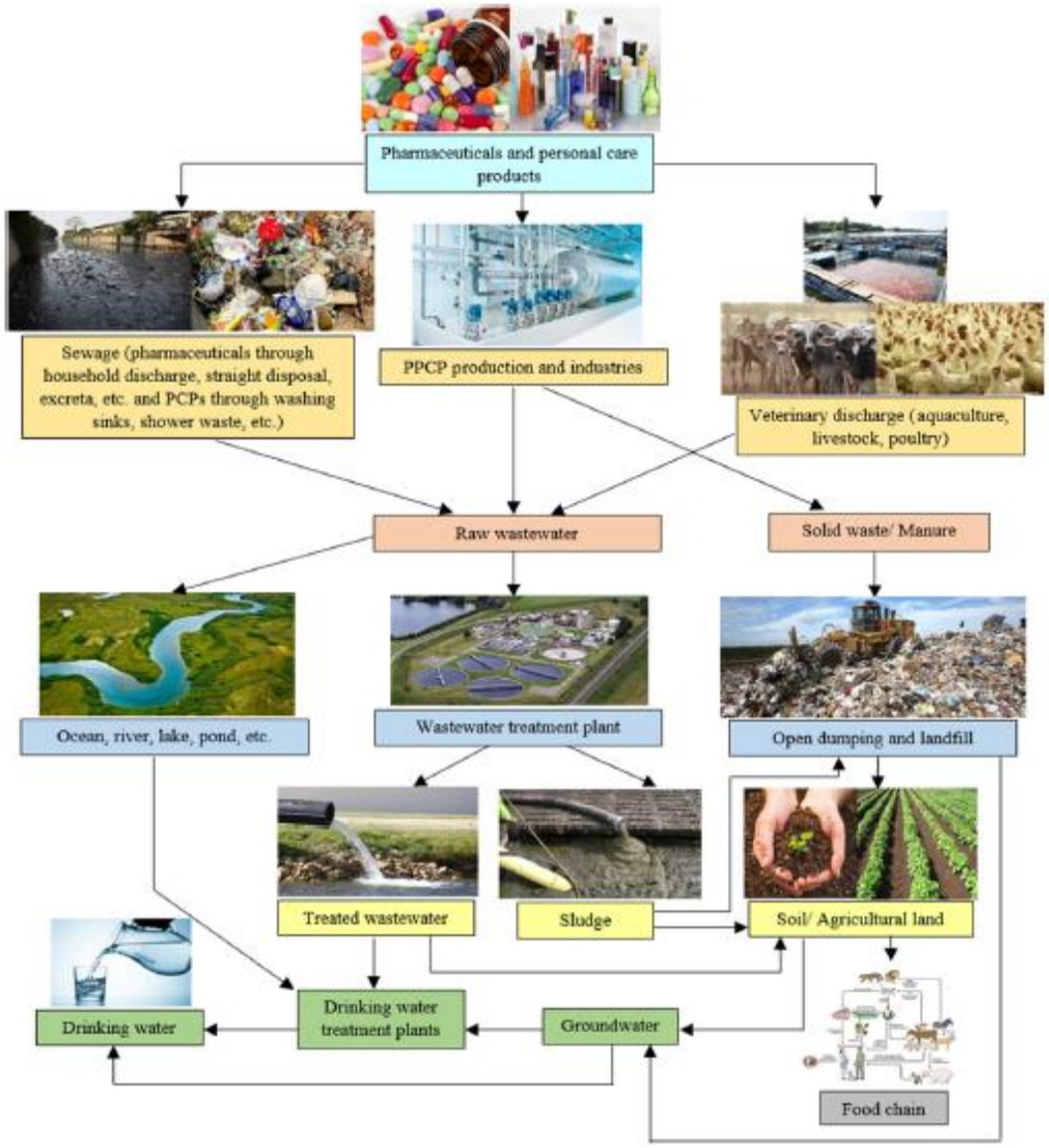

Figure 2-1:Sources, environmental fate, and transport of PPCPs (Morone et al., 2019)

Table 2-1: List of selected personal care products with their INCI, CAS number, and function (Díaz-Cruz, 2015)

Name	INCI	Abbreviation	CAS no	Function
Methyl p-hydroxybenzoate	Methyl Paraben	MeP	99-76-3	Preservative
5-Chloro-2-(2,4-dichloro phenoxy) phenol	Triclosan	TCS	3380- 34-5	Biocide
2-Ethylhexyl 4-methoxycinnamate	Ethylhexyl methoxycinnamate	EHMC	5466- 77-3	UV filter

Table 2-2: Functions and main properties of the selected PCPs (Wang & Wang, 2016)

PCP	Function	Molecular weight (MW)	$LogK_{ow}$
Triclosan	Destroy and kill unwanted germs and parasites	289.5	4.76
Methylparaben	Prevent decomposition by microbial growth or by undesirable chemical changes	152.1	1.96
Ethylhexyl methoxycinnamate	Protect the skin from the sun's ultraviolet radiation, and reduces sunburn and other skin damage	290.4	6.1

2.2.1. Disinfectant and antiseptic- triclosan

Triclosan (TCS) with the IUPAC name 5-chloro-2-(2.4-dichloro phenoxy) phenol is commonly used as an antimicrobial agent in antiseptics, household disinfectants, and medical devices. It can be used as a preservative in shampoos, hand soaps, toothpaste, deodorants, and other personal care products. It is also an antifungal agent in textiles, packaging, and functional clothing. Due to the extensive use of these products in households, TCS is emitted in large amounts, leading to its traces in the environment. According to Claudia & Magrini (2017), this compound should be considered a priority pollutant as exposure to humans can result in endocrine disruption, thyroid function impairment, liver carcinogenesis, and oxidative stress. TCS is known for its instability and lipophilicity, as it can be converted into chlorinated derivatives resulting in more toxic compounds. It can bioaccumulate in plants and animals, including aquatic life. It is degraded to dioxins and is harmful to marine bacteria at levels found in the environment (Díaz-Cruz, 2015).

The presence of TCS in the aquatic environment has the following effects (Juliano & Magrini, 2017):

- it exhibits toxicity to algae species
- alters benthic bacterial communities' composition resulting in the development of cyanobacteria over algae
- Exhibits teratogenic responses
- death in the embryos and larvae of zebrafish
- shows endocrine disruption in fish

Another concern is that antimicrobial compounds such as TCS can cause bacterial resistance against antibiotics and may also be related to allergic sensitization in children (Díaz-Cruz, 2015). Due to its hydrophobic properties, during conventional wastewater treatment, despite TCS being found in effluent wastewaters, it has high removal rates showing a slight tendency to accumulate in sludge and sediments, where it can persist (Díaz-Cruz, 2015).

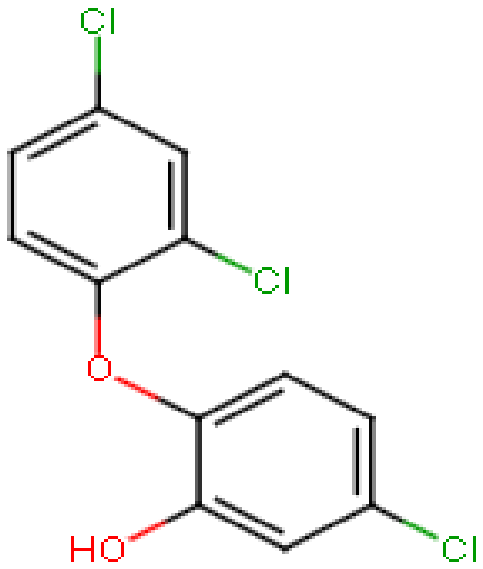

Figure 2-2: Structural formula for Triclosan (National Center for Biotechnology Information, 2020b)

2.2.2. Preservatives-Methylparaben

Methylparaben (MeP) forms part of the preservatives used for their antimicrobial properties. Parabens are characterized by their broad spectrum of activity against yeasts, moulds, and bacteria, their chemical stability, low toxicity, and low cost (Juliano & Magrini, 2017). Parabens' effectiveness as antibacterial and fungicidal, with their low production cost, low toxicity, and the lack of a suitable alternative, makes them ubiquitous (Díaz-Cruz, 2015). It is mostly used in pharmaceuticals, food products, and cosmetics. The structural formula is shown in figure 3.

Paraben removal in wastewater treatment is reported to be effective, with a percentage removal higher than 90%; however, traces of these parabens are found in the tissues of fish, marine birds, and their eggs and marine mammals (Juliano & Magrini, 2017). Recently, concerns were raised about the effect of parabens on humans and aquatic life. Recent studies show that parabens display endocrine-disrupting activities, which may be linked to human breast cancer, pending scientific evidence. However, based on past reviews, it would be negligent in underestimating the possible concerns for human health of the continuous introduction of parabens into the environment (Juliano & Magrini, 2017). The potential endocrine disruption of parabens is associated with the interference of the vitellogenin plasma concentration in some organisms, such as rainbow trout and Japanese medaka fish (Juliano & Magrini, 2017).

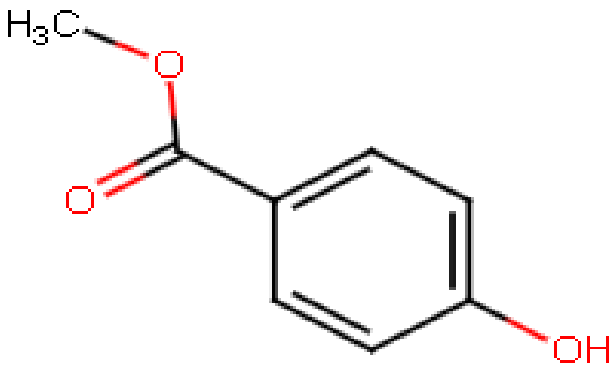

Figure 2-3: Structural formula or methylparaben (National Center for Biotechnology Information, 2020c)

2.2.3. UV filter- Ethylhexyl methoxycinnamate

Ethylhexyl methoxycinnamate (EHMC), octyl methoxycinnamate, is a commonly used UV filter in sunscreens and other cosmetic products (Fennell et al., 2017). It is structured as shown in figure 5 below. One consumer can use EHMC in many categories of PCPs, increasing its exposure to the environment. A study by Manová et al. (2015) provided the first comprehensive information about EHMC aggregate exposure levels in multiple PCP categories. In this study, it was reported that PCPs like sunscreen, lip care, face cream, hand cream, make-up foundation, lipstick, and aftershave contributed to the exposure of EHMC to the population in all seasons at various levels. EHMC levels are found between ng/L to µg/L even in tap water, and it has been noted that due to the high consumption of the cosmetic product in summer, their concentration is ten times higher than that in winter (Gackowska, 2020).

Recent studies show that the frequent usage of EHMC has led to its widespread in different environments such as surface water, swimming pool water, marine organisms, and wastewater in treatment plants. The availability of this compound in wastewater enhances human exposure, creating health concerns. This UV filter has raised a debate in the scientific community about its potential endocrine-disrupting effects on the human population, aquatic life, and wildlife (Manová et al., 2015).

According to Díaz-Cruz (2015), EHMC is one of the UV filters that can alter the transcription profile in fish and genes related to the production of sexual hormones. It has also been reported that EHMC is one of the interactive products in the environment. Xu et al. (2020) stated that EHMC accumulates in aquatic organisms and produces degradation products that show high ecology toxicity. The study provided information that the presence of EHMC in high-altitude rivers can disturb the nitrogen transformation process by stimulating N_2O production, increasing pressure on global warming.

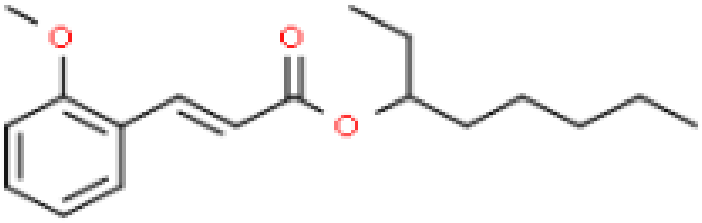

Figure 2-4: Structural formula for Ethylhexyl methoxycinnamate (National Center for Biotechnology Information, 2020a)

2.3. Membrane technology

2.3.1. Membrane Bioreactor

Membrane Bioreactors (MBR) is a hybrid process consisting of a biological treatment method combined with membrane filtration to remove various pollutants from wastewater to produce high-quality effluent. It is characterized by its high removal of bacteria, low footprint, stable operation performance, reduction of excess sludge production, and ability to operate under highly suspended solids producing a higher effluent quality that can be reused in various industries (Oota et al., 2005; Jalilnejad et al., 2018; Murakami, 2008). Conventional activated sludge (CAS) comes short regarding fluctuations in effluent flow rates and composition, making it less desirable as a treatment resulting in its effluent not meeting the required discharge limits for reuse. However, over the past years, MBRs have provided the qualities needed to fill the gaps left by the CAS, making it more desirable as a treatment technique (Ezugbe & Rathilal, 2020).

Though MBR may seem efficient in wastewater treatments, it has drawbacks of fouling and cleaning topping the list, hence the need for additional treatments. Although applicable as a treatment technique, it has been reported that further treatment, such as ozone or activated carbon, may be required to remove the yellowish-brown colour found in an MBR effluent (Oota et al., 2005). As previously mentioned, ECs are very complicated, and MBRs cannot effectively remove all types due to their complexities. The EC removal efficiency by MBR can be affected by several factors, such as conductivity, organic load, pH, sludge age, and temperature (Chtourou, 2018).

MBR is often coupled with additional treatments, mostly RO/ NF, to remove PCPs (Alturki et al., 2010; Wang et al., 2018). Several studies have investigated the use of an MBR-integrated system to remove EC. Due to the complementarity of the MBR-RO/NF hybrid system, Wang et al. (2018) successfully removed PPCPs from municipal wastewater using this system, with an average removal of 95% for most of them. Jalilnejad et al. (2018) found that MBR effluent was not suitable for irrigation purposes, but when coupled with RO and NF, the effect that the use of MBR effluent would've caused was reduced. It was also noted that using an MBR-RO system could effectively reduce SS and COD, providing a higher-quality effluent suitable for reuse, making this integrated system a considerable alternative for the recovery and reuse of treated wastewater for irrigation (Dolar et al., 2012; Aziz & Ojumu, 2020).

2.3.2. Reverse Osmosis

Reverse Osmosis (RO) is a pressure-driven process commonly used for selective separation, purification, and concentration (Wenten & Khoiruddin, 2015). It is also described as a diffusion-controlled process where the mass transfer of permeate through the RO membrane is governed by diffusion (Wenten & Khoiruddin, 2015). The RO system is used in the separation of dissolved solutes from water through a semi-permeable membrane that only allows water to diffuse into and out of the membrane

It is applied as the final step in water treatment to reuse and recover valuable components. Studies have shown that RO can treat industrial wastewater with a recovery of 80% or more, successfully removing inorganic and organic compounds with pressure under 60 bar (Wenten & Khoiruddin, 2015). It is further reported that using RO as a secondary or tertiary wastewater effluent filtering step allows the reclaimed water's direct consumption. RO, as part of the membrane-based method, has demonstrated high effectiveness in removing various components compared to other methods. Due to its characteristics, it can effectively remove organic molecules with low molecular weight. The effluent from RO systems can also be reused in industries (Mikhak et al., 2019).

In wastewater, RO membranes are used to remove the dissolved solids and harmful pollutants in municipal sewage effluent, municipal wastewater, dumpsite and landfill leachate, electroplating wastewater, sugary wastewater, wastewater from the dairy industry, tannery wastewater, and olive mill wastewater, name a few (Wenten & Khoiruddin, 2015).
Baker (2012) used the following equations to describe the solution-diffusion mechanism used in RO, where the water flux is linked to the concentration gradient across the membrane given

$$j_i = A(\Delta P - \Delta \pi) \qquad (1)$$

Where J_i is the water flux, ΔP describes the difference in pressure across the membrane, Δπ is the difference in osmotic pressure across the membrane, and A is a permeability constant. The equation also shows that when the applied pressure is higher than the osmotic pressure, water flows from the concentrated to the dilute salt-solution side of the membrane (ΔP>Δπ). When the applied pressure is lower than the osmotic pressure, water flows from the dilute to the membrane's concentrated salt-solution side (ΔP<Δπ). When the pressures are equal ΔP=Δπ, no low flow occurs.
Equation 2 describes the salt flux across a RO membrane

$$J_i = B(C_{JO} - C_{JL}) \qquad (2)$$

B is the salt permeability constant, C_{JO} salt concentration in the feed and C_{JL} salt concentration in the permeate solution. The salt concentration in the feed is higher than that of the permeate solution (Baker, 2012); therefore, equation 2 can be simplified into equation 3

$$J_i = B * C_{JO} \quad (3)$$

Equation 3 shows the proportionality of the water flux to the applied pressure. Equation 4 shows that the salt flux is independent of pressure, which means that the membrane selectivity (represented by R) changes as the pressure increases.

$$R = \left(1 - \frac{C_{JO}}{C_{JL}}\right) * 100\% \quad (4)$$

Like any other process, it also has limitations caused by membrane characteristics and hydrodynamics within the membrane module, such as low permeation flux, inadequate selectivity, membrane durability, membrane fouling, high equipment, and operating cost rendering the process inefficient (Wenten & Khoiruddin, 2015). The technology has made significant improvements, such as using a new membrane material module, changes to the process design, introduction of pre-treatments, and energy recovery, leading to cost reduction and motivating the commercial application of this technology. Pre-treatment such as coagulation-flocculation-sedimentation are very useful in fouling; the coagulants or coagulant aids used can effectively increase membrane permeability (Mikhak et al., 2019). These pre-treatments, including electrocoagulation, help reduce pollutant load, minimizing fouling.

2.3.3. Nanofiltration

NF membrane forms part of the commonly known pressure-driven membranes, MF, UF, RO, and NF. NF membrane pore sizes are smaller than UF and MF but larger than RO, ranging from 1 to 10 nm. NF is a pressure-driven separation technique often used to separate ultrasmall pollutants in water (Rienzie et al., 2019). It uses ionic separation and sieving to separate the solute from the solution. The molecules can easily be separated based on their water charges or molecular weights (Abdel-Fatah, 2018).

NF is often used where the retained component has a high molecular weight and is also a minor component, with osmotic pressures, not a problem (Baker, 2012). NF membranes can separate solutes or chemicals from solution, produce bio-materials, drug industry, and flavours, recover fine chemicals from outlet streams in medical applications, and feed additives.
These membranes have also gained popularity as a replacement for RO, as they can recover delicate and expensive materials for profits, lower energy expenses, and even drink water (Abdel-Fatah, 2018).

According to Abdel-Fatah (2018), NF membranes have the following advantages:

- they do not require chemical treatment for the reduction of hardness
- no heating or cooling of feed is needed, thus reducing separation costs
- Mechanical stirring is also not required to maintain gentle molecular separation
- They can handle a large volume of feed continuously at a stable permeate flow rate

Their pore size limits the application of these membranes, and they are replaced only after little use compared to the used filter, which unfortunately increases costs (Abdel-Fatah, 2018). Like any other technique, it needs to be operated at the right conditions, and as part of the membrane family, fouling is an issue during operation. To decrease membrane fouling parameters such as feed pH, the permeate flow rate, concentrate and feed temperature must be controlled (Abdel-Fatah, 2018). Membrane selection is also essential, as proper selection and operation may delay fouling. In addition, Abdel-Fatah (2018) reported that a higher pressure could help maintain a stable permeate flux, whereas cleaning may be a requirement in some cases.

NF membranes are mainly used in various industries, as listed below, as mentioned by Abdel-Fatah (2018):

- Desalination of food industries such as dairy, baker's yeast beverage products, fish meal, juice processing, meat processing, olive processing, soft drinks, and sugar industry,
- Pharmaceutical and biotechnology applications
- Purification spent clean-in-place chemicals.
- Removals of Metal, Nickel, and Chrome plating from metal finishing industries and the leather industry,
- Whey partial desalination,
- Application in the chemical industry,
- Textile dyes desalination and brighteners of optical

Table 2-3: The benefits of NF in wastewater treatment (Abdel-Fatah, 2018)

Application	**Permeate**	**Concentrate**	**Benefits of NF**
Whey/Whey permeate	Salty wastewater	Desalted whey concentrate	Allows the recovery of lactose and whey protein concentrate with reduced salt content
Textile	Dyes	Water, salts, BOD, COD, and colour	NF is used to desalt dyes resulting in a higher-value product
Caustic cleaning solutions	Caustic cleaning solution	BOD, COD, suspended solids, caustic cleaner	Allows caustic cleaning solution to be recycled, resulting in reduced cleaning chemical costs
Recycle acid solutions	Acid solution	BOD, COD, calcium, suspended solids, acidic water	Allows acid solution to be recycled, resulting in reduced cleaning chemical costs
Water	Softened water	Hard water	Potable water production. Softened water reduces scaling on equipment and heat exchange surfaces
Antibiotics	Salty waste product	Desalted, concentrated Antibiotics	NF produces high-value pharmaceutical products
Pharmaceutical Industry	Drug Industry	Salty waste product	Increases the value of a pharmaceutical product

2.3.4. RO and NF in wastewater treatment

Numerous studies have investigated RO and NF membrane use in wastewater as an individual treatment or part of an integrated system. They have shown the removal efficiency of several pollutants in various industries. One of them focuses on PPCPs removal in secondary wastewater. While other treatment methods can remove other contaminants, they are not fully efficient in eliminating all PPCPs present, hence detecting surrounding receiving water bodies. Secondary conventional treatments aim to reduce organic matter and readily biodegradable nutrients, as shown in Table 4 (Kaur et al., 2019).

RO/ NF is also used to remove COD, TDS as a measure of turbidity, and inorganics such as ammonia, nitrogen and phosphates. Aziz & Kasongo (2021) evaluated the use of UF/RO/NF in removing inorganic material from municipal water. The study reported the highest rejection for tested parameters at a controlled pH of 6,5 using XLE. The COD removal was up to 99% and recorded turbidity below 1NTU due to increased pH, suggesting that controlled pH could effectively reduce COD and turbidity. The study also highlighted that the highest average removal of ammonia (98%), phosphates (97%), and phosphorus (98%) were recorded at a pH of 6,5 using XLE, suggesting the dominant removal mechanism was due to electrostatic interactions. Lim et al. (2021) compared XLE and NF270 in removing ammonium as a function of pressure, feed pH, and initial ammonium concentration. The results showed that both membranes were effective, but XLE outperformed NF270 in all areas. The COD removal was also reduced from 114-50mg/L for NF270 and 27mg/L for XLE. It further supports that these membranes are effective at lowering COD and inorganics.

In the landfill leachate treatment, coagulation and adsorption had a COD, turbidity and ammonium nitrogen (NH_4-N) removal of 65,7%, 87% and 15,2%, respectively. At the same time, XLE, NF90, and NF270 recorded 85,7%, 79,4%, and 37,1% for COD, 79,2%, 82,9%, and 7,4% NH_4^+-N, and 99,4%, 99,2%, and 99,6% for turbidity, respectively (Strmecky et al., 2016).

Table 2-4: Various treatments for PCPs

Personal Care Products	Treatment 1		Treatment 2		NF/RO	
	remarks	**reference**	**remarks**	**reference**	**remarks**	**reference**
Triclosan	Grit tanks, primary sedimentation, anoxic bioreactor, aerobic bioreactor, and clarifiers collectively removed 99.8% (167-0,3g/day) of TCS	(Roberts et al., 2016)	The use of adsorption and biodegradation to treat sewage and greywater under aerobic conditions had removal efficiencies of 96%(21,9-1,11µg/L) and 98% (15,6-0,35µg/L) for sewage and greywater, respectively	(Zeeman et al., 2010)	NF had a removal efficiency of 57.1% (1862-798ppb)	(Ogutverici et al., 2016)
Methylparaben	The use of adsorption-activated sludge and UV radiation had a removal	(Sun et al., 2014)	Adsorption and fixed-bed column experiments had 60% (5-2mg/L) and 30%(0,5-0,35mg/L)	(Chtourou, 2018)		

	efficiency between 81.6-91%, with adsorption alone removing 71.6% (100-20ng/L)		removal efficiencies, respectively.			
Ethylhexyl methoxycinnamate	The use of adsorption and biodegradation to treat sewage and greywater under aerobic conditions had removal efficiencies of 99.6% (7,1-0,003µg/L) and 49%(15,5-7,9µg/L) for sewage and greywater, respectively.	(Zeeman et al., 2010)	Coagulation-flocculation, ozonation, and continuous microfiltration had an average removal of 28-43% (54-116ng/L).	(Li et al., 2007)	Removal EHMC by NF and RO had an efficiency of 72% (35-10ng/L) and49% (17-9ng/L), respectively	(Krzeminski et al., 2017)

Table 2-4 shows that integrated systems are more effective in removing PCPs than individual methods, even though integrated systems sometimes have low efficiency compared to NF and RO. In a study conducted by Li et al. (2007), the results concluded that coagulation-flocculation, ozonation, and continuous MF had an average removal of EHMC between 28-43%, compared to RO and NF with an efficiency of 49% and 72%, respectively (Krzeminski et al., 2017). RO and NF are preferred for PPCP removal over conventional treatment methods for their high selectivity (Morone et al., 2019). They exhibit admirable qualities that allow an excellent performance and removal rate higher than 85% for almost all pharmaceutical ingredients (Rienzie et al., 2019). The efficiency of these membranes differs depending on the type of membrane used and the operating conditions. Numerous studies have investigated NF and RO's use in removing selected PPCPs, and the results vary, but they all show high efficiency.

The two systems are based on a semi-permeable membrane, and the main difference is that RO removes all particles, including vitamins and minerals essential for drinking water (Freyria et al., 2018). At the same time, NF gives a coarser filtration without removing minerals. Due to the difference in pore sizes, NF shows a higher removal rate for larger molecules.

The removal rate of PPCPs varies due to the difference in their physicochemical characteristics. Wang et al. (2018) investigated using an integrated MBR-RO/NF system to remove 27 PPCPs in municipal wastewater; MBR-NF resulted in 13/27 compounds concentration below detection limits and MBR-RO with 20/27. It was the result of the difference in removal mechanisms. When compared, the integrated system had a removal rate above 95% and more for most compounds, while MBR alone had a rate between 41.08% and 95.51%.

Liu et al. (2011) compared the use of NF to that of RO in treating biologically treated textile effluent. The results showed that the NF membrane had a higher COD reduction rate due to the NF's sieving removal mechanism. As previously mentioned, the membranes have various uses in different industries, and their characteristics allow them to be better than the others depending on the requirements for the application.

The variety of compounds in PCPs will result in different rejection trends depending on the physicochemical properties of the compound investigated (Freyria et al., 2018). The removal efficiency for the PCPs will vary, with some showing higher removal efficiency using NF while others have a higher removal efficiency using RO. The identical NF with a removal efficiency of 72% for EHMC had a removal efficiency of 57.1% for TCS (Krzeminski et al., 2017; Ogutverici et al., 2016).

2.3.5. MBR-RO/NF integrated treatment system for the treatment of CECs in municipal wastewater

The MBR-RO/NF hybrid system has been reported to be successful in removing CECs, SS, and COD from municipal wastewater, providing high-quality effluent that can be reused with significantly fewer environmental health concerns (Dolar et al., 2012; Wang et al., 2018; Jalilnejad et al., 2018; Aziz & Ojumu, 2020). Coupling MBR with RO/NF enhances the system performance ensuring a higher removal of trace organic compounds. Several studies reported that MBR-RO resulted in stable RO permeate flux in long-term use and reduced membrane fouling (Alturki et al., 2010).

Alturki et al.(2010) coupled MBR with NF270, NF90, BW30, and ESPA2 to remove 40 CECs from municipal wastewater. Out of the 40 compounds, including Ibuprofen (IBU), Bisphenol A (BPA), Diclofenac (DCF), and Triclosan (TCS), the hybrid system successfully resulted in effluent with a number of these compounds below detection. MBR-RO had 7(ESPA2), and 14(BW30) compounds detected in the effluent, while MBR-NF resulted in 16(NF270) and 12(NF90) compounds in the permeate. These results suggest that MBR-RO had a better performance than MBR-NF. The results were complemented by another study that observed that MBR-RO achieved better results than MBR-NF (Wang et al., 2018). Out of the 27 PPCPs that were being removed using the integrated systems, MBR-RO effluent had 7 compounds detected, while MBR-NF had a record of 14. The systems both recorded an excellent PPCPs rejection above 95% for most of them. A combination of MBR-XLE and MBR-NF90 can achieve levels below detection, while MBR-NF270 records 90-99% removal of CECs (Racar et al., 2020).

The coupling of MBR with RO/NF enhances the removal of CECs by providing the necessary removal mechanism where the other treatment is limited to improve and collectively remove the target compounds (Alturki et al., 2010; Dolar et al., 2012; Wang et al., 2018). MBR is limited in removing hydrophilic and biologically persistent trace organic compounds, which can be complemented using RO/NF membranes through steric hindrance or size exclusion mechanisms. Studies show that only after RO/NF can the permeate be reused without restrictions as per European Union (EU) and World Health Organisation (WHO), depending on the membrane used, as the efficiency of the membranes is affected by the physicochemical properties of the CECs, solution chemistry, and membrane properties (Alturki et al., 2010; Racar et al., 2020).

2.3.6. Membrane selection

NF has the advantage of retaining minerals that cannot be retained by RO (Kaur et al., 2019). Membrane selection is essential to remove the required parameters effectively. Different membrane materials for both NF and RO show and will show other micro-pollutant rejection trends based on the physicochemical properties of the targeted compounds (Freyria et al., 2018). The membranes must be analyzed first before use for their properties, as shown in Table 5. The contact angle is measured, followed by scanning electron microscopy (SEM) to study the surface morphology of the membrane.

Table 2-5: Membrane properties (Lin et al., 2014)

Membrane characterization	**NF (NF270)**	**RO (XLE)**
Molecular Weight Cut-Off	300	100
Pure water permeability	17.8	8.8
Average pore diameter (nm)	0.84	-
Root mean square roughness	9.0±4.2	129.5±23.4
Contact angle	64.1±10.5	66.3

2.4. Factors affecting membrane-based water treatment

2.4.1. Physicochemical properties of target compounds and membrane properties

Molecular weight and molecular weight cut-off

It is common knowledge that compounds have different physical and chemical properties. Those properties play a vital role in their removal. The molecular weight of these compounds is one of the properties that influence their reduction in technologies such as RO systems. Several studies have mentioned that when removing PPCPs, size exclusion was often the dominant removal mechanism for RO membrane when the molecular weight is greater than the MWCO of the membrane (Kim et al., 2018; Wei et al., 2020). It was supported by an observation of the removal efficiency of TCS using XLE, NF270, and NF90 (Lin et al., 2014). The TCS rejection followed the NF270 > NF90 > XLE, the same order as the MWCO NF270-300>NF90-200>XLE-100. Another study also further supported that the compound with the highest removal happens to have the most significant molecular weight. Compounds with relatively high molecular weight (carbamazepine (CBM), sulfamethoxazole (SMX), and atrazine (ATZ)) had a high removal compared to small compounds (phenol (PHN) and 4-chlorophenol (4CP)) (Heo et al., 2013).

Hydrophobicity, surface charge, and dissociation constant

PPCPs contain ionizable functional groups that exist in forms that are pH dependent by affecting the ionization state of the PPCPs as the result of the acid dissociation constant (pKa)(Wang et al., 2019; Wei et al., 2020). The hydrophobicity of the neutral compounds results in hydrophobic interactions and pore-filling behaviour. The interaction between PPCPs and membranes plays a significant role in removal efficiency. The PCPs exhibit hydrophobicity, with a log K_{ow} value of 4.76, 1.96, and 6.1 for TCS, MeP, and EHMC, respectively. Membranes contain charges measured as zeta potential, related to the feed pH, making the pH the determinant of the membrane charge quantity and properties (Wei et al., 2020). The membrane charge is comparative to the absolute zeta potential value; if the value is greater than zero, it indicates that the membrane surface is positively charged.

2.4.2. Water quality and process parameters

pH

The feed pH is considered one of the process variables that play a vital role in removing PPCPs and the performance of the RO system (Wei et al., 2020). It affects the rejection capabilities of polyamide (PA) composite membranes by changing the membrane surface charge, the hydrophobicity, and the adsorption of dissociable organic compounds, consequently, their rejection (Dang et al., 2014; Kucera, 2015). The change in feed pH determines the charge quality and properties of the membrane surface and also the ionization state of PPCPs due to the dissociation constant (pKa) (Wei et al., 2020).

Numerous studies have investigated the effect of feed pH on PA membrane performance and the removal of PCPs. The recommended operation pH ranges between 2-11. Lim et al. (2021) investigated the effect of pH (2-10) on the performance of XLE and NF270 by measuring permeate flux. The results showed that the flux fluctuated with the increase in feed pH for investigated membranes, 116.22-135.04 $L/m^2 \cdot h$ for the NF270 membrane and 71.67 -74.71 $L/m^2 \cdot h$ for XLE. It was also noted that NF270 had a higher flux due to its larger pore size. There was a noticeable change in permeate flux for the NF270 with the change in feed pH. Alkaline conditions had higher recorded flux than acidic conditions, while XLE showed a stable flux record, suggesting that pH had more effect on NF270. These results were further supported by a study by Lin et al. (2014). Both studies reported that the change in feed pH altered NF270 membrane properties. Alkaline conditions had higher permeate flux due to the increased negative membrane surface charge resulting in larger and looser pore structures.

As previously mentioned, the change in feed pH influences the rejection of PPCPs. Various studies have investigated the effect of pH on PPCP removal using membranes such as XLE, NF270, and NF90(Lin & Lee, 2014; Lin et al., 2014). When evaluating the rejection of PPCPs (TCS, CBZ, IBU, SMZ, SMX) using membranes (XLE, NF90, NF270) as a function of pH, it was found that XLE had the highest PPCP rejection and that the rejection increased with the increase in pH for all membranes(Lin & Lee, 2014). The study indicated that the rejection for XLE (86-99%) was a result of size exclusion, while NF270 (23-92%) and NF90 (57-97) rejection were dominated by electrostatic repulsion as a result of the change in pH and varying ionization constants. It was further supported by Lin et al. (2014). They observed that the rejection of TCS followed the order of NF270 > NF90 > XLE due to pore size difference and change adsorption

due to the change in pHs for all membranes due to electrostatic repulsion between the dissociated TCS and membrane surface.

Temperature

It has been suggested that temperature affects the performance of RO systems. Manufacturers often recommend the maximum operational temperature to be 45°C as a significantly higher temperature alters the structure of the membrane, making it denser and difficult for water to pass through the membrane (Kucera, 2015). Temperature affects the system flux and rejection. The salt rejection decreases with increasing temperature while flux increases(Mohammed et al., 2014; Kucera, 2015; Wei et al., 2018). At relatively higher temperatures, the salt diffusion is reportedly higher and fouling decreases. With increasing temperature, the viscosity and density decrease, and the permeability coefficient of water increases, allowing the water to flow easily through the membrane.

The same phenomenon is observed in removing PPCPs(Wei et al., 2020). The increase in temperature generates thermal energy, which increases the diffusivity of the investigated PPCPs, reducing the water viscosity and increasing the MWCO of NF membranes, making it easier for PPCPs to pass through. While the effect of temperature on the removal of PCPs is poorly studied, studies have shown the influence of temperature in the removal of pharmaceuticals using NF membranes(Wei et al., 2018; Wei et al., 2020).

Flux

Flux is defined as the rate of permeate measured per unit surface area of the membrane. The operating pressure influences temperature, recovery, feed concentration of dissolved solids, and pH (Kucera, 2015). The flux increases with an increase in operating pressure and temperature and decreases with the increase in total dissolved solids in the feed solution. The feed pH alters the membrane properties, affecting the water flux, and while this may be the case for membranes such as NF270, for some membranes like XLE, the pH effect is insignificant (Lim et al., 2021).

Salt rejection

RO systems are often used for high-contaminant removal, and salt rejection is measured to monitor performance. It is defined as the percentage removal of salt or contaminants from the feed solution. It can assess RO membranes' performance and indicate when the membrane needs to be replaced or cleaned (Puretec water, n.d.; Baker, 2012). TDS is often used to indicate salt content to calculate salt rejection; for an increase in feed TDS, the water driving force decreases due to the increase in osmotic pressure on the feed side. This, in turn, results in high TDS concentration in the permeate and a decrease in the system flux (Kucera, 2015).

Pressure

RO is a pressure-driven process, so any change in the operating pressure affects the system performance directly through flux and indirect salt rejection (Kucera, 2015). When the pressure increase, so does the flux. As a result of salt passage found in RO membranes, when the flux increase with the increasing pressure, more water passes through the membrane, decreasing the salt passage and resulting in a higher salt rejection (Mohammed et al., 2014; Kucera, 2015). When the effect of pressure was investigated on the performance of XLE and NF270, Lim et al. (2021) reported that the increase in pressure increased the permeate flux for both membranes due to the increased driving force that allowed more solvents to pass through the membrane. It was also noted that the permeate flux was relatively higher due to the large hydrophilicity and MWCO for NF270.

Recovery

Recovery measures the percentage of the feedwater that is converted into permeates. Usually, RO systems have a recovery rate between 80–85%, with a 15–20% brine flow containing salts, CEC, and other pollutants (Alrehaili et al., 2020). The water flux and salt rejection are noted to be affected by recovery. An increase in recovery increases the feed side osmotic pressure, slowly decreasing the water flux as the pressure nears the applied pressure. The water driving force will be lost, resulting in zero flux (Kucera, 2015).

2.5. Review of previous studies on the removal of CECs from wastewater

As previously mentioned, WWTPs are one of the most significant sources of PCPs. Depending on their physicochemical properties, some compounds are destroyed during the wastewater treatment process, while some are left undamaged or transformed into metabolites (Ebele et al., 2016). The results in compounds with unknown toxicity and persistence were found in receiving water bodies. The recent availability of sensible and precise analytic techniques that can measure concentrations as small as nanograms, such as liquid and gas chromatography-mass spectroscopy (LC-MS & GC-MS), can be used to detect and characterize PPCPs in water (Freyria et al., 2018). Seeing these compounds has led to various treatment methods to remove PPCPs, as shown in Table 2-6 below.

Although conventional treatment methods and advanced oxidation processes have been applied as a treatment for CECs, they have limitations. An example of these limitations is a study by Redding et al. (2009), who used a simple design, cheap, and easy operation adsorption process for EDCs/PPCPs. While adsorption for some compounds was considered successful, the difference in the concentration of the 40 compounds made it less practical for higher concentrations, limiting its use when factors such as seasonal variation are considered. Another limitation was that the high organic matter loading might lead to the blocking of active adsorption sites.

To show the different technologies used in removing PPCPs, Xu et al. (2017) reviewed the studies looking at the advantages and disadvantages of using technologies such as adsorption, biological technology, advanced oxidation process, separation, and integrated processes. The biological treatment centres its technology on efficiency, treatment performance, and utilizing processes such as sorption, plant uptake, and biological degradation. While it is simple and uses less energy, it is time-consuming and limited by seasonal variations and secondary contamination with sludge.

An example of an advanced oxidation process was the degradation of diclofenac and clofibric acid using UV photolysis by Kim et al. (2013). Even though the degradation of the target compounds was successful, the process cannot be applied in large-scale operations.

Table 2-6: Mechanisms, advantages, and limitations of various treatment technology (Morone et al., 2019)

Treatment technology	Mechanism	Advantages	Limitations	References
Conventional treatment methods				
Biological treatment	Microbes use PPCPs as a carbon source and mineralize them	Simple, minimum energy consumption	Time-consuming, seasonal variations, secondary contamination with sludge	Xu et al. (2017)
Sand filtration	Formation of biofilm on the filtration medium helps in biodegradation of PPCPs	Removes suspended solids	Unpredictable since some PPCPs might not biodegrade	Matamoros et al. (2009)
Separation process	Membrane filtration is based on pore size, while MBRs rely on retaining the sludge for biodegradation	Effective PPCP removal, high selectivity	Membrane fouling, issues with the disposal of rejected concentrate	Radjenovi'c et al. (2009)
Passive treatment	Adsorption into the matrix of wetland, aerobic and anaerobic biodegradation and photodegradation	Low-energy requirements, less costly	Longer HRTs, unfeasible for large volumes of wastewater	Hijosa-Valsero et al. (2010)
Adsorption	Uptake of PPCPs onto the surface and porous matrix, the interaction between adsorbent and PPCP	Simple design, cheap, easy operation	High organic matter loading might lead to the blocking of active adsorption sites	Redding et al. (2009)
Advanced Oxidation Process				

Conventional Fenton	Generation of hydroxyl and other radicals Conventional	Faster reaction rate, minimal chemical usage, easy generation of hydroxyl radicals, high efficiency of mineralization Broad	Limited pH range, the requirement of an additional neutralization step, the need for excess H_2O_2, a vast amount of iron-containing sludge generation Excess	Bokare and Choi (2014)
Fenton like		Broad pH range	Excess chemical consumption, the formation of toxic by-products Large-scale	Tayo et al. (2018) Kim
Photocatalytic methods	PPCP degradation through the generation of nonspecific ROS upon excitation with UV light Generation	Complete mineralization, absorption wavelength range can be extended in visible light	Large-scale application is difficult	Kim et al. (2014a)
Ozonation	Generation of highly oxidizing and reactive hydroxyl species through ozone degradation into water	High disinfection potential	Less stability and low solubility of ozone in water, the short half-life of ozone, energy-consuming	Derco et al. (2015)

2.6. Membrane transport models

Transport models for membranes are essential to help determine helpful information regarding the membrane's ability to retain solutes and permeate certain substances. A suitable model enables an accurate prediction of the membrane performance (flux and rejection prediction) by optimizing the process to enhance its efficiency (Ang & Mohammad, 2015). It also results in less time and energy consumption due to reduced number of experiments. The application of models differs due to different membrane properties and fouling. The following figure shows the classification of other transport models and solutes.

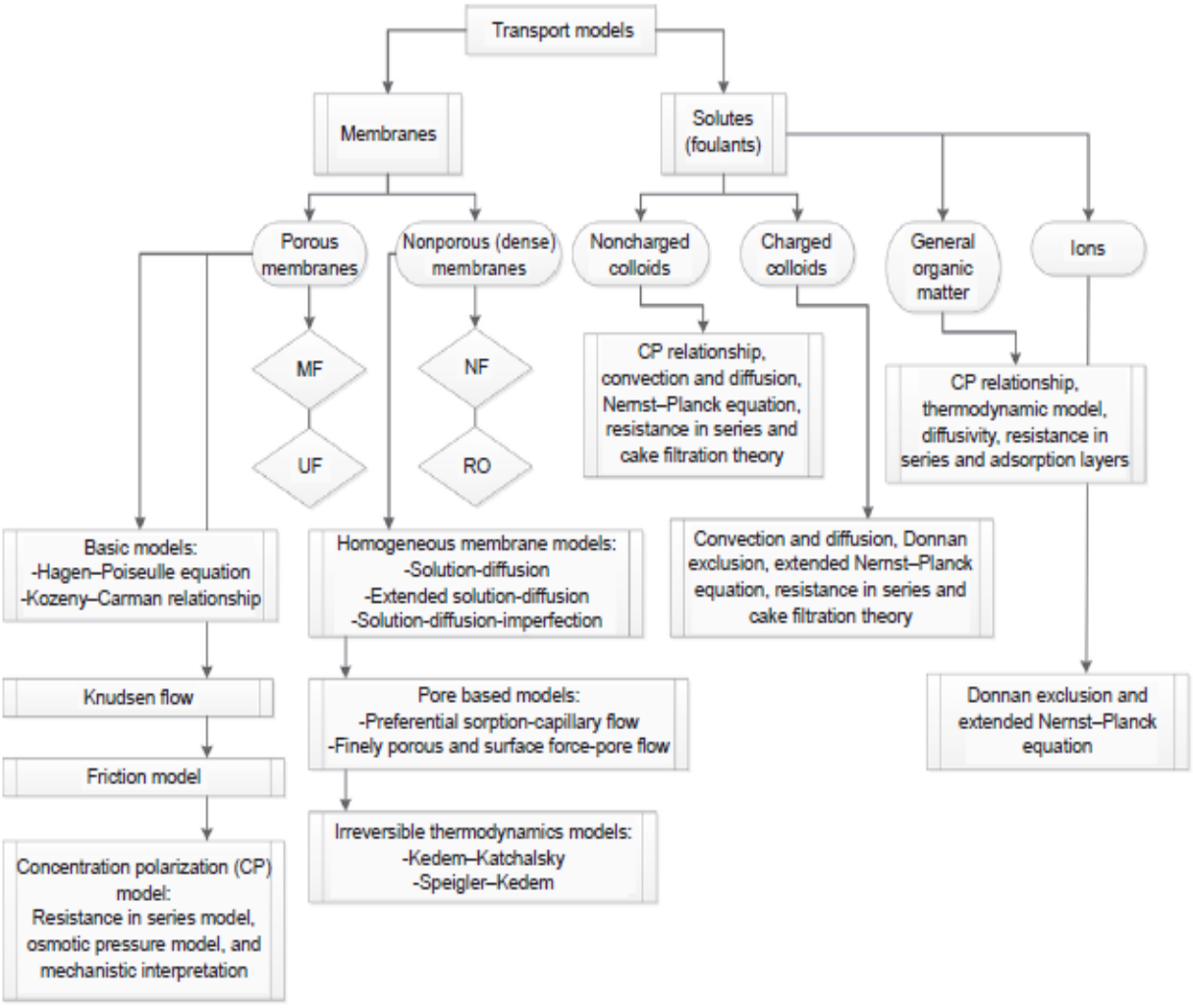

Figure 2-5: Classification of models based on the different membranes and solutes (Ang & Mohammad, 2015)

As mentioned before, the application of a transport model is also influenced by the type of membrane used. Since the study focuses on applying NF/RO membranes, this section will look at the model used for the two membranes. Given that there are changing parameters in the

investigation, the transport model had to include the effect of water chemistry (i.e., pH of the feed). Different models are employed in removing trace organic compounds using RO/NF. These include irreversible thermodynamics models, mass transport models, and artificial neural network models (Ang & Mohammad, 2015). Although all the models have advantages, their limitations cannot be ignored, making it difficult to find a suitable transport model. That said, the extended solution diffusion model is considered the most appropriate model for this study. The model characterized the structural descriptors of polyamide composite membranes (XLE, NF90, & XLE), understanding the effects of feed water chemistry on membrane transport and interfacial and structural properties (Wang, 2014).

The volumetric water flux (J_w) linked to pressure is shown in the equation below, where the pressure difference and osmotic pressure are represented as ΔP and Δπ, respectively

$$j_i = A(\Delta P - \Delta\pi) \tag{5}$$

Where A, the water permeability constant, is given by

$$A = \frac{k_w D_{w,m} V_m}{\Delta x R_G T} \tag{6}$$

Where the water solubility (k_w) is the ratio of the equilibrium water concentration in the membrane ($C_{w,m}$) to the equilibrium water concentration in the feed side ($C_{w,f}$), as shown below

$$k_w = \frac{C_{w,m}}{C_{w,f}} \tag{7}$$

$$C_{w,m} = C_{w,p}\varepsilon \tag{8}$$

With $C_{w,m}$ defined as the product of the equilibrium water mass concentration in the membrane pore and the porosity(ε), the water-membrane pore coefficient (ϕ_w) is then defined as follows

$$\emptyset_w = \frac{C_{w,p}}{C_{w,f}} \tag{9}$$

The simplified definition of water solubility then becomes,

$$k_w = \emptyset\varepsilon \tag{10}$$

Where w, m, p, and f denote water, membrane, pore, and feed, respectively.
Given the water-membrane partition model in Eq (9) and the water diffusion coefficient ($D_{w,m}$) in Eq (10)

$$\emptyset_w = (1-\lambda_w)^2 \exp\left(-\frac{\Delta G_{w,m}}{kT}\right) \tag{11}$$

$$D_{w,m} = k_d D_{w,\infty} \tag{12}$$

With the assumption that the measured temperature (T) is the default temperature, by properly substitution in Eq 5, the volumetric water flux then becomes

$$J_w = \frac{k_d D_{w,\infty}}{\Delta x}(1-\lambda_w)^2 \exp\left(-\frac{\Delta G_{w,m}}{k_B T}\right)\frac{V_m}{R_g T}(\Delta P - \Delta\pi) \tag{13}$$

Where Δx is the effective pore length, R_g is the gas constant, V_m is the molar volume of water, and K_B is the Boltzmann constant. $\Delta G_{w,m}$ is the water-membrane interaction energy, and λ_w is the water stokes radius (rw) ratio to the membrane pore size (r_p). The membrane's physical properties can then be used to obtain the water solubility (A_w) and then calculate $\Delta G_{w,m}$ using the interfacial energies and surface tension.

$$\Delta G_{w,m} = -2A_w(\sqrt{\gamma_w^{LW}\gamma_m^{LW}} + \sqrt{\gamma_w^{+}\gamma_m^{-}} + \sqrt{\gamma_w^{-}\gamma_m^{+}} \tag{14}$$

$$A_w = \frac{\pi r_w^2}{2} \tag{15}$$

The varying pH is reported to affect the membrane water permeability (Wang et al., 2014). By measuring the membrane water permeability at different pH values, the solute flux (J_s) is expected to change. The solute transportation is due to solute diffusion and solvent permeation; therefore, the solute flux is given by

$$J_s = -k_d D_{s,\infty}\frac{dc}{dx} + \frac{J_w}{\varepsilon}k_c c \tag{16}$$

Where k_d and k_c are the hindrance coefficients, $D_{s,\infty}$ is the solute diffusivity in bulk calculated using the Stokes-Einstein equation, and c is the solute concentration within membrane pore, in this case, the concentration of the compounds tested. The flux equation is derived under the conditions below, where β is the concentration polarization factor (CPF).

$c = \emptyset_s \beta C_f$ at x=0

$c = \emptyset_s C_p$ at x=Δx

The rejection is one of the critical measures of the membrane's performance. Therefore, the measured rejection must be accurate. Ang & Mohammad (2015) defines the concept of concentration polarization (CP) as the accumulation of retained solutes in the membrane boundary at the feed side. The CPF is added to obtain a more accurate rejection (R_o).

$$R_o = 1 - \frac{C_p}{C_f} = 1 - \frac{\beta \emptyset_s k_s}{1 - (1 - \emptyset_s k_s)\exp\left(-\frac{J_w k_c S}{k_d D_{s,\infty}}\right)} \tag{17}$$

The ratio of Δx/ε gives the structure factor (S), and other variables are defined in the following equation

$$k_d = \frac{6\pi}{k_t} \tag{18}$$

$$k_c = (2 - \emptyset)\frac{k_s}{2k_t} \tag{19}$$

$$k_t = \frac{9}{4}\pi^2\sqrt{2}(1-\lambda)^{-\frac{5}{2}}\left[1 + \sum_{n=1}^{2} a_n(1-\lambda)^n\right] + \sum_{n=1}^{4} a_n + 3\lambda^n \tag{20}$$

$$k_a = \frac{9}{4}\pi^2\sqrt{2}(1-\lambda)^{-\frac{5}{2}}\left[1 + \sum_{n=1}^{2} b_n(1-\lambda)^n\right] + \sum_{n=1}^{4} b_n + 3\lambda^n \tag{21}$$

$$\emptyset_s = (1-\lambda_s)^2 \exp\left(-\frac{\Delta G_{mws}}{kT}\right) \tag{22}$$

$$\begin{aligned}\Delta G_{mws} = 2A_s \Bigg[& \sqrt{\gamma_s^{LW}\gamma_w^{LW}} + \sqrt{\gamma_m^{LW}\gamma_w^{LW}} - \sqrt{\gamma_m^{LW}\gamma_s^{LW}} - \gamma_w^{LW} \\ & + \sqrt{\gamma_m^+}\left(\sqrt{\gamma_s^-} + \sqrt{\gamma_m^-} - \sqrt{\gamma_w^-}\right) + \sqrt{\gamma_m^-}\left(\sqrt{\gamma_s^+} + \sqrt{\gamma_m^-} - \sqrt{\gamma_w^+}\right) \\ & - \sqrt{\gamma_m^-\gamma_s^+} - \sqrt{\gamma_m^+\gamma_s^-}\Bigg]\end{aligned} \tag{23}$$

The physicochemical properties of the solute, membrane properties, and water chemistry play a vital role in determining the organic solute rejection by NF/RO membranes (Wang, 2014). Therefore, the parameters mentioned, measured, calculated, or obtained from the literature will be used in the model to get the solute flux and solute rejection under any given operating condition.

2.7. Analytical methods and screening

2.7.1 Sample Preparation

Sample preparation is considered one of the most critical stages of analysis. It is frequently used to improve analysis or chromatographic analysis through concentration of analytes, sample fractionation, and clean-up (Moldoveanu & David, 2015). Samples such as WTP effluent have trace amounts of PCPs; extraction techniques are then used to pre-concentrate and clean up samples before analysis to remove compounds that may interfere and to achieve low detection limits (Castro, 2016). Like other techniques, sample preparation needs to fulfil specific standards. Osunmakinde et al. (2013) reported that those standards include robustness, simplicity, cost efficiency, environmentally friendly, and reproducible.

Solid-phase extraction (SPE) is a commonly used sample preparation method. It is often used for its simplicity and capability to concentrate analytes and isolate organic components such as PCPs from aqueous samples. While its simplicity and economy make it an even more attractive method, it also has a complex method development and production process (Campıns-Falco et al., 2012; Stone, 2017). Figure 2-7 shows SPE to paint a picture of what is required and the steps involved, while Stone (2017) describes each step in detail.

Set up	A vacuum or positive pressure manifold for cartridges or plates is necessary to perform SPE
Internal Standards	Mix internal target standards with the sample.
Acidification	Change the pH of the sample to a pH that maximizes retention of analytes on the stationary phase
Conditioning	SPE bed requires conditioning with methanol or acetonitrile to activate the stationary phase
Loading	The sample is loaded onto the cartridge/plate
Washing	One or more wash solutions to remove matrix and exogenous interferences
Drying	The SPE bed is dried with air or nitrogen to remove residual water and solvent.
Elution	The waste container is then replaced with a collection container, and

elution solvent is applied to flush analytes from the stationary phase into the collection vessel.

Reconstitution — The eluate is evaporated using a gentle stream of nitrogen, and a reconstitution solution is added; the containers are sealed, mixed, and introduced to chromatography

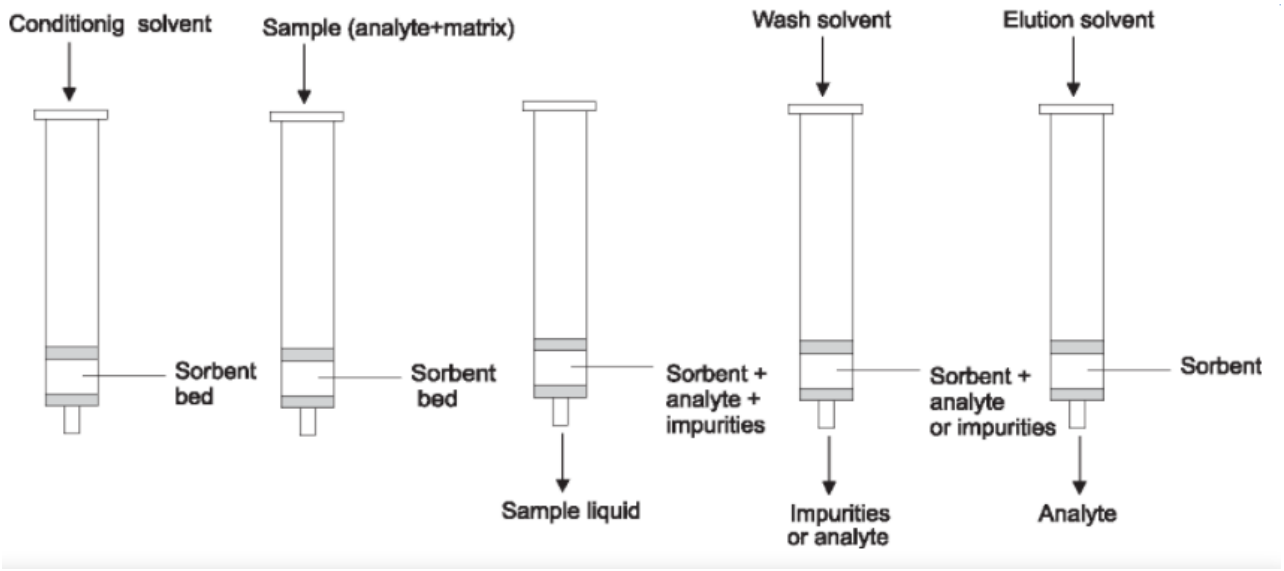

Figure 2-6: Solid phase extraction (Biziuk & Zwir-Ferenc, 2006)

2.7.2. Instrumental Analysis

Following extraction, an appropriate analytical method must be selected to identify and quantify the target compounds. The PPCPs analytes from SPE are employed in gas chromatography and liquid chromatography coupled with mass spectrometry (MS) for the qualitative and quantitative analysis of PPCPs (Shen et al., 2019). Quality by managing consistency between the sample and the target component through peak time and quantity by generating a standard curve by injecting different concentration levels of chosen standard (Pang et al., 2016). These two methods provide a sensitive, selective, and accurate analysis. Coupled with MS, the technique provides a highly sensitive and selective method for analyzing the complex low levels nature of PPCPs (Osunmakinde et al., 2013).

The type of instrument used usually depends on the physicochemical properties of the analytes and the availability of resources(Castro, 2016). An example of studies using these methods, including High-performance liquid chromatography (HPLC), can be seen in Table 2-7, and further explanation of their operation is provided below.

Table 2-7: Concentration of PCPs and the analytical technique used for detection in wastewater

PCP	Concentration	Analytical technique	Reference
Triclosan	2000-5000µg/L	HPLC	(Ogutverici et al., 2016)
	9898ng/L	HPLC	(Najmi et al., 2020)
	>0,1µg/L	GCMS	(Cabeza et al., 2012)
	2µg/L	HPLC	(Alturki et al., 2010)
	800µg/L	HPLC	(Lin & Lee, 2014)
	9,68ng/L	GCMS	(Heath et al., 2018)
	3,2mg/L	UPLC	(Mamo et al., 2018)
	0,1mg/L	HPLC	(Chtourou, 2018)
Methylparaben	114000ng/L	HPLC	(Najmi et al., 2020)
	151ng/L	GCMS	(Heath et al., 2018)
	0,5mg/L	HPLC	(Chtourou, 2018)
	100ng/L	LCMS	(Sun et al., 2014)
Ethylhexyl methoxycinnamate	84ng/L	HPLC	(Najmi et al., 2020)
	9,5ng/L	GCMS	(Cabeza et al., 2012)
	17-64ng/L	GCMS	(Krzeminski et al., 2017)
	34-2128ng/L	GCMS	(Li et al., 2007)

Liquid Chromatography (LC)

LC, a column chromatography, regards liquid as a mobile phase and is preferred for its capability to separate complex samples(Pang et al., 2016). Coupling with MS allows relative molecular mass and structural characteristics to be identified through qualitative by the relationships of the peak and compound content which the peak represented. LCMS/MS is often preferred for its increased analytical sensitivity and selectivity to assay polar and semi-polar compounds with the same molecular mass but different product ions by allowing the separation and detection of compounds in complex water matrices (Castro, 2016). Its analysis generates large datasets containing valuable information that could be extracted and used to obtain qualitative or quantitative information. The chemical composition of a sample using various data mining and statistical tools for multi-class compound characterization (Stavrianidi, 2020).

LC is be modified into a modern application known as high-performance or high-pressure liquid chromatography (HPLC), which uses the same principle as previously mentioned by having the mobile phase pushed through the stationary phase using pumps to speed up the process while also guaranteeing a high sensitivity (Aniszewski, 2007; Houck & Siegel, 2015; Pang et al., 2016). LCMS and HLPC have been and continue to be employed in detecting PPCPs, as noted in various studies in Table 2-7. Another example is a study by Yuan et al. (2020) where an HPLC system was successfully used to identify and quantify 15 PPCPs, including TCS, CBM, and SMX, with a concentration range of 100-500ng/L from river water samples.

Gas Chromatography (GC)

GC is used for the identification and separation of non-polar and semi-polar toxicants widely as the result of its resolution, accuracy and precision, wide dynamic concentration range, potential, sensitivity, specificity, and high degrees of reproducibility (Feng et al., 2019; Piechocka et al., 2020; Zahbi, 2022). A derivatization step is added before GC injection to increase volatility, polarity and thermal instability to obtain sharp peaks, better separation and higher sensitivity(Castro, 2016). It also expands the applicability of GCMS to more compounds by achieving higher sensitivity.

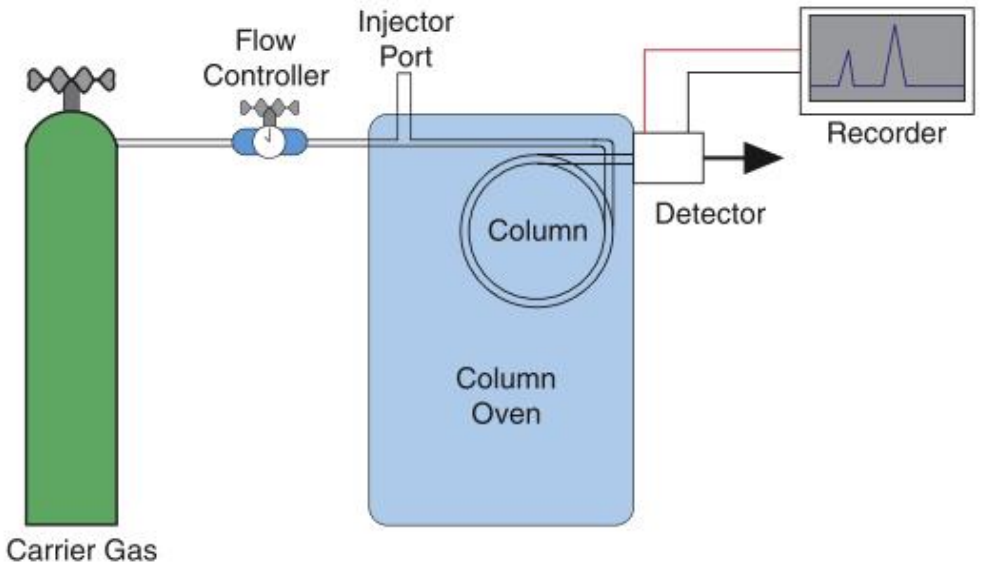

Figure 2-7: Gas Chromatograph (Houck & Siegel, 2015)

GC also uses a similar principle as LC. Figure 2-7 shows that GC operation can be explained using the visible components. Houck & Siegel (2015) details that the mobile phase, an inert gas, often helium, is forced through the stationary phase under pressure. It then purges the entire system of oxygen to prevent the analyte from burning when heated. The analyte mixture combined with the mobile phase is passed through the injector under pressure and then carried into the column with the stationary phase. The molecular and polarity of the analyte, including the temperature of the stationary and mobile phases, determines the traverse time on the column. Their polarities will determine if the mixture separates at low or high temperatures. Therefore, starting with a low temperature and gradually increasing the temperature is advisable to ensure complete separation of the detector. The signal received from the analyte is converted into a small electric current which is then computerized and displayed as a triangular peak on a monitor. During GC analysis, under the same conditions, the retention time of an analyte remains the same, and coupled with MS, an analyte can be analysed by providing structural information used for the identification of the compounds in addition to quantification(Houck & Siegel, 2015; Feng et al., 2019). One of the applications for GCMS is PCPs. Basaglia et al. (2011) used GCMS to accurately detect trace levels of 23 PCP, including fragrance constituents musk xylene and ketone, from water samples. Examples of other studies can be found in Table 2-7.

2.8. Membrane surface characterization

An essential part of any study is understanding the influence of every component used. The same applies to membrane filtration. Membrane properties and their effect need to be known before an investigation. Membrane characterization allows the user to understand the influence of the membrane surface morphology and structure on the permeation, rejection, and fouling behaviour of RO and NF membranes, which enables them to choose membranes based on their desired separation performance (Vrijenhoek et al., 2001; Khulbe et al., n.d.). Through this process, physical surface morphology, surface chemical properties, surface zeta potential, and specific surface chemical structure can be characterized to help accurately predict the behaviour of the membranes, such as permeate flux(Vrijenhoek et al., 2001). It includes describing the membrane to choose a suitable membrane based on the pore size and pore size distribution, surface roughness and structure, electrokinetic characteristics, chemical properties (hydrophobic/hydrophilic), and chemical composition.

2.8.1. Fourier Transform Infrared Spectroscopy

Fourier transform infrared spectroscopy (FTIR) is used as a qualitative analysis tool to identify the characteristic functional groups from the spectral bands by identifying the conjugation between the nanomaterial and the adsorbed biomolecule. It provides vital information on the molecular structure of organic and inorganic components through non-destructive chemical characterization (Chen et al., 2015; Torres-Rivero et al., 2021).

Scanning of the samples using an FTIR spectrometer uses a source that emits radiation passing through an interferometer to the detector, where the signal is amplified and converted to a digital signal by the A/D converter and amplifier, after which the signal is transferred to the computer where the Fourier transform is carried out (Titus et al., 2019). The recorded radiation ranging between 10,000–100cm^{-1} is sent through the sample, where some radiation is absorbed. The rest passes through to the detector and is converted, resulting in a recorded unique FTIR spectrum between 4000-400cm^{-1} for every molecule, aiding in chemical identification.

One of the standard applications of FTIR is membrane characterization. Morris et al. (2022) used FTIR to study the impact of an antiscalant on the surface of the XLE polyamide (PA) thin-film composite (TFC) membrane before and after fouling. Through this analysis, they could distinguish between the various chemical groups found on the surface of an XLE virgin membrane, as shown in

Figure 2-8. At 3000cm^{-1}, they observed aliphatic-C-H bond stretching and aromatic C-H stretching bond at 2900cm-1, while some peaks helped identify the membrane's polysulfone support. Further peak assignments for polyamide membranes can be found in Table 2-8.

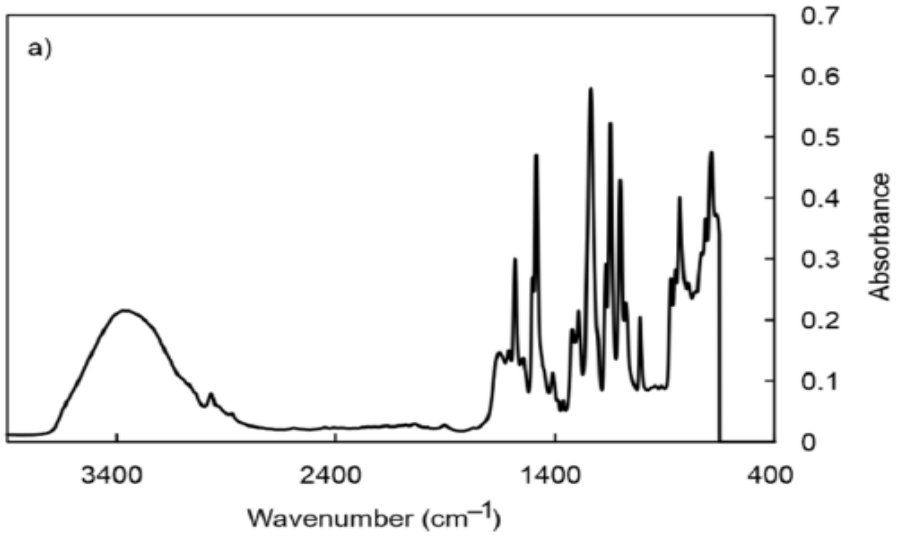

Figure 2-8: ATF-FTIR spectrum of an XLE virgin membrane (Morris et al., 2022)

Table 2-8: FTIR peaks and assignments for polyamide membranes

Peak (cm^{-1})	Peak assignment and features	References
3100-3000	Aromatic hydrocarbon	(Sachit & Veenstra, 2017)
840-800		
1300-1200	Aromatic ethers	
2990-2850	Aliphatic hydrocarbon	
1460-1350		
1550-1300	Inorganic carbonate	
880-700		
1664	Amide I band (C=O)	(Al-abri et al., 2022)
1609	(C=C) ring vibration of the polyamide layer	
1484 & 1410	Aliphatic C-H deformation and C-O stretching and O-H deformation of phenol	
1243	C-O-O asymmetric stretching	

	vibration of the polysulfone support layer	
2920	Aliphatic C-H stretching	(Adel et al., 2022)
1631	Amide C=O stretching	
1448	C=C ring vibration of polyamide	
1154	C-O antisymmetric stretching	(Oatley-radcliffe, n.d.)
1105	C-O and C-C stretching	
1015		

2.8.2. Scanning Electron Microscopy

Scanning Electron Microscopy (SEM) is a technique used to characterize nanoparticles' morphology and chemical composition using its high resolution and high imaging speed for direct imaging and dimensional measurements of micro and nanostructures (Torres-Rivero et al., 2021). An electron beam with low energy is radiated to the material. It scans the surface of the sample, where several different interactions occur, resulting in the emission of photons and electrons from or near the sample surface (Omidi et al., 2017). The receiving signals are detected with the detectors used for the SEM mode to characterise the material forming an image.

One of the applications of SEM is membrane characterization. It can be used to determine pore size in the case of a porous membrane and measure its thickness. (2016) described an unmodified porous membrane as free from defects and with a uniform structure with small holes. Diop et al. (2011) performed various membrane characterization analyses on XLE and NF270 membranes, including SEM. The cross-sectional images shown in figure 7 showed similar thickness between the membranes and identical structural layers consisting of a microporous active layer where separation takes place and a macroporous layer responsible for the mechanical resistance. The comparable difference in total thickness was reported to result in a difference in permeability and accounting for the difference in pore size. Permeability is directly proportional to applied pressure and inversely proportional to the thickness of the filter layer (Diop et al., 2011).

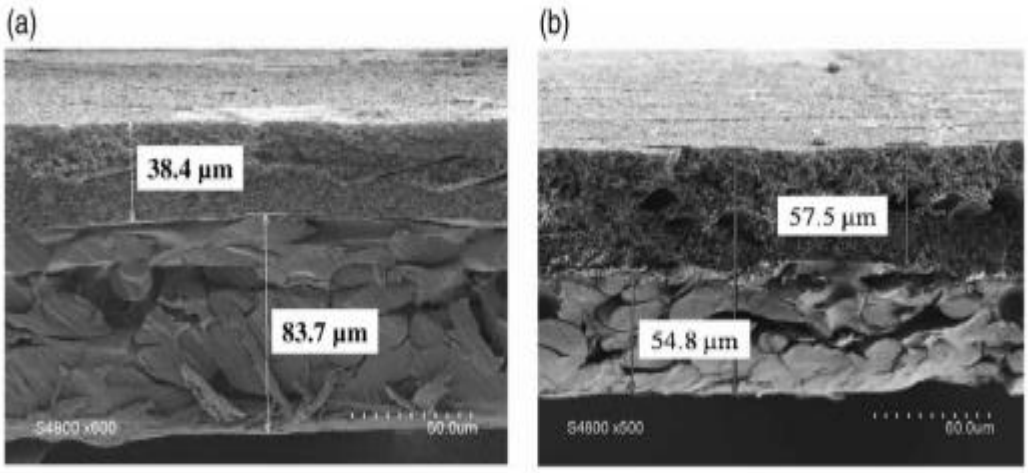

Figure 2-9: SEM cross-sectional images of NF270 (a) and XLE (b) virgin membranes (Diop et al., 2011)

Coupling SEM with energy-dispersive X-ray spectroscopy (EDX, EDS) allows future characterization through element analysis. EDX is used for semi-qualitative and semi-quantitative analysis to determine the element and chemical composition accompanying electron microscopy (Torres-Rivero et al., 2021). The scaling in membranes depending on the type and density of the charge and the structure of the surface can be monitored through an image of the topography of the surface provided by Atomic force microscopy (AFM), while the contact angle is used to measure the membrane and solute interfacial tensions and water/solute–membrane interaction energies (Diop et al., 2011; Wang et al., 2014; Kowalik-klimczak, 2016).

2.9. Effect of SARS-CoV-2 in the detection of PCPs in untreated wastewater

The outbreak of the COVID-19 disease in December 2019 resulted in a series of events that affected the way of living. The noticeable devastating impact of the epidemic, like compromised health and high death rates, where the centre of publicised information to curb the spread and limit the effect of the disease. However, it has been reported that studies show that the change brought about by the pandemic resulted in a reduction in pollution, cleaner beaches, environmental noise reduction, and the reduction in greenhouse gas emissions to the atmosphere while also leading to an increase in domestic solid residues, reduction in recycling, and the increased production of plastic material used for personal protection equipment (PPE) (Bandala et al., 2021).

Many people relied on several drugs to treat various symptoms related to COVID-19, which ended in WWTP with increased concentration (Chen et al., 2021). PPCP usage increased due to the high demand for antibiotics, disinfectants, and COVID-19-related drugs such as caffeine, diclofenac, carbamazepine, etc. (Anand et al., 2022). These drugs may be released into the environment, making their impact and treatment even more complex. As a result of the unanticipated effects on mental health and lifestyle due to COVID-19, Alygizakis et al. (2021) reported that between the years 2019 and 2020, there was a 196% increase of anionic detergents and surfactants found in PCPs in wastewater from Athens. It was reported to be a result of lockdown measures which meant staying and working from home, social distancing, frequent hand-washing and surface-disinfection

Chapter 3

Research Methodology

3. Methodology

3.1. Introduction

This chapter gives a detailed outline of the use of equipment and material, including all the experimental procedures followed when conducting experimental runs. A description of the instrumentation used is also included. This research will use the quantitative experimental approach.

This project is divided into two sections:

- Bench scale reverse osmosis study
- GC-MS analysis

All experiments were conducted at the Cape Peninsula University of Technology, Bellville, Chemical Engineering, and Chemistry Building in the Environmental Engineering Water Laboratory 1.18.

3.2. RO system process description

3.2.1. Experimental Setup

This study uses a synthetic make-up of the municipal MBR secondary effluent as feed. The feed was a composition of A 13l de-ionized water blended with organic and inorganic substances, spiked with selected commercial model PCPs (TCS, MeP, and EHMC). The research project was conducted on a bench-scale RO Cell (SEPA CF Cell), with a high-pressure, low-flow rate hydra cell pump used to pump the feed water through the membrane cell. A water bath unit was used to control the varying temperature conditions, while a potable meter was used to monitor the system's pH. The valves in the system were used to regulate the flow and pressure around the system. The permeate was discharged into a holding tank while the concentrate was recycled back to the feed tank. An automated software system controlled the plant. The feed velocity was set manually on the variable speed drive (VSD). Data was captured and recorded accordingly.

Photo 3-1: RO bench-scale system in the Environmental Engineering Research Laboratory (September 2022)

Photo 3-2: Heating and cooling unit in the Environmental Engineering Research Laboratory (September 2022)

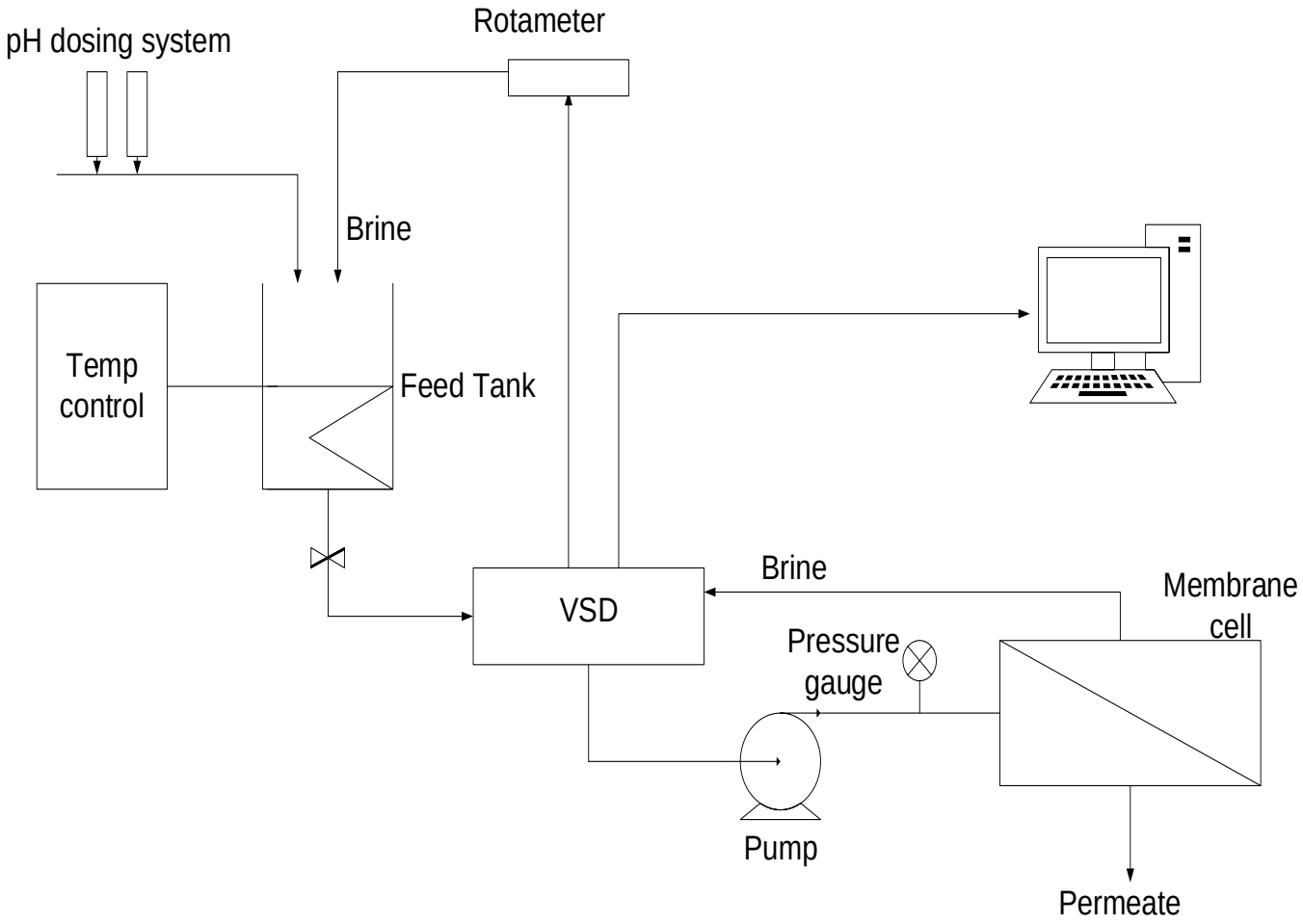

Figure 3-1: Schematic PFD diagram of the RO bench-scale system

Table 3-1: RO bench-scale equipment

1	water bath
2	Variable speed drive (VSD)
3	Hydraulic pump
4	RO SEPA CF membrane cell
5	Hydra cell Pump
6	Computer (control station) with software

3.2.2. RO System operation

The experimental runs were divided into short and long experiments. The short-run was 8 hours long, with EC, TDS, and temperature readings were taken every 45 minutes. The long run was 24 hours, with a measurement interval of 2 hours. All operating conditions were set manually on the system. The timeline of the 8-hour is shown below.

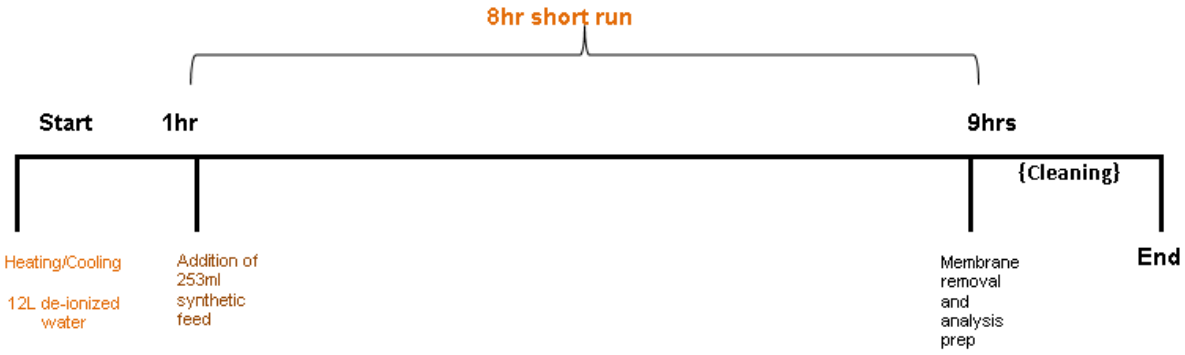

Figure 3-2: Timeline for the short-run experiment

The feed temperature was set to the desired condition on the water bath. While the feed was heating up or cooling to the experiment condition, a new membrane prior soaked in de-ionized water for 24 hours was placed in the membrane holder inside the membrane cell. The synthetic feed was added to the feed tank then sulphuric acid or sodium hydroxide was added to the feed to adjust pH to the desired condition. The pressure is set to 10 bars. When the system is stable, the conductivity and TDS of the feed, brine, and permeate were measured.

3.2.3. RO start-up procedure

1. The cell body was separated, top from bottom
2. The feed spacer and permeate carrier were cut to the size and shape of the shim. The permeate carrier was placed on the cell top while the feed spacer was at the bottom.
3. The membrane previously soaked in de-ionized water and cut from an XLE-4040 or NF270-4040 DOW FilmTech membrane was further cut and shaped to fit the rectangular dimension 14.5cm x 9.5cm, covering a surface area of 0.014m^2 where permeation occurs. The membrane is placed in the cell, with the shiny side covering the cell's bottom.
4. The cell was reassembled and placed in the cell holder. The hydraulic pump pressurises the system, setting the piston pressure between 12-14 bar.

5. The feed tank was transferred to the tank.
6. Feed temperature is set to the condition of the run to either heat or cool the feed.
7. The valves were all opened then the pressure was set to 10 bars for all runs.
8. Once the required temperature had been reached, and the system was stable, the synthetic feed was added to the feed tank's DI water, creating the required feed composition.
9. pH was set to the experiment condition by adding H_2SO_4 or NaOH as needed.
10. An alarm was set on the HI-5522 high-grade bench-top meter for the experiment pH range to alert the user when pH needs to be adjusted manually, ensuring constant pH.
11. After the system had stabilized in the required operating conditions, EC, TDS, and temperature for the feed, brine, and permeate were measured.

3.2.4. Membrane Cleaning

The membranes used for all experiments were soaked for 24hrs in de-ionized water. The cell was cleaned without having to scrub the cell mechanically. It was done using the feed pump to circulate de-ionized water in the system 45 minutes before every experimental run. Before the new set of operating conditions, the cell was mechanically scrubbed by installing a new membrane before flushing the system with de-ionized water for 45 minutes.

3.2.5. Membrane replacement

Figure 3-3: Membrane replacement (Sterlitech Corporation, 2017)

1. Release pressure from the system using the hydraulic pump
2. The membrane cell was removed from the cell holder
3. The cell body was then separated, top from bottom
4. The spacer was placed in the cell bottom
5. A new membrane was installed in the cell bottom
6. The permeate carrier was placed in the cell top
7. After installation, the cell body was reassembled
8. The cell was inserted back into the cell holder
9. The cell system was pressurized to 12 bar using the hydraulic pump, ready for the next experimental run

Operating limits

Table 3-2: XLE4040 (RO) membrane operating limits

Membrane type	**Polyamide thin film composite (Filmtech)**
Maximum operating temperature	45°C
Maximum operation pressure drop	0.9 bar
pH range, continuous operation	2-11
pH range, short-term cleaning	1-13
Maximum feed silt density	SDI 5
Free Chlorine Tolerance	<0.1 ppm

Table 3-3: NF270 (NF) membrane operating limits

Membrane type	**Polypiperazine Thin-Film Composite (Filmtech)**
Maximum operating temperature	45°C
Maximum operation pressure drop	1 bar
pH range, continuous operation	3-10
pH range, short-term cleaning	1-12
Maximum feed silt density	SDI 5
Free Chlorine Tolerance	<0.1 ppm

Table 3-4: RO system operation conditions

Feed Solution	Synthetic MBR secondary municipal wastewater
Feed Pressure (bar)	10
Piston Pressure (bar)	12
Feed velocity (Hz)	12.83±0.15
Membrane dimension	14.5cm x 9.5 cm
Area (m^2)	0.013775
PCP Concentration (average)	
MeP (µg/L)	458.15
TCS (µg/L)	453.15
EHMC (µg/L)	450
Feed pH	3-10
Feed Temperature (°C)	15-35

3.2.6. Equipment used during operation

The HI-5522 high-grade bench-top meter was connected to the feed tank to monitor the pH and temperature, with an alarm to indicate if the two parameters were outside the set conditions and needed to be adjusted. The pH of the feed was adjusted using diluted sulphuric acid and sodium hydroxide.

Figure 3-4: HI5522-02 Laboratory research grade benchtop pH/ISE/EC meter

A 10ml glass cylinder and a stopwatch were used to measure the flow rate of the permeate.

Figure 3-5: 10ml glass measuring cylinder (left) and stopwatch (right)

COD and ion analysis

COD was used to measure the quality of the samples as an indication of the effectiveness of the treatment. The COD reactor was used as a digester, while the photometer was used to detect the COD after reaction time and for the in-house ion analysis.

Figure 3-6: Thermo-reactor (left) and HI83399 multi-parameter photometer with COD (right)

The total dissolved solids, conductivity, and temperature for the feed, brine, and permeate were measured every 45 minutes using the portable EC/TDS/ temperature, which was later used to calculate the salt rejection.

Figure 3-7: HI99300 EC/TDS/ temperature meter

Turbidity

The measurement of TDS was characterized by the turbidity of the feed and the permeate. This was done in-house before and after every run using the pictured portable turbidity meter.

Figure 3-8: WTW Portable turbidity meter

3.2.7. Experimental design

The experimental layout in Table 3-5 was designed to investigate the influence of pH, temperature and the selected membranes on removing the parameters listed as responses. The pH conditions 3, 6, and 10 and temperatures 15, 25, and 35°C were chosen based on the membrane manufacturers' continued operation recommendations to avoid compromising the quality of the membranes and the experimental results. The values are all within the operating limits.

Table 3-5: Summary of experimental runs

Run	pH	Temperature	Membrane
2	3	25	XLE
3	3	25	NF270
9	3	15	XLE
11	3	35	XLE
13	3	35	NF270
16	3	15	NF270
4	6	35	NF270
5	6	15	XLE
8	6	15	NF270
15	6	35	XLE
1	10	35	XLE
6	10	25	XLE
7	10	35	NF270
10	10	15	NF270
12	10	25	NF270
14	10	15	XLE

No of Runs	32
Hours	8
long run (hrs)	24
Runs per day	2

3.2.8. Synthetic feed make-up (MBR effluent)

The feed was prepared every second day by blending organic and inorganic substances diluted with de-ionized water to make a feed composition as shown in Table 10, then stored at 4°C for two days. The compounds were measured individually by mass using an analytical balance and then diluted with de-ionized water. The stock solution for TCS, MeP, and EHMC was made by dissolving the compounds in analytical-grade methanol. The 1L feed was divided into four 250ml individually spiked with 1ml stock solution of each PCP before the start of the experiment.

Photo 3-3: Synthetic MBR effluent (left) and permeate (right)

Table 3-6: Feed composition for synthetic wastewater MBR effluent

Compound	**Concentration (mg/L)**
Sucrose ($C_{12}H_{22}O_{11}$)	12.5
Protein (meat extract)	4.27
Ammonium Chloride (NH_4Cl)	0.68
Dipotassium phosphate of (K_2HPO_4)	0.28
Manganese sulfate monohydrate ($MnSO_4 \cdot H_2O$)	1.31
Calcium Chloride hexahydrate ($CaCl_2 \cdot 6H_2O$)	1.23
Glucose ($C_6H_{12}O_6$)	12.5
Ammonium sulfate ($(NH_4)_2SO_4$)	4.17
Monopotassium phosphate (KH_2PO_4)	0.56
Magnesium sulfate heptahydrate ($MgSO_4 \cdot 7H_2O$)	1.31
Sodium bicarbonate ($NaHCO_3$)	1.88
Ferric Chloride hexahydrate ($FeCl_3 \cdot 6H_2O$)	8.75×10^{-3}

3.3. Solid Phase Extraction (SPE) and Gas Chromatography-Mass Spectrometry (GC-MS)

The target compounds selected for this study included Triclosan (TCS), Methylparaben (MeP), and Ethylhexyl methoxycinnamate (EHMC). Their physio-chemical properties are presented in Table 2-2, chapter 2, section 2.4.1

PCPs addition

The PCPs were measured in its chemicals mass and weighed on an analytical balance. The weighed quantities were dissolved in 4000µl of methanol stock solution, of which 1ml was used to spike the 13l feed. The process was done for each PCPS.

Sample preparation for PCPs GCMS analysis

Samples are collected every 45min for the reverse osmosis experimental run. The samples are in 1L Schott glass bottles autoclaved at 120°C. After RO, the samples undergo preparation for quantitative analysis for the removal of PCPs. Mass spectrometry was performed using an Agilent 7000 triple quadrupole mass spectrometer with positive electro-spray modes (ESI+).

3.3.1. Solid Phase Extraction (SPE)

The analytes were extracted using solid phase extraction.

- Permeate samples (200ml) from each run were filtered with Glass Fibre Filters (0,7 microns, 47mm).
- The samples were acidified to pH 2 with sulphuric acid and then spiked with 30 µL of Bisphenol A as an internal standard with a 0.2mg/ml concentration.
- To improve the SPE extraction, the cartridges 60mg HLB SPE tubes were conditioned with 3mL ethyl acetate: acetone (50% volume) followed by 3ml of methanol.
- 50mL of the 200ml sample was then loaded into the tubes.
- After loading, 3 mL of water with 5% methanol was used to wash the tubes.
- They were then left to dry under vacuum for 1 hour.
- The tubes were eluted with 6 mL ethyl acetate: acetone (1:1), then placed in a centrifuge and mixed at 5000rpm for 10 minutes.

- After centrifugation, the samples are placed in a heating block set to 42°C and dried under a gentle stream of nitrogen to dryness.

The dried extracts were reconstituted and derivatized with 40 µL of N-methyl- N-(trimethylsilyl) trifluoroacetamide (MSTFA) in 80µL of ethyl acetate.

Apparatus for SPE extraction

The permeate was filtered using Glass Fibre Filters (0,7 microns, 47mm) to remove solids before SPE. The setup was made of a Buchner flask and funnelled connected to a vacuum source to assist and speed up the filtration

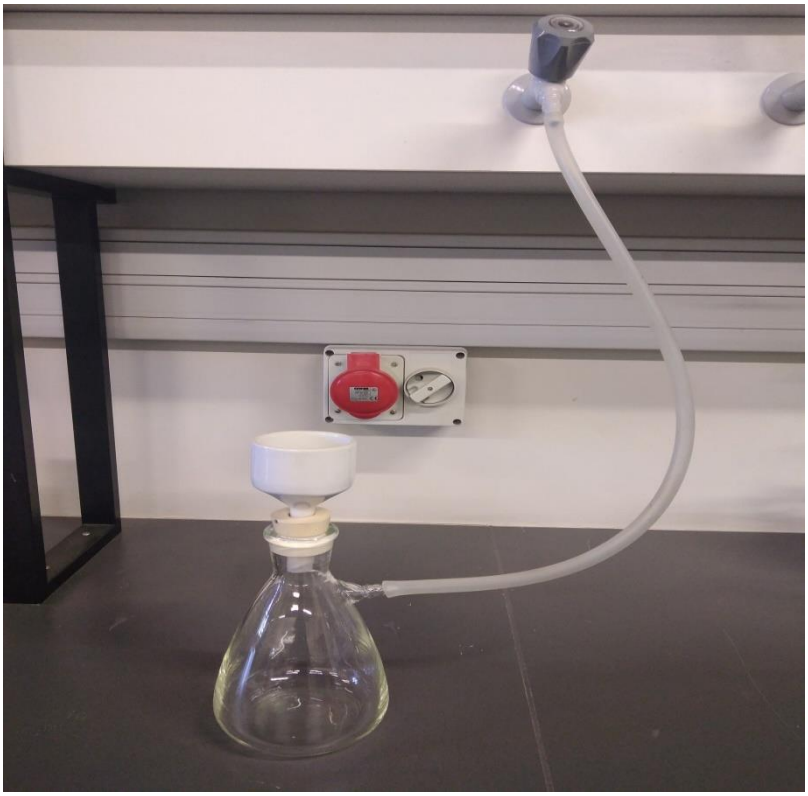

Photo 3-4: Filtration setup using vacuum

The pH of the samples was adjusted to 2 and then spiked with internal standard (BPA) before SPE by using the pH edge meter

Figure 3-9: HI2002-02 pH/ ORP pH meter

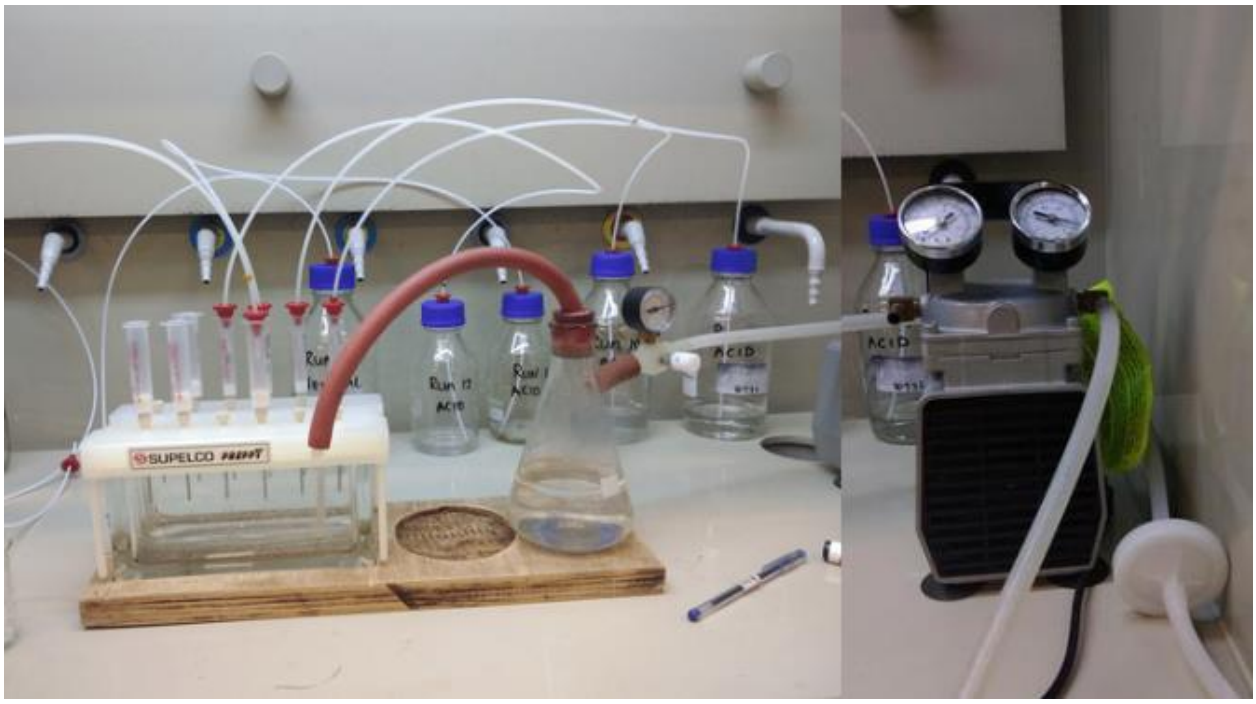

Photo 3-5: SPE station (September 2021)

3.3.2. Gas Chromatography Spectrometry (GC-MS)

The samples were analyzed using an Agilent 7890B/7000C GC/MS triple quad using a J&W 122-5532G DB-5MD and DG column. The operating conditions were as follows:

Table 3-7: GC conditions

Inlet temperature	240°C
Transfer line temperature	280°C
Ion source	230°C
Injection volume	1µL using autosampler
Injection mode	Split ratio: 14:1 (15 times dilution)
Injector pressure	14.6 psi
Gas carrier	Constant ultrapure helium flow rate (column): 1 mL/min
Oven program	100°C: hold 0.5 min, 100-200°C: 15°C/min, hold 2 min, 200-300°C: 13°C/min with a total run time of 16.86 min

The mass spectrometry was operated in Electron-Impact (EI) mode of 70 eV, with a gain factor of 3, solvent delay of 7 minutes, and at 2.2 cycle/ sec with dwell time for each compound as shown by table 12, 450ms/ cycle. The post-run time was 9.06 minutes.

Table 3-8: Selected Ion Monitoring (SIM) method

	MS1 mass	MS1 resolution	Dwell (ms)
BPA	357	Unit	5
MeP	209	Unit	90
TCS	200	Unit	250
EHMC	178	Unit	10

3.4. Membrane characterization

The membranes before and after treatment were characterized by Attenuated total reflectance-Fourier Transform Infrared (FTIR), Scanning Electron Microscopy- Energy Dispersive X-Ray Analysis (SEM-EDX), and zeta potential to study the surface morphology changes. The analysis was done internally (ATR-FTIR) and externally (SEM-EDX and zeta potential).

3.4.1. FTIR analysis

The membrane samples (XLE and NF270) and PCP were characterized employing an FTIR spectroscopy with an ATR single reflection diamond crystal-based module. Spectra were recorded at 1 cm^{-1} resolution, and 48 scans were made for samples before and after treatment with the PCPs at a nominal incident angle of 45° and wavelength between 400-4000 cm^{-1}. The recorded results were normalized to compare the spectra and for accurate representation.

3.4.2. SEM

Before and after treatment, the top surface morphology for the membrane samples was investigated using Nova NanoSEM. The images were scanned at 1000x and 5000x magnification, horizontal field width (HFW) of 298µm and 59.7µm, respectively, with a working distance of 6-6.2mm, and at landing electron of 20 kV for all samples.

Chapter 4

Results and discussion

4. Results and Discussion

The results presented are divided into the following**:**

- Membrane surface characterisation by SEM and ATR-FTIR
- RO process
- GCMS results

Statistical analysis

All statistical analysis was performed using Excel 2020. Variation between individual samples was assessed using ANOVA: two factors with replication. Significant variance was shown for P-values (below 0.05 to below 0.0001).

4.1. Membrane surface characterization

The surface interface characterizes membranes to the environment they are in contact with ATR-FTIR, and SEM EDX was used to analyse the membrane surface characteristics.

4.1.1. FTIR

ATR-FTIR was used to examine the presence of the PCPs on the RO and NF polyamide (PA) Thin film composite (TFC) membranes. The analysis provided a suitable method of identifying selected functional groups on the membrane surface, allowing for differentiation between the virgin and the membranes undergoing remedial treatment.

Spectra were recorded at 1 cm^{-1} resolution, and 48 scans were made for samples before and after treatment with the PCPs at a 45° nominal incident angle. The FTIR spectra were recorded with wave numbers ranging from 400-4000 cm^{-1} but zoomed in for interpretational purposes to show peaks ranging from 800-1600cm^{-1}. The data were normalised to allow for a more accurate representation and straightforward spectra comparison. The Figures below show the spectra of XLE and NF270 virgin membranes and a long-run treatment at pH 6, 35°C.

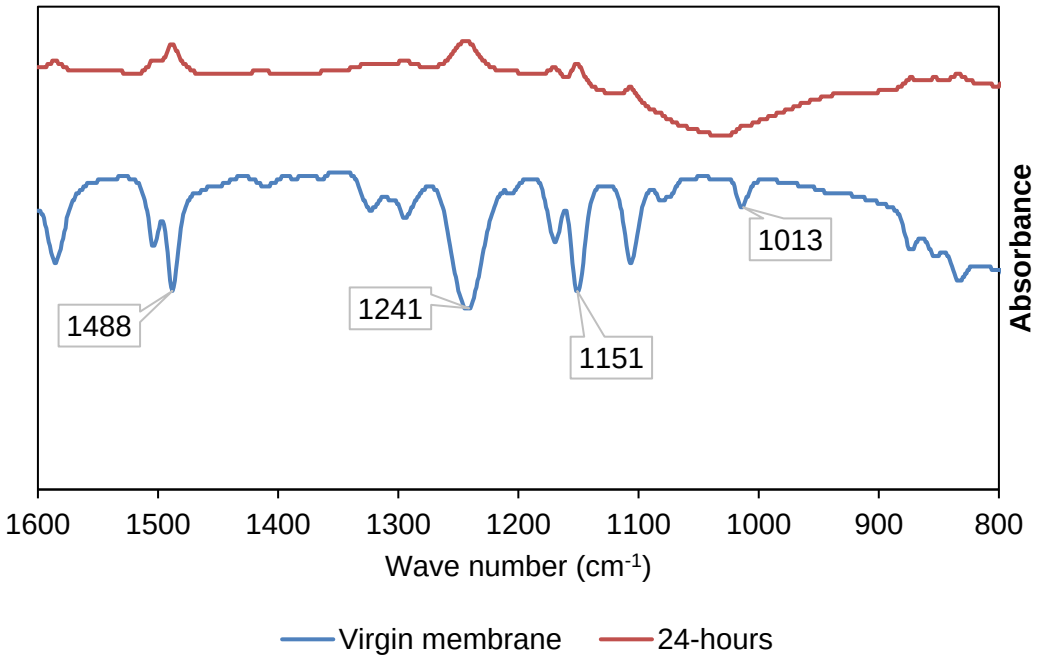

Figure 4-1: FTIR spectra of NF membrane before and after a 24-hour run at pH 6 and feed temperature 35°C

Figure 4-1 shows a significant difference between NF270 before and after treatment. The peaks for the virgin membrane are steep and visible, showing the various functional groups. The multiple peaks for both membrane samples are indicated. The indicated peaks in the spectra are consistent with the results of a fouling study on NF270 and NF90 (Bastrzyk et al., 2014). The FTIR results showed a weak peak of 1488cm$^{-1,}$ indicating aliphatic deformation(Al-abri et al., 2022). The membranes exhibit peaks at wave numbers 1488, 1241, 1151, and 1013 cm^{-1}, with 1488cm^{-1} a possible indication of the polysulfone support layer (Morris et al., 2022). Peaks between 1600-1400cm -1 are characteristics of a carbonyl functional group (C=O) (Tang et al., 2007).

While both membranes show the same peaks, the virgin membrane show pronounced peaks. The virgin membrane shows a peak at 1013cm$^{-1,}$ which, as shown by Table 2-8 (chapter 2), shows C-O and C-C stretching; however, the 24-run samples show deformation at the same peak. This may result from the high temperature; as previously mentioned, that high temperature alters the membrane (Kucera, 2015). The amplitude differs, suggesting a

change in the functional group and disappearing polysulfone support later for the fouled membrane.

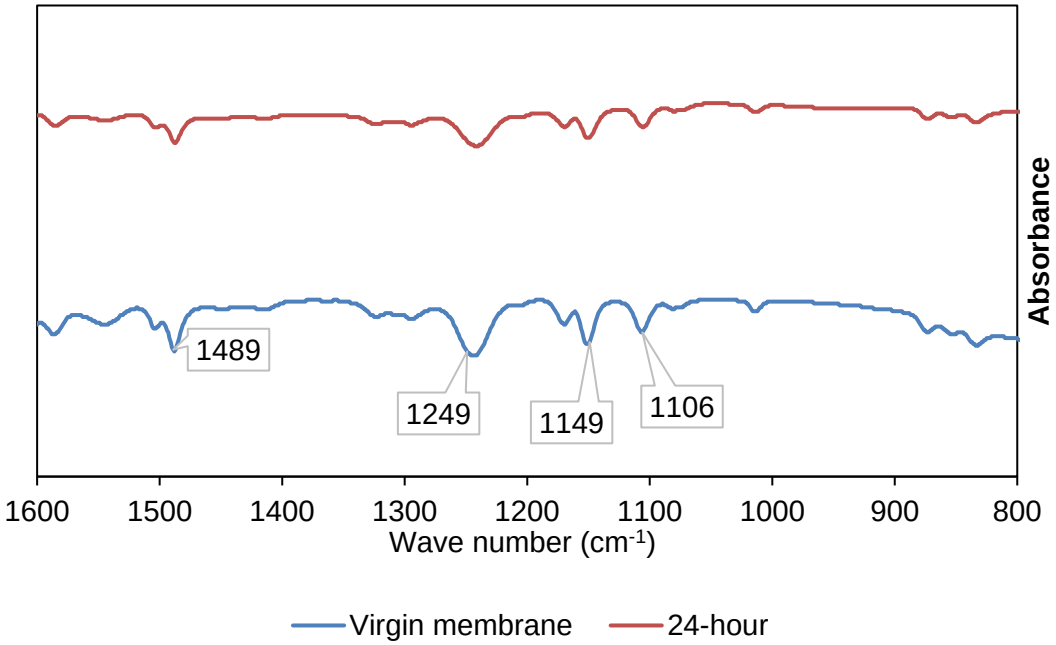

Figure 4-2: FTIR spectra for RO membranes before treatment and after a 24-hour run at pH 6 and feed temperature of 35°C

The trend of the spectra shown in Figure 4-2 for the XLE virgin membrane and XLE after a long treatment (pH 6 at 35°C) was similar. The virgin membrane had broad peaks, while the sample after treatment exhibited peaks with smaller amplitudes. The observation on the spectra included a C-C and C-O stretch, possible C-O antisymmetric stretch, C-O-C asymmetric stretch vibration of the polysulfone layer, and aliphatic C-H deformation at peaks 1106, 1149, 1249, and 1489 cm^{-1}, respectively (Oatley-Radcliffe, n.d.; Adel et al., 2022; Al-abri et al., 2022) Peak 1149 cm^{-1} could be the O=S=O stretching vibrating layer indicative of the polysulfone support (Siew et al., 2022). When comparing NF270 to XLE, the spectrum of NF270 suggested a most significant effect of pH on the membrane than it did for XLE(Lin et al., 2014).

4.1.2. SEM analysis

SEM was used to qualitatively observe the membrane's surface before and after short and long-run treatment. The surfaces depicted in Figures 4-3 to 4-5- were scanned at 5000x magnification, with a Horizontal Field Width (HFW) of 59,7µm, a working distance of 6mm, and a landing electron of 20kV using a Nova NanoSEM. The analysis is coupled with EDX to analyze element composition before and after treatment. Figure 4-3 shows SEM images of NF270 virgin membrane (A) and images of NF270 after an 8-hour at 35°C for varying feed pH. Kowalik-klimczak (2016) described a porous membrane as having uniform and defect free morphology, as observed in the virgin membrane A. The membrane consists of macroporous polyester mechanical support, microporous polysulfone support and a thin polyamide top layer where separation occurs (Kowalik-klimczak, 2016; Ramdani et al., 2021). After treatment, there are significant changes in the surface morphology of the membranes compared to the virgin membrane, as expected due to the deposited PCPs and inorganic material from the feed during treatment. There is a noteworthy difference in the membrane structures with the varying feed pH, suggesting that feed pH plays a significant role in the removal of PCP and deposition of pollutants on the surface of the membrane. While there are no cross-sectional images to collaborate the change in thickness due to deposition, image B-D shows the change in the uniformity often found in porous membranes(Sachit & Veenstra, 2017).

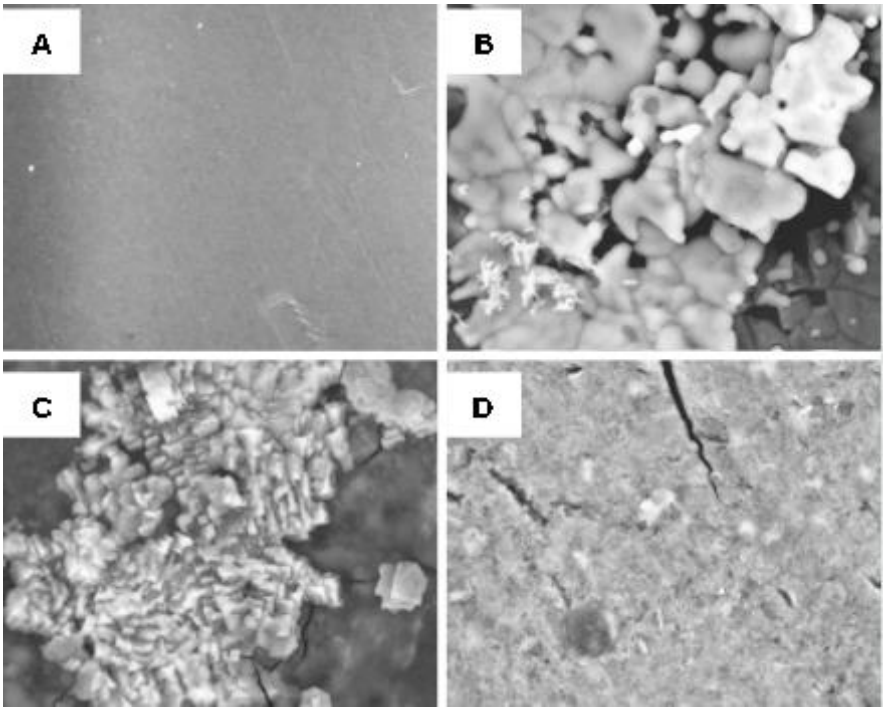

Figure 4-3: SEM images of NF270 virgin membrane (A) and NF270 after an 8-hour RO treatment at 35°C, with feed pH set to 3, 6, and 10 (B-D)

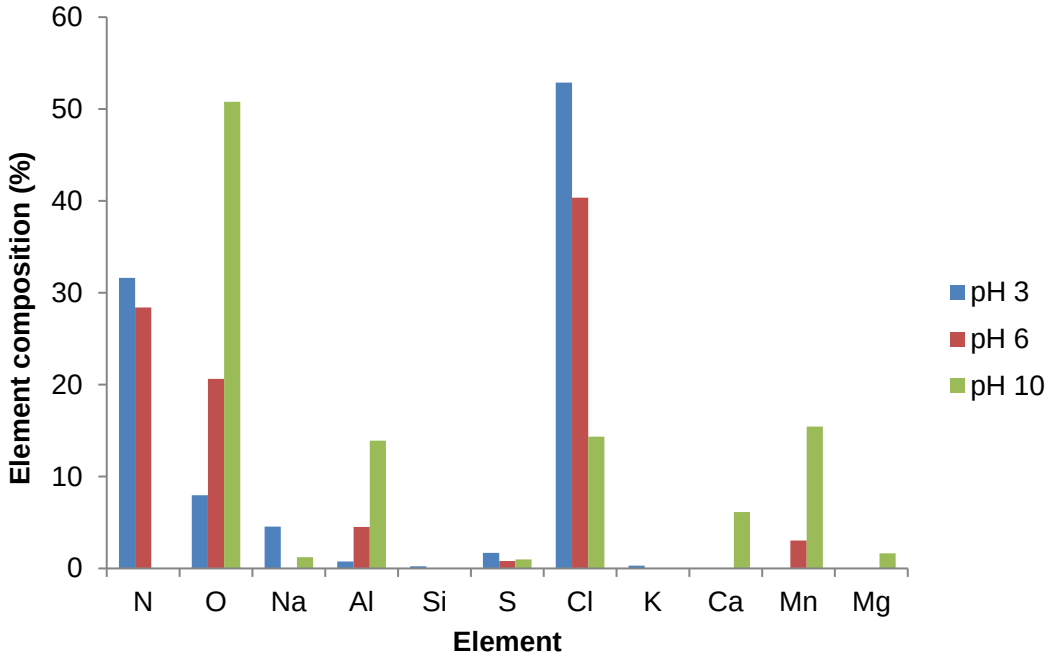

Figure 4-4: Element analysis of NF270 after an 8-hour set at temperature 35°C at varying feed pH 3, 6, and 10

Table 4-1: Element composition of RO and NF before treatment

element	Weight percentage	
	RO	NF
C	76,08(0,44)	76,14(0,32)
O	18,41(0,38)	17,56(0,53)
S	5,51(0,11)	6,3(6,28)
Total	100	100

EDX was used to analyze the elemental composition of each membrane at varying conditions. Looking at the influence of the changing experimental needs, Figure 4-4 shows the difference in element composition of the NF270 membrane at pH 3, 6, and 10 at 35°C. The composition of the virgin membranes is shown in Table 4-1. The results show that the membrane RO and NF contain 78,08% and 76,14% of C and 5,51% and 6,3% of S, respectively. In polyamide membranes, C represents the aromatic functional group, while S represents the microporous substrate, polysulfone (Sachit & Veenstra, 2017). The changing conditions all showed the lack of the aromatic functional group, as indicated by the absence of C. The polysulfone layer is also considerably affected by the change in pH. In turn, mechanical support affects the polyamide layer responsible for the separation and, subsequently, the permeate flux(Lau et al., 2019). The element analysis showed a significant difference in element composition and the constituents before and after treatment, as expected due to their presence in the feed (Table 3-6) and as the results of the filtration through different operating conditions. While some elements are abundant, like N (31,62%) and Cl (52,87%) in pH 3, and O (50,79%) in pH 10, some are not present, like Mg and Ca in both pH 3 and pH 6, indicating less foulant deposition. It should also be noted that while elements are abundant after treatment for all conditions, the virgin membranes show only the presence of O, C, and S (Figure 4-8), indicating the lack of foulants as opposed to the membrane samples after treatment.

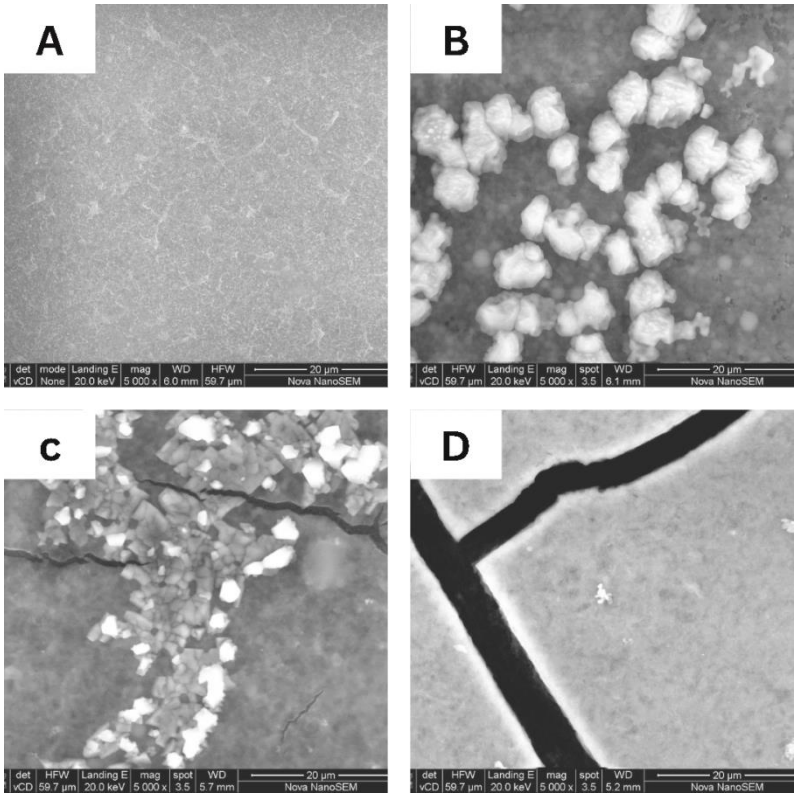

Figure 4-5: SEM images of XLE virgin membrane (A) and XLE after an 8-hour RO treatment at 35°C, with feed pH set to 3, 6, and 10 (B-D)

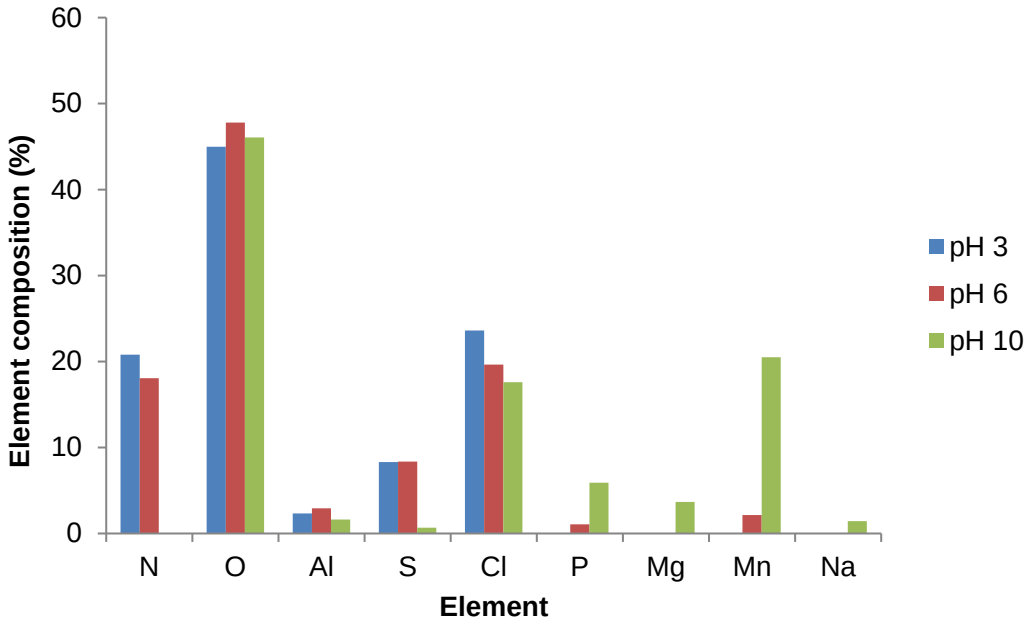

Figure 4-6: Element analysis of XLE after an 8-hour RO treatment set at temperature 35°C at varying feed pH 3, 6, and 10

Figures 4-5 and 4-6 show the SEM images and element analysis of the XLE membrane at different operation conditions. As expected, the virgin membrane (A) is uniform and undamaged compared to the samples C-D used for treatment, showing significant deposition of foulants. Image B, representing pH 3 at 35°C shows localized foulant deposition, which is supported by the few element compositions in Figure 4-6, S(8,3%), which indicates the polysulfone layer present in polyamide membranes(Sachit & Veenstra, 2017) and O (44,98%), Cl (23,61%), Al (2,3%), and N (20,79%) present in the feed solution. The results show that at pH 10, the membrane contains a high deposition of O (46,06%), Cl(17,6%)**,** and Mn (20,5%). The difference in structure suggests a significant difference in layer thickness which subsequently describes the changing permeability as the feed conditions change for each experiment. As Diop et al. (2011) noted that the difference in thickness will account for the difference in pore size and will result in a difference in permeability as permeability is directly proportional to applied pressure and inversely proportional to the thickness of the filter layer. Compared to NF270, there was no significant difference in the elemental analysis for XLE due to the change in pH. It is supported by studies which indicate that pH has less effect on XLE (Lin et al., 2014; Lim et al., 2021). While the constituents vary, the analysis reported the same abundant element (O) 44,98%, 47,8%, and 46,06% for pH 3, 6, and 10, respectively. The element ratio was different, and pH 10 had more element deposition than pH 3, pH 6, and its untreated version. It results from the porous fouling layer at high pH(Lin et al., 2014).

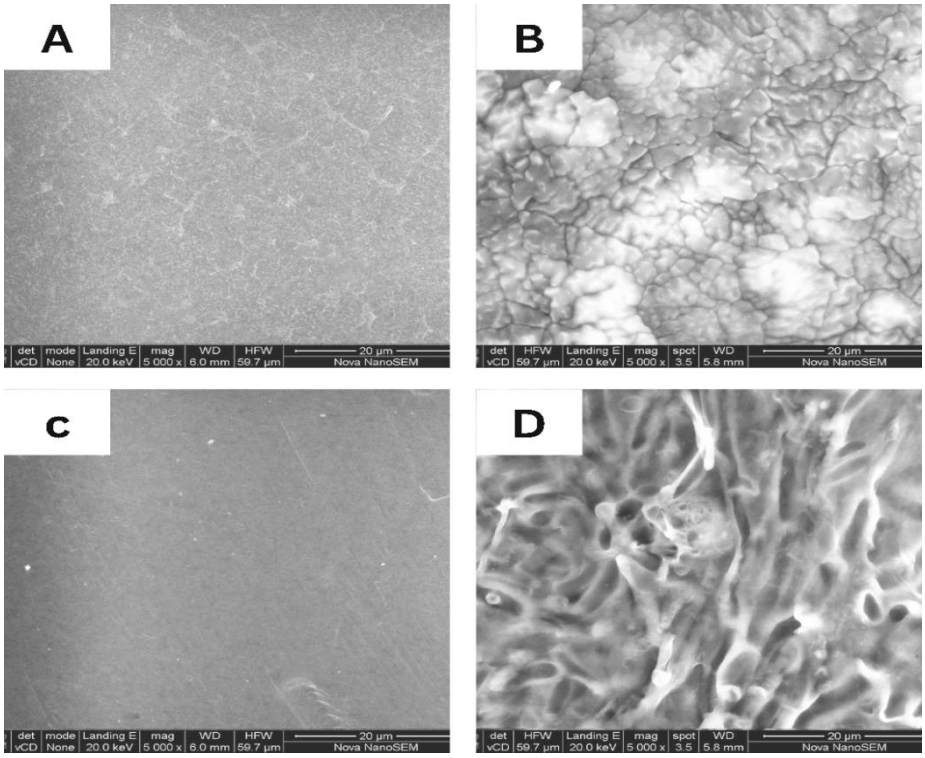

Figure 4-7: SEM images of XLE (A) and NF270 (C) virgin membrane and XLE (B) and NF270 (D) after a long run (24 hours) at pH 6 and temperature 35°C

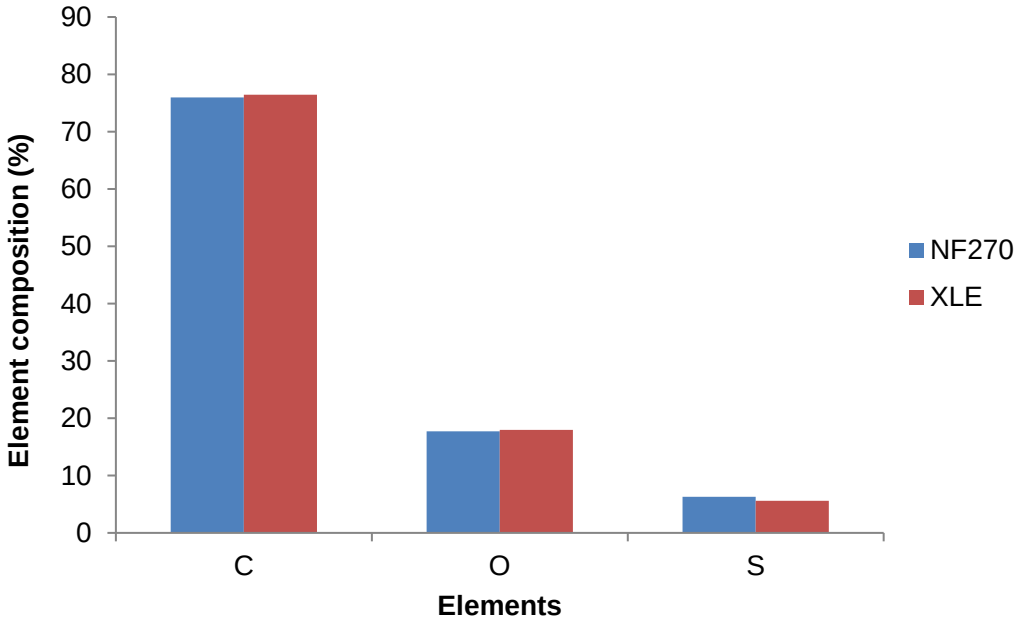

Figure 4-8: Element analysis for XLE and NF270 virgin membrane

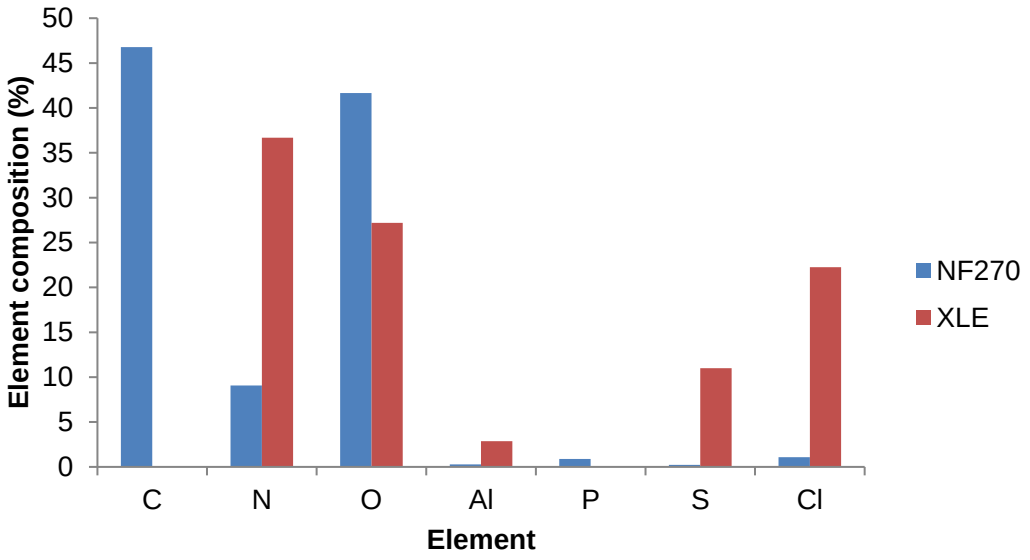

Figure 4-9: Element analysis for XLE and NF270 long run (24 hours) at pH 6 and temperature 35°C

The research included a study of the effects on the operating conditions after 24 hours to assess the applicability of the membranes at the chosen optimum condition for a more extended period. As previously mentioned, using RO/NF results in a possible high-quality wastewater treatment plant (WWTP) effluent that can be reused. However, they face the problem of fouling(Lin et al., 2014; Kim et al., 2018; Lopera et al., 2019; Adel et al., 2022). As a result, finding solutions to reduce fouling in long time use is imperative. The Figures above show the difference before and after the 24-hour treatment, with Figures 4-8 and 4-9 comparing the SEM images and element analysis, respectively, of XLE (A-B) and NF270 (C-D) membranes before and after 24-hour treatment with conditions set at feed temperature of 35°C and pH 6. It was to study the effect of pH and temperature over a relatively extended period. The images for virgin membranes (A and C) appear clean and smooth. While changes may be observed after treatment, there is more uniformity in the SEM images of the long runs compared to short runs, which showed localized foulant deposition, showing that the membranes underwent further changes over a more extended period. The images also support that pH and temperature alter the membranes' structure (Wei et al., 2020; Lim et al., 2021).

4.2. RO system performance

All experiments were conducted in a crossflow membrane unit with a flat sheet membrane cell (GE Osmonics). The effective membrane area was (0.013775 m^2) with dimensions of (14.5cm X 9.5 cm). After reverse osmosis treatment, synthetic secondary wastewater was analysed to study the treatment efficiency of RO and NF polyamide (PA) thin-film composite (TFC) membrane under different working conditions. Experimental runs were carried out at controlled temperatures of 15, 25, and 35°C and varying pH 3, 6, and 10.

Table 3-5 summarises all the experimental runs carried out at different feed conditions. Experimental runs were performed using the RO membrane, and the NF membrane was carried under the same conditions. The effluent concentrations of the inorganics are shown in Tables 4-1.

4.2.1. Flux and salt rejection

To evaluate the system performance, the two membranes (XLE and NF270) were monitored at certain intervals, 45 minutes for the 8 hours and 2 hours for the long run. Their performance was assessed by measurement of the salt rejection and flux as they are reported to be the key factors in analysing the performance of the RO system (Idrees, 2020). The following figures show the same axes' average flux and rejection over time.

The 8-hour experiments were conducted under changing feed pH (3, 6, and 10) and feed temperature (15, 25, and 35°C). While the different paired feed conditions were controlled, the RO system needed to be monitored to evaluate its performance and compare the performance of each membrane at the other experimental conditions and the overall performance of XLE and NF270.

The RO system performance was observed through changes in salt rejection and flux. Figure 4-10 shows the average flux and salt rejection of XLE and NF270 over 495 minutes at pH 6 and temperature 35°C. At these conditions, both membranes proved to be effective. XLE had an average salt rejection of 91,68%, while NF270 recorded an average of 82,41%. It can be seen in Appendix H, for the same set feed pH, XLE recorded the highest rejections

when the feed temperature was set a 35°C and low retention at 15°C while NF270 performed well at a feed temperature of 15°C compared to 35°C.

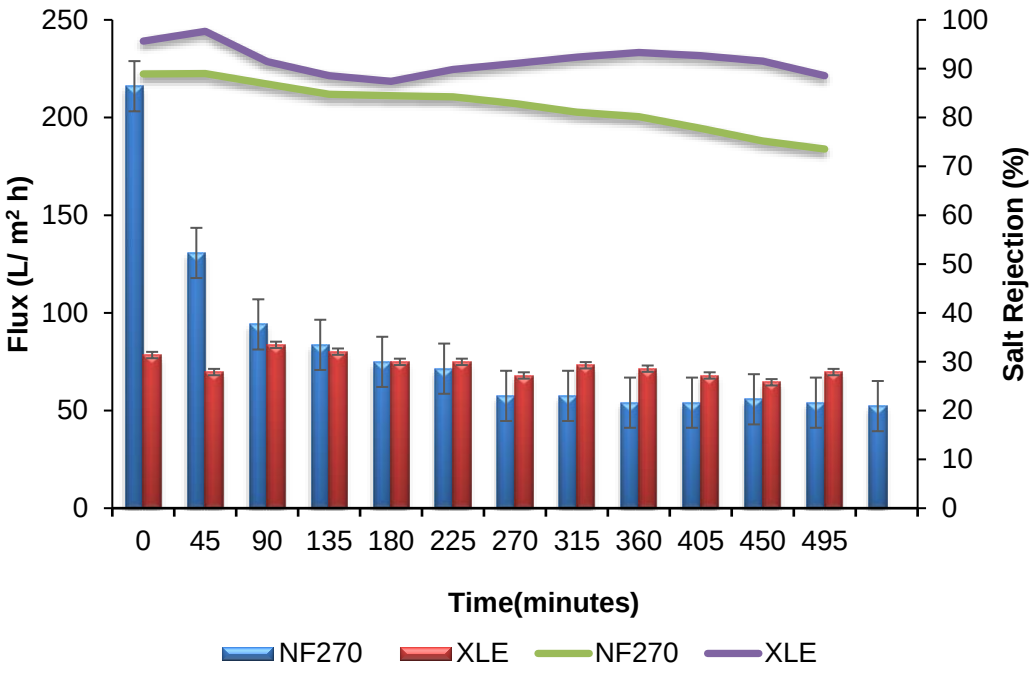

Figure 4-10: Flux and rejection of XLE and NF270 after an 8-hour at feed pH 6 and 35°C

This suggests that while both membranes had high rejection, the temperature played a considerable role in salt retention. As the temperature increased from 15°C to 35°C, the feed viscosity decreased, leading to decreased fouling on the membrane surface(Mohammed et al., 2014). The salt rejection for NF270 also declined over time due to slight temperature changes during experiments. According to Kucera (2015), For every 1 ° C change in temperature, there is a 3% change in water flux and a temperature change results in a slight shift in salt rejection.

Wang et al. (2014) observed that XLE and NF270 membranes are less pHs sensitive with increased feed pH. However, the salt rejection significantly decreased with the decrease in pH; pH 3 reported significantly lower salt rejection than pH 6 and 10 for both membranes. It has been reported that the rejection of inorganic and organic material may be controlled by electrostatic repulsion (size exclusion), steric hindrance (pore size), water chemistry, and membrane surface properties (Braghetta et al., 1997).

There is a considerable difference in the flux for the two membranes. NF270 recorded the highest average flux (216,34-85,37 L/m h) over time compared to XLE (83,63- 64,46 L/m h). The relatively higher permeate flux for NF270 may be attributed to the large hydrophilicity and MWCO for NF270(Lim et al., 2021).t was also observed that the flux increased with feed temperature while salt rejection decreased for both membranes. Kucera (2015) reported that higher temperature alters the structure of the membrane, making it difficult for water to pass through the membrane. As a result, manufacturers recommend the operating temperature to be less than 45°C as a temperature above that value will make the membrane dense. These results agree with the results observed by Mohammed (2014). As previously mentioned, the increase in temperature results in a decrease in feed viscosity; it also results in a reduction of feed solution viscosity. It is attributed to the rise in the permeability coefficient of water increase, the solubility of solute increases and, consequently, a higher diffusion rate of solute through the membrane (Jin et al., 2009; Mohammed et al., 2014; Gedam et al., 2012).

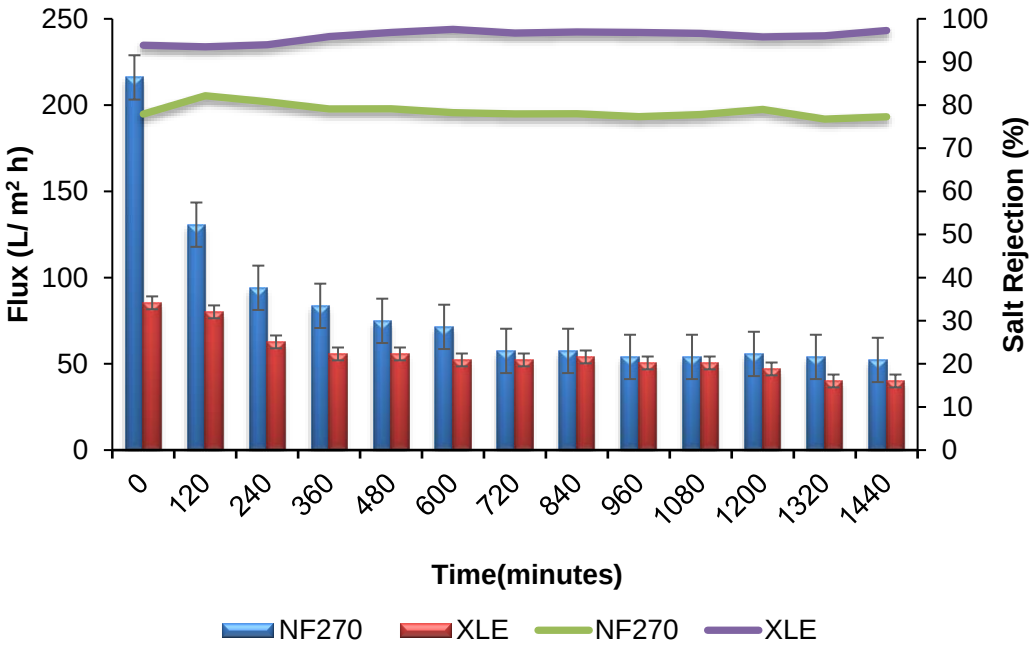

Figure 4-11: Flux and rejection of XLE and NF270 after a long run at feed pH 6 and 35°C

The investigated RO membranes (XLE and NF270) were subjected to a 24-hour longer experimental run to evaluate their performance over a more extended period at conditions where the highest rejection was recorded for possible industrial use. Figure 4-11 shows the average flux and salt rejection of XLE and NF270 at pH 6 and temperature 35°C. The performance of the membranes for the short and long run exhibited the same trend, showcasing their viability for extended operation. However, NF270 showed a significant decrease in flux starting at the 6th hour compared to the initial high flux reading, after which

the flux stabilized for both membranes. The flux decrease may also indicate fouling as fouling decreases the membrane performance, shortening its life (Vrijenhoek et al., 2001; Aziz & Kasongo, 2019). Filtration results in the deposition of the feed constituents being filtered on the surface of the membrane resulting in a progressive decline in flux(Nanda et al., 2010). Noticeable changes can be observed in the NF270 as it is the most influenced by pH and temperature; pH change is insignificant with XLE (Lim et al., 2021). The feed pH results in the difference in the membrane hydrophilicity and charge, influencing the retention of solutes, while as a result of the higher temperature, the MWCO of the NF membrane is increased, which favours the permeation of the feed constituents, which further blocks the surface of the membranes resulting in the formation of a fouling layer (Nanda et al., 2010; Kucera, 2015; Wei et al., 2020). While this may be the case, the controlled feed pH and temperature aid in the decrease in membrane fouling, suggesting possible long-term use(Abdel-Fatah, 2018).

It is important to note that the operating conditions and membrane properties play a vital role in the performance of a RO system. With the considerable difference in membrane properties, it was observed that changing pH and temperature resulted in overall high performance for the NF270, making it an XLE alternative (Wei et al., 2020). The feed pH alters the membrane properties, affecting the water flux, and while this may be the case for membranes such as NF270, for some membranes like XLE, the pH effect is insignificant (Lim et al., 2021). The operating conditions provided an advantage by increasing permeation through membrane surface interaction and provided performance stability where needed(Lin et al., 2014; Kucera, 2015; Wei et al., 2020; Lim et al., 2021)

4.2.2. COD and turbidity removal

Turbidity and COD were among the parameters tested to evaluate and compare the performance and effectiveness of using XLE and NF270 to treat MBR effluent. A multi-parameter photometer and turbidity meter were used to quantify the sample contents before and after treatment. The results were subsequently used to calculate the percentage removal for both parameters. Samples were prepared and measured for all experimental conditions to investigate the effect of pH (3, 6, and 10) and temperature (15, 25, and 35°C) on COD and turbidity removal.

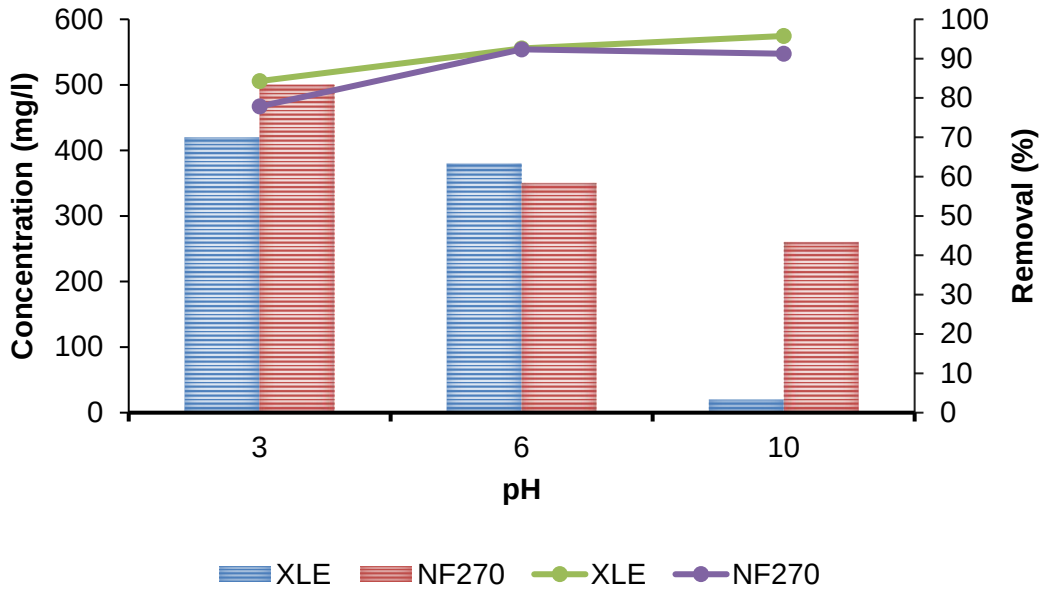

Figure 4-12: COD final concentrations and percentage removal after an 8-hour using XLE and NF270 at varying feed pH and 35°C

The initial concentration of the COD ranged from 5258-1852 mg/L while the permeate recorded concentration was between 2782-20mg/L. The high values resulted from the presence of methanol that was used to dissolve the investigated PCPs. An increase in methanol content has been reported to increase COD concentration (Fan et al., 2020). Figure 4-12 displays the resulting average COD concentration and percentage removal after 8-hour treatment at pH 3, 6, and 10 at a feed temperature of 35°C using XLE and NF270. The results showed that COD percentage removal increased with increasing pH and temperature. It was supported in a study by Aziz & Kasongo (2021), where it was reported that with increasing pH, hydroxide ions concentration increases, increasing hydroxyl free radicals and that a higher pH results in higher osmotic flow, which contributes to high COD removal.

XLE recorded its highest removal (95,76%) at 35°C at pH 10 and lowest reduction (84,29%) at 15°C and feed pH of 3. NF270 removed 92,36% at pH 6 at a feed temperature of 15° C, the lowest removal of 77,86% at pH 3 and a feed temperature of 15°C. The results showed that XLE was better at removing COD compared to NF270. It was comparable to a study by Kosutic & Dolar (2014), which reported that XLE and NF90 had better removal efficiency than NF270. The difference between the COD removal efficiency is explained by the difference in their membrane properties which influences the formation of a second layer

formed by the feed constituents through absorption on the membrane surface filtration (Liu et al., 2011a). It further explained that under the same operating conditions, the fouling rate also determines the strength of the Donnan effect on the membrane surface and, therefore, COD removal.

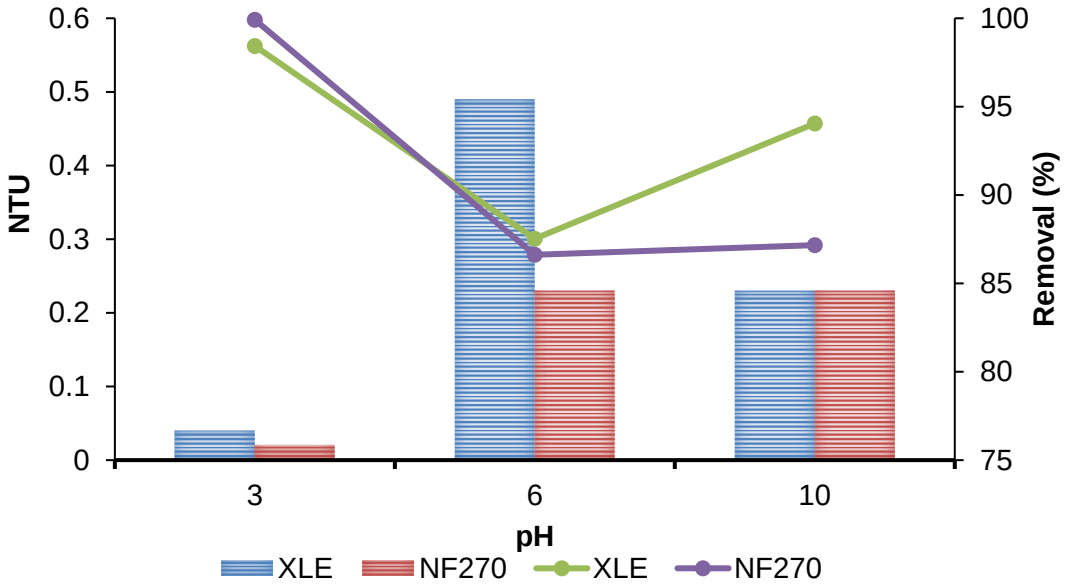

Figure 4-13: Final Turbidity and percentage removal after an 8-hour using XLE and NF270 at varying feed pH and 35°C

Turbidity is often used to measure solid foulants, which may help determine the effluent's potential environmental health concern. The results in Figure 4-13 indicated that investigated membranes efficiently removed turbidity. Both membranes showed a similar removal trend suggesting a comparable influence of pH in turbidity removal. However, NF270 recorded the highest overall turbidity removal of 99,91% at pH 3. XLE also recorded the highest reduction of 98,43% at pH 3 and 35°C feed temperature.

It indicates that NF270 was more efficient at turbidity removal compared to XLE. Strmecky et al.(2016) had the same observation where XLE, NF90, and NF270 recorded 99,4%, 99,2%, and 99,6% for turbidity, respectively, supporting NF270 as the better performer. Loose membranes are often preferred over removing foulants with larger MW to reduce fouling in tight membranes.

The results also document that both membranes had the lowest removal at pH 6 and a feed temperature of 15°C. NF270 reported the highest permeate concentration of 0,71NTU, while XLE reported 1,06 NTU. These values may both be considerably low, but the effect varies. The Department of Water Affairs and Forestry (1996) said that turbidity between 0-1 NTU presented no significant risk that may be associated with transmission of infectious micro-organisms or health effects resulting from the presence of suspended solids. On the other hand, samples with values ranging between 1-5 NTU present a possibility of disease transmission.

4.3. Removal of inorganics

The removal of inorganic material in the MBR effluent was used as another parameter to compare the investigated membranes. The concentration of ammonia and phosphates was measured using a multi-parameter photometer for all samples before and after experimental runs. The measured concentration was used to calculate these compounds' overall percentage removal to evaluate each membrane's performance at the set experimental conditions, determining the condition with the highest removal and the potential effect of the final concentrations on the environment or industrial usage.

The permeate quality of RO and NF units of selected inorganics are summarised in Tables 4-2 and 4-3. These tables show the average concentrations and percentage removal of inorganics found in the effluent of the two membranes at three different pH (3,6,10).

Municipal wastewater consists of various waste runoffs containing CECs, including perfluorinated compounds (PFCs), pharmaceuticals and personal care products (PPCPs), brominated flame retardants (BFRs), pesticides, steroid hormones, surfactants through direct discharge from industries, hospitals, domestic wastewater, and aquaculture facilities, making the removal of inorganics complex (Wenning & Martello, 2014; Wang et al., 2017; Oluwole et al., 2020; Aziz & Kasongo, 2021). Due to limitations, MBR effluent usually requires further treatment, such as RO, to remove inorganics and heavy metals (Abdel_Kader, 2015).

Tables 4-2 and 4-3 show the effluent concentration and percentage removal of ammonia with significant differences observed between the two membranes at variable pH: ($p=0,0035$ for XLE and NF270 membranes at pH 3; $p=0,0084$ for XLE and NF270 at pH 6; $p=1,5x10^{-5}$ for XLE and NF270 at pH 10; $\alpha=0,05$) with standard deviation in parenthesis at varied feed pH and 35°C after treatment of MBR effluent. The effluent concentration and percentage removal of phosphate ions ($p=1,1x10^{-5}$ for XLE and NF270 at pH 3, $p=9, 9x10^{-6}$ for XLE and NF270 at pH 6, and $p=0,13$ for XLE and NF270 at pH 10;$\alpha=0,05$) for RO and NF at varied feed pH and at 35°C after treatment of MBR effluent.

The analysis showed that XLE reported the highest removal of 94,83% for NH_3 and 94,84% for NH_3-N at pH 6 at 35°C, while NF270 recorded all highest values for ammonia ions at pH 6. The lowest removals were recorded pH for both XLE (57,01%) and NF270 (40,71%). The high concentration of NH_3-N indicates eutrophication and eco-toxicity (Reza & Chen, 2021). When analysing the removal of NH_3-N using membrane filtration, Kosutic & Dolar (2014)

reported that XLE and NF270 removed 88,9% and 37,1%, respectively, at a pH range of 7,87- 8,22. It further supports that XLE has higher removal efficiency compared to NF270. The difference in efficiency can be explained by the difference in size and density of the pore structure of the membranes, which facilitates solute retention and result in high ammonium permeability for NF270 as membrane properties change at extreme acidic and alkali conditions (Diop et al., 2011; Lim et al., 2021). It can be noted that both membranes recorded the lowest concentrations at feed pH 6 and low temperature 15°C making it the ideal condition for ammonia removal.

Table 4-2: Final concentration of the inorganics after the short-run treatment of MBR effluent using RO and NF with varying feed pH (3, 6, and 10) at 35°C

Membrane	**Parameter**	**pH**		
		3	**6**	**10**
RO	NH_3	0,43 (0,52)	0,6 (0,70)	5,2 (4,90)
	NH_4^+	0,4 (0,56)	0,64 (0,65)	5,5 (5,20)
	NH_3 -N	0,33 (0,44)	0,49 (0,67)	4,3 (4,05)
	P	0,08 (0,05)	N.D (0,01)	0,11 (0,12)
	PO_4^{3+}	0,25 (0,16)	N.D (0,03)	0,35 (0,36)
	P_2O_5	0,19 (0,12)	0,01 (0,03)	0,26 (0,27)
NF	NH_3	2,4 (1,90)	2,2 (1,70)	10,1 (9,55)
	NH_4^+	2,6 (2,05)	2,3 (1,85)	10,7 (10,10)
	NH_3 -N	2 (1,60)	1,8 (1,65)	8,3 (7,85)
	P	0,68 (0,64)	0,05 (0,04)	0,1 (0,25)
	PO_4^{3+}	2,1 (1,90)	0,16 (0,11)	0,4 (0,80)
	P_2O_4	1,57	0,12	0,3

		(1,44)	(0,08)	(0,60)

Values are averages from n=2 samples where the standard deviation is in parenthesis

Table 4-3: Percentage removal of the inorganics after the short-run treatment of MBR effluent using RO and NF with varying feed pH (3, 6, and 10) at 35°C

Membrane	**Parameter**	**Recovery**		
		3	**6**	**10**
RO	NH_3	94,19 (0,22)	94,83 (2,31)	64,63 (1,44)
	NH_4^+	94,94 (1,32)	94,80 (2,64)	64,52 (1,36)
	NH_3 -N	94,59 (0,89)	94,84 (1,91)	64,46 (1,56)
	P	96,19 (1,28)	100,00 (0,52)	94,50 (0,58)
	PO_4^{3+}	96,15 (1,35)	100,00 (0,42)	94,26 (0,41)
	P_2O_5	96,12 (1,51)	99,74 (0,26)	94,35 (0,44)
NF	NH_3	73,33 (5,30)	84,06 (4,64)	40,94 (0,17)
	NH_4^+	72,63 (5,58)	84,25 (3,81)	40,88 (0,34)
	NH_3 -N	72,97 (4,97)	84,21 (1,06)	40,71 (0,39)
	P	77,33 (5,42)	96,67 (1,71)	96,97 (13,57)
	PO_4^{3+}	76,67 (6,48)	96,44 (1,89)	96,08 (12,65)
	P_2O_5	73,83 (8,29)	96,47 (1,94)	96,05 (12,73)

Values are averages from n=2 samples where the standard deviation is in parenthesis

The removal of phosphates was recorded to be relatively higher for the XLE than NF270. It concurred with the study by Dolar et al.(2011), where XLE was compared to other membranes, including NF90, for the removal of phosphates resulting in a reduction higher

than 95%, also relatively higher than NF membranes. It was reported that rejection of phosphates depends on the membrane used and that phosphates ions are harmful and have molecular weight similar to RO and NF90 membrane making size exclusion the dominant removal mechanism. At pH 10, the rejection of phosphorus follows the pattern of the MWCO; the higher the MWCO, the lower the phosphorus removal (Chai et al., 2019). XLE had samples with a concentration below detection, while NF270 reported a concentration of 0,05mg/L (P) and 0,16mg/L (PO_4^{3+}) for the same conditions (pH 6 35°C). The membranes also reported the lowest removal of 93,68% for XLE at feed pH of 10 at 35°C and 22,86% at feed pH 3 and a temperature of 15°C. Phosphate removal decrease with decreasing feed pH (Dolar et al., 2011). It shows that the change in pH significantly affected the physicochemical properties. Chai et al. (2019) investigated the effect of pH on removing phosphates using NF membranes, including NF270 and NF90. Results showed that phosphorus is absorbed into the membrane structure at alkaline conditions (pH 10 and 13.5) compared to lower pHs (pH 1.5 and 5). The NF270 membrane outperformed other membranes owing to its desirable performance under solid alkali solution.

Table 4-4: Characteristics of NF and RO effluent average water quality at pH 6 and 35°C with reuse criteria for wastewater in different applications (Üstün et al., 2011; Emongor et al., 2005; Hansen et al., 2016; Asano et al., 1988; Aziz & Kasongo, 2021)

Parameter	Irrigation	cooling systems	NF	RO
COD (mg/l)	<50	<30	325	350
NH_3	<6,08	<1	2,2	0,6
P	<1,5	-	0,05	-
PO_4^{3-}	<2	<7	0,16	-
TDS (mg/l)	<200	-	22,5	11,58
pH	6,5-8,4	6,8-7,2	6±0,5	6±0,5
EC ($\mu s/cm^{-1}$)	<250	<1445	45,17	11,58

The results in Table 4-4 indicate that the removal of ammonia, phosphorus and phosphates by NF and RO are within the range of irrigation and cooling systems specifications and international guidelines for reuse. The TDS and EC also support this within range for reuse, suggesting that the investigated membranes were effective enough to offer the effluent for

reuse purposes, specifically in cooling systems and irrigation. The only limiting parameter is the COD for both irrigation and cooling systems. The values 325mg/L for NF and 350mg/L for RO may not paint a clear picture of the effluent due to the methanol used to dissolve PCPs used in the investigation. As mentioned in section 4.2.2, the methanol level in a water solution results in increased COD.

RO has been reported to effectively reduce water consumption in cooling towers by using effluent as an alternative to freshwater usage (Hansen et al., 2016). While reclaimed wastewater is encouraged for cooling systems, ensuring the water quality doesn't interfere with the industrial tower operation is imperative. Asano et al. (1988) noted that the significant problems associated with water quality in cooling systems include scaling, corrosion, biological growth, and fouling in heat exchangers and condensers. The parameters noted in Table 4-4 play a massive role in these issues. The presence of nutrients such as phosphates and phosphorus encourages biological growth, which may result in deposits on hot surfaces reducing efficiency in heat exchangers due to scaling. In contrast, phosphorus deposits inhibit heat transfer and water flow resulting in fouling. TDS increase electric conductivity resulting in accelerated corrosion.

Good-quality water effluent provides the agricultural sector with a substitute water source for irrigation when freshwater is scarce due to drought and inconsistent rainfall (Emongor et al., 2005). There is an emphasis on good quality because, like in cooling towers, water contaminants or constituents need to be known before reused for irrigation to ensure no damage is caused to agriculture production, groundwater quality, and soil conditions (Emongor et al., 2005; Üstün et al., 2011).

High values of TDS and EC prevent plants from absorbing water due to ion concentration in the soil, resulting in physiological drought. While phosphates (PO_4^-) are credited for eutrophication, high levels of ammonia (NH_3^+) can result in quality problems in crops and excessive growth (Emongor et al., 2005).

4.4. Chemical Analysis

This study used a synthetic membrane bioreactor (MBR) municipal secondary effluent as the feed water. The feed was spiked with personal care products (PCP), Triclosan (TCS), Methylparaben (MeP), and Ethylhexyl methoxycinnamate (EHMC). Two commercial membranes, i.e. RO and NF, were investigated. Composite samples were collected and stored at 4°C before the clean-up and concentrating step through SPE to improve detection during further analysis. The personal care products activity was assessed using GCMS.

4.4.1 Personal care products (PCP) in the influent

The synthetic secondary municipal wastewater feed solution was dosed with target analytes in the 450-478,85µg/l range. Each contaminant was dosed at the same concentration for each experimental run. The averages used for this study are within the scope of previously reported studies and can be seen in Table 2-7 (chapter 2).

Standard calibration curves were generated using linear regression analysis showing good fits to the data (R^2 = 0.991-0.9925) through the use of BPA as an internal standard, over the established concentration range (0,1 - 15µg/L), excluding where this concentration range fell below the detection limits of a particular compound. A six-point calibration was performed for each personal care product, and possible fluctuations in signal intensity were checked by injection of standard solution at two concentrations after each 4–6 injections. Method detection limits (MDL) were determined from spiked water samples as the minimum detectable amount of analyte with a signal-to-noise ratio of 3.

4.4.2. Personal care products (PCP) in the effluent

The removal of CECs using membrane filtration was reported to be influenced by the physicochemical properties of the CEC (e.g. molecular weight, charge, etc.), membrane properties and operating conditions (membrane pore size, porosity, direction, and pressure), and water quality conditions (e.g. pH, solute concentration, temperature, background inorganics, etc.) (Kim et al., 2018). The research used a RO system to evaluate the removal of TCS, MeP, and EHMC from municipal secondary MBR effluent using XLE and NF270 under varying conditions. Feed temperature and pH were varied and controlled throughout

the experiments to investigate their effect on removing the selected PCPs and comparing the RO membranes. The breakdown of the experimental runs is shown in Table 3-5 (Chapter 3). To characterize the concentration of the PCPs after treatment, SPE was used to extract the target compound from the treated samples to achieve the desired sensitivity for GC-MS.

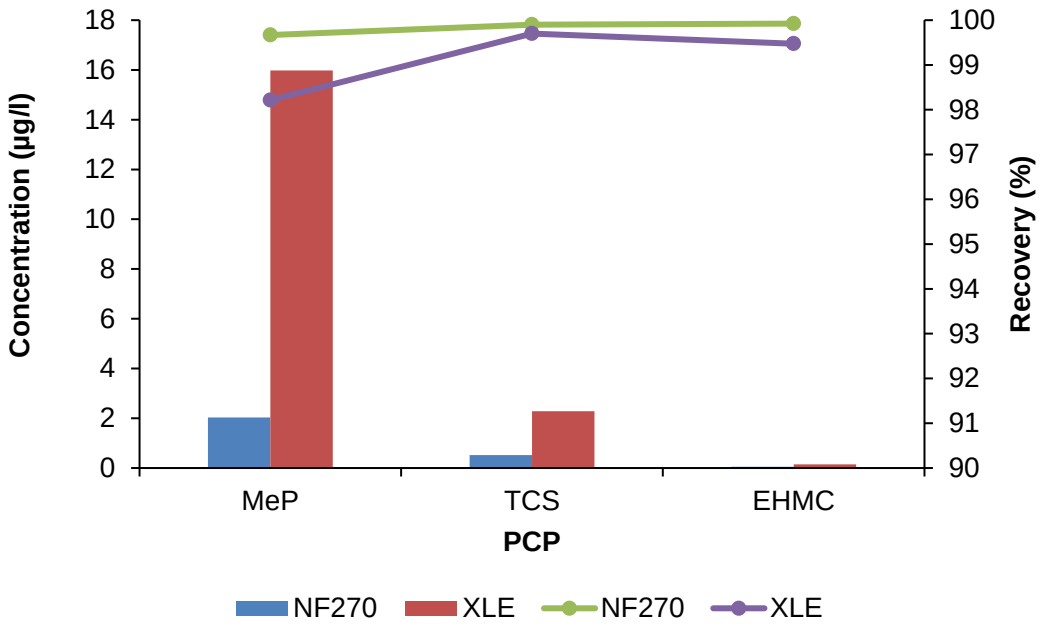

Figure 4-14: Concentration and percentage removal of personal care products after 8-hour treatment at pH 6 and at 35°C with XLE and NF270 membranes

4.4.1. The effect of physicochemical properties

As a result of the difference in size, charge, and hydrophobicity, solute-membrane interactions were evaluated. The composition of the PCPs in the MBR effluent was characterized before and after treatment. Figure 31 shows the permeate concentration (p= 0,28 α=0,05) and percentage removal of TCS, MeP, and EHMC using XLE and NF270 at pH 6 and a feed temperature of 35°C for a short experimental run. The overall results showed that EHMC (XLE=99,97%, NF270= 99,99%) had the highest removal for both membranes, followed by TCS (XLE=99,50%, NF270=99,88%), then MeP (XLE=96,52%, NF270=99,57%). The results also correlate with their molecular size. The compound with the highest removal happens to have the most significant molecular weight (EHMC-290g/mol)

followed by TCS (289g/mol), then MeP (152,1g/mol), making size exclusion one of the dominant removal mechanisms (Wang & Wang, 2016). This observation was supported by a study where compounds with relatively high molecular weight (carbamazepine (CBM), sulfamethoxazole (SMX), and atrazine (ATZ)) had high removal compared to small compounds (phenol (PHN) and 4-chlorophenol (4CP)) (Heo et al., 2013). The hydrophobicity of the compound also plays a role in its retention. After filtration of synthetic PPCP wastewater, TCS, one of the most vital hydrophobic compounds, was found in the polyamide and polysulfone layers of RO membranes suggesting that PPCPs can be rejected by hydrophobicity adsorption effect (Wei et al., 2020).

Table 4-5: Concentration of personal care products at 35°C with RO and NF membranes for 8 hours

Membrane	PCP pH	MeP	TCS	EHMC
RO	3	0,51 (0,13)	0,57 (0,20)	0,25 (0,03)
	6	15,98 (10,99)	2,28 (1,29)	0,15 (3,13)
	10	0,33 (28,37)	0,79 (81,23)	0,03 (27,10)
NF	3	1,57 (0,07)	3,29 (0,29)	0,3 (0,01)
	6	2,03 (0,14)	0,52 (0,10)	0,05 (0,42)
	10	4,51 (0,51)	3,94 (1,93)	0,06 (0,03)

Values are averages from n=2 samples where the standard deviation is in parenthesis

4.4.2. The effect of membranes properties and operating conditions

The PCP retention was considerably high for all experimental conditions. Both membranes effectively removed the trace amounts of the selected compounds with an initial concentration range of 450-478,85µg/L. XLE and NF270 have successfully removed PCPs(Kim et al., 2018; Wei et al., 2020; Lim et al., 2021).

During a study of the effect of silica fouling on the removal of PPCPs using RO/NF membranes, TCS was one of the PCPs investigated at varying pH (3, 5, 8, 10). The results showed that rejection followed the NF270 > NF90 > XLE, the same order as the MWCO NF270-300>NF90-200>XLE-100 as a result of its hydrophobicity (log k_{OW}= 4,76) as shown in Table 2-2 (chapter 2) (Lin et al., 2014). RO/NF membranes are reported to use size exclusion (steric hindrance), electrostatic repulsion, and hydrophobic interactions between membrane and solute to remove organic compounds (Lin & Lee, 2014). The initial stage of filtration is reported to be adsorption onto the membrane, then later followed by a steric/ size exclusion mechanism (Kim et al., 2018). The MWCO between XLE and NF270 result in a difference in PCPs retention. NF270 is considered a loose membrane with a larger pore size than XLE. The results in Figure 4-14 support the statement. XLE had a removal efficiency of 99,57%, 99,50%, and 96,52% for EHMC, TCS, and MeP, respectively. NF270 recorded removal for EHMC, TCS, and MeP to be 99,99%, 99,88%, and 99,57%. The compound with the highest removal has the most significant molecular weight (Table 2-1 chapter 2) (Heo et al., 2013).

The concentrations for the PCPs are significantly higher for NF270. For feed pH 3 at 35°C XLE recorded concentrations for EHMC, MeP, and TCS of 0,25, 0,51, and 0,57µg/L respectively, compared to NF270 EHMC, MeP, and TCS were 0,3, 1,57, and 3,29µg/L**.** It is attributed to size exclusion and electrostatic repulsion due to the change in pH, which has been reported that rejection increases with pH for all membranes**.** The results were consistent with the study conducted by Lin & Lee (2014), where rejection for XLE (86-99%) was a result of size exclusion, while NF270 (23-92%) and NF90 (57-97) rejection were dominated by electrostatic repulsion as a result of the change in pH and varying ionization constants.

The change in pH and temperature was expected to affect the removal mechanism and, subsequently, the PCP removal efficiency. An increase in temperature results in an addition in MWCO of NF and thermal energy generation, increasing the diffusivity of PPCPs and decreasing the viscosity of the water (Wei et al., 2020). The results showed no change in PCP rejection as a result of temperature. For NF270 at feed pH 10 and varying temperatures, the rejection for all the PCPs is consistent at 99% and above values. The results were consistent with another published study. While investigating the influence of temperature on phthalate esters (PAEs) removal using NF, the temperature change affected the permeate flux. Still, it showed no effect on rejecting PAEs(Wei et al., 2016). These results were attributed to the bucking effect between the permeating solute molecules and the permeating flux (Wei et al., 2020).

Table 4-3 shows the final concentration of the samples with significant differences between the membranes (standard deviation in parenthesis) ($p=1, 93x10^{-5}$ for XLE & NF270 at pH 3, p=0,28 for XLE & NF270 at pH 6, and p=0, 20 for XLE & NF270 at pH 10; α=0, 05) at feed temperature of 35°C for an 8-hour run. From the results, it can be observed that the concentration changes with the changing pH. EHMC initially had a concentration of 450µg/L, which was removed to 0,25µg/L for XLE and 0,3µg/L for NF270 at pH 3. The concentration was reduced to 0,03µg/L for both membranes at pH 10. Lin & Lee (2014) reported that a change in pH could result in a difference in the membrane surface charge and the ionic state of the PPCPs. When RO membranes and PPCPs have the same charge, the removal efficiency is reported to be higher and lower when opposite (Wei et al., 2020).

While NF and RO have proven to be successful at PCP removal, RO outperformed NF. It is due to the interaction between membrane properties, the physicochemical properties of the three PCPs, and the influence of pH and temperature. Generally, the removal mechanism of the PCPs is a result of size exclusion, electrostatic repulsion, and hydrophobicity(Wei et al., 2020). As a result of the difference in MWCO of the membranes, size exclusion provides RO with an advantage.

Chapter 5
Conclusion and Recommendations

5.1. Conclusion

The reduction of COD, micropollutants and contaminants of emerging concerns in municipal secondary MBR wastewater by low pressure and extra-low energy PA TFC membranes for effluent discharge or possible recycle application was investigated. Extensive research was done on changing a RO system's operating variables (feed pH and temperature) and whether those changes efficiently enhance the elimination of COD, inorganics, and CECs.

Detailed selected qualitative analyses were investigated on membrane surface characteristics using Scanning Electron Microscopy (SEM), Attenuated Total Reflection-Fourier Transform Infrared Spectroscopy (ATR-FTIR), and Energy Dispersive X-Ray Spectroscopy (EDX) before and after RO experimental runs. During the ATR-FTIR analysis, the varying pH and temperature resulted in changes in the membrane structure, more so for NF270 than XLE. The mechanical support layer (polysulfone) was compromised due to changing pH resulting in varying rates of fouling, which increased with pH as indicated by FTIR and EDX analysis. The amounts of foulants supported this, showed by EDX and the deposition in SEM images.

The results showed that COD percentage removal increased with increasing pH and temperature and that XLE was better at removing COD than NF270. XLE recorded its highest percentage removal of 95,76 for COD at feed pH 10 at 35°C, while results showed 92,36 COD removal for NF270 at pH 6 and 35°C. The two membranes showed a comparable influence of pH in TDS removal. However, NF270 recorded the highest overall TDS percentage removal of 99,31, whilst the XLE recorded 98,43. The selected inorganic removal showed that the XLE outperformed NF270 for phosphates and ammonia. The XLE membrane at a pH of 6 and temperature of 35°C removed phosphates and ammonia 100 and 96,4%. At the same time, the NF270 membrane reported an average of 87,34 and 97,78 percentage removal, respectively.

RO and NF membranes exhibited exceptional removal rates (>80%) for most PCPs. The lowest concentration of micropollutants recorded was 0.03µg/l for EHMC with the RO membrane at a pH 3 and a feed temperature of 35°C, achieving a 99,99 percent rejection. The RO membrane performed better overall compared to the NF.

Finally, COD, TDS, Inorganics, and selected pharmaceuticals (EHMC, MeP, and TCS) removal using the RO bench-scale unit with RO and NF membranes at the predetermined process variables were successful for potential future reuse applications.

5.2. Recommendations

Further studies should look at the following suggestions for characterizing membranes with Atomic Force Microscopy (AFM) to understand the effect of the change in roughness or overall membrane surface morphology on PCP treatment. The zeta potential should be determined to understand the impact of pH better. Future studies should also include more larger PCPs to better appreciate their physicochemical properties and effect on their removal. Finally, fouling at the suggested pH 6 and temperature of 35°C should be tested at extended RO periods with cost analysis.

References

References

Abdel_Kader, A.M. 2015. A Review of Membrane Bioreactor (MBR) Technology and Their Applications in the Wastewater Treatment Systems. *Desalination and Water Treatment*, 32: 111–119.

Abdel-Fatah, M.A. 2018. Nanofiltration systems and applications in wastewater treatment : Review article. *Ain Shams Engineering Journal*, 9(4): 3077–3092. https://doi.org/10.1016/j.asej.2018.08.001.

Acero, J.L., Benitez, F.J., Leal, A.I., Real, F.J. & Teva, F. 2010. Membrane filtration technologies applied to municipal secondary effluents for potential reuse. *Journal of Hazardous Materials*, 177(1–3): 390–398. http://dx.doi.org/10.1016/j.jhazmat.2009.12.045.

Adel, M., Nada, T., Amin, S., Anwar, T. & Mohamed, A.A. 2022. Groundwater for Sustainable Development Characterization of fouling for a full-scale seawater reverse osmosis plant on the Mediterranean sea : membrane autopsy and chemical cleaning efficiency. *Groundwater for Sustainable Development*, 16(March 2021): 100704. https://doi.org/10.1016/j.gsd.2021.100704.

Al-abri, M., Kyaw, H.H., Al-ghafri, B., Tay, M., Myint, Z. & Dobretsov, S. 2022. Autopsy of Used Reverse Osmosis Membranes from the Largest Seawater Desalination Plant in Oman. *Membranes*, 12(671).

Alrehaili, O., Perreault, F., Sinha, S. & Westerhoff, P. 2020. Increasing Net Water Recovery of Reverse Osmosis with Membrane Distillation Using Natural Thermal Differentials Between Brine and Co-Located Water Sources : Impacts at Large Reclamation Facilities. *Water Research*.

Alturki, A.A., Tadkaew, N., Mcdonald, J.A., Khan, S.J., Price, W.E. & Nghiem, L.D. 2010. Combining MBR and NF/RO membrane filtration for the removal of trace organics in indirect potable water reuse applications. *Journal of Membrane Science*, 365(1–2): 206–215. http://dx.doi.org/10.1016/j.memsci.2010.09.008.

Alygizakis, N., Galani, A., Rousis, N.I., Aalizadeh, R., Dimopoulos, M. & Thomaidis, N.S. 2021. Science of the Total Environment Change in the chemical content of untreated wastewater of Athens , Greece under COVID-19 pandemic. *Science of the Total Environment*, 799(149230). https://doi.org/10.1016/j.scitotenv.2021.149230.

Anand, U., Adelodun, B., Cabreros, C., Kumar, P. & Abhijit, S.S. 2022. Occurrence ,

transformation , bioaccumulation , risk and analysis of pharmaceutical and personal care products from wastewater: a review. *Environmental Chemistry Letters*, 20(6): 3883–3904. https://doi.org/10.1007/s10311-022-01498-7.

Andrii, B., Adriaan, J., Lucia, H.L., Grietje, Z. & Huub, R. 2013. Electrochemical oxidation of personal care and household products in the aerobically treated grey water. , (Figure 2): 176–177.

Ang, W.L. & Mohammad, A.W. 2015. Mathematical modeling of membrane operations for water treatment. In *Advances in Membrane Technologies for Water Treatment*. Elsevier Ltd: 379–407. http://dx.doi.org/10.1016/B978-1-78242-121-4.00012-5.

Aniszewski, T. 2007. Alkaloid Chemistry. In *Alkaloid Chemistry, Biological Significance, Applications and Ecological Role*. 61–139.

Asano, T., Mujeriego, R. & Dickson Parker, J. 1988. Evaluation of industrial cooling systems using reclaimed municipal wastewater. *Water Science and Technology*, 20(10): 163–174.

Aziz, M. & Kasongo, G. 2019. Scaling prevention of thin film composite polyamide Reverse Osmosis membranes by Zn ions. *Desalination*, 464(April): 76–83. https://doi.org/10.1016/j.desal.2019.04.021.

Aziz, M. & Kasongo, G. 2021. The Removal of Selected Inorganics from Municipal Membrane Bioreactor Wastewater Using UF / NF / RO Membranes for Water Reuse Application : A Pilot-Scale Study. *Membranes*, 11(117).

Aziz, M. & Ojumu, T. 2020. Exclusion of Estrogenic and Androgenic Steroid Hormones from Municipal Membrane Bioreactor Wastewater Using UF / NF / RO Membranes for Water Reuse Application. *Membranes*, 10(37).

Baker, R.W. 2012. *Membrane Technology and Application*. Third Edit. Newark, California: John Wiley & Sons Ltd.

Bandala, E.R., Kruger, B.R., Cesarino, I. & Leao, A.L. 2021. Impacts of COVID-19 pandemic on the wastewater pathway into surface water: A review. *Science of the Total Environment*, 774(145586).

Basaglia, G., Pasti, L. & Pietrogrande, M.C. 2011. Multi-residual GC-MS determination of personal care products in waters using solid-phase microextraction. *Analytical and Bioanalytical Chemistry*, 399(6): 2257–2265.

Bastrzyk, J., Gryta, M. & Karakulski, K. 2014. Fouling of nanofiltration membranes used for separation of fermented glycerol solutions ‡. *Chemical papers*, 68(6): 757–765.

Biziuk, M. & Zwir-Ferenc, A. 2006. Solid Phase Extraction Technique – Trends , Opportunities and Applications. *Polish Journal of Environmental Studies*, 15(5).

Braghetta, B.A., Digiano, F.A. & Member, W.P.B. 1997. pH AND IONIC. : 628–641.

Brunner, A.M., Bertelkamp, C., Dingemans, M.M.L., Kolkman, A., Wols, B., Harmsen, D., Siegers, W., Martijn, B.J., Oorthuizen, W.A. & Thomas, L. 2020. Science of the Total Environment Integration of target analyses , non-target screening and effect-based monitoring to assess OMP related water quality changes in drinking water treatment. *Science of the Total Environment*, 705: 135779. https://doi.org/10.1016/j.scitotenv.2019.135779.

Cabeza, Y., Candela, L., Ronen, D. & Teijon, G. 2012. Monitoring the occurrence of emerging contaminants in treated wastewater and groundwater between 2008 and 2010 . The Baix Llobregat (Barcelona , Spain). *Journal of Hazardous Materials*, 239–240: 32–39. http://dx.doi.org/10.1016/j.jhazmat.2012.07.032.

Campıns-Falco, P., Sevillano-Cabeza, A., Herraez- Hernandez, R., Molins-Legua, C., Moliner-Martınez, Y. & Verdu-Andres, J. 2012. Solid-phase Extraction and Clean-up Procedures in Pharmaceutical Analysis. *Encyclopedia of Analytical Chemistry*.

Castro, M.M.M. 2016. *Assessment of musk and UV filter compounds in wild mussels collected in Portugal coast*. Universidade do Porto.

Chai, Y.K., Lam, H.C., Koo, C.H., Lau, W.J., Lai, S.O. & Ismail, A.F. 2019. Performance evaluation of polyamide nanofiltration membranes for phosphorus removal process and their stability against strong acid / alkali solution q. *Chinese Journal of Chemical Engineering*, 27(8): 1789–1797. https://doi.org/10.1016/j.cjche.2018.09.029.

Chen, X., Lei, L., Liu, S., Han, J., Li, R., Men, J., Li, L., Wei, L., Sheng, Y., Yang, L., Zhou, B. & Zhu, L. 2021. Science of the Total Environment Occurrence and risk assessment of pharmaceuticals and personal care products (PPCPs) against COVID-19 in lakes and WWTP-river-estuary system in Wuhan , China. *Science of the Total Environment*, 792: 148352. https://doi.org/10.1016/j.scitotenv.2021.148352.

Chen, Y., Zou, C., Mastalerz, M., Hu, S. & Gasaway, C. 2015. Applications of Micro-Fourier Transform Infrared Spectroscopy (FTIR) in the Geological Sciences — A Review. *International Journal of Molecular Sciences*: 30223–30250.

Chtourou, M. 2018. *Pharmaceutical and Personal Care Products removal by advanced treatment technologies.* University of Girona.

Dang, H.Q., Price, W.E. & Nghiem, L.D. 2014. Factors governing the rejection of trace organic contaminants by nanofiltration and reverse osmosis membranes. *Faculty of Science, Medicine and Health*.

Department of Water Affairs and Forestry. 1996. *SOUTH AFRICAN WATER QUALITY GUIDELINES DOMESTIC*. Second. S. (CSIR E. S. Holmes, ed. Pretoria.

Dhodapkar, R.S. & Gandhi, K.N. 2019. 3. Pharmaceuticals and personal care products in aquatic environment: chemicals of emerging concern? In *Pharmaceuticals and Personal Care Products: Waste Management and Treatment Technology*. Elsevier Inc.: 63–86. http://dx.doi.org/10.1016/B978-0-12-816189-0.00003-2.

Díaz-Cruz, M.S. 2015. *Personal Care Products in the Aquatic Environment*. D. Barceló, ed. Springer.

Diop, S.N., Diallo, M.A., Diawara, C.K. & Cot, D. 2011. Intrinsic properties and performances of NF270 and XLE membranes for water fi ltration. *Water Science & Technology: Water Supply*, 11(2): 186–193.

Dolar, D., Gros, M., Rodriguez-mozaz, S., Moreno, J. & Comas, J. 2012. Removal of emerging contaminants from municipal wastewater with an integrated membrane system , MBR – RO. *Journal of Hazardous Materials*, 239–240: 64–69. http://dx.doi.org/10.1016/j.jhazmat.2012.03.029.

Dolar, D., Vucic, B. & Košutic, K. 2011. RO/NF treatment of wastewater from fertilizer factory — removal of fluoride and phosphate. *Desalination*, 265: 237–241.

Ebele, J.A., Abdallah, M.A. & Harrad, S. 2016. Pharmaceuticals and personal care products (PPCPs) in the freshwater aquatic environment. *Emerging Contaminants*, 3(2017): 1–16. http://dx.doi.org/10.1016/j.emcon.2016.12.004.

Emongor, V.E., Khonga, E.B., Ramolemana, G.M., Marumo, K., Machacha, S. & Motsamai, T. 2005. Suitability of Treated Secondary Sewage Effluent for Irrigation of Horticultural Crops in Botswana. *Journal of Applied Sciences*, 5(3): 451–454.

Ezugbe, E.O. & Rathilal, S. 2020. Membrane Technologies in Wastewater Treatment. *Membranes*, 10(89).

Fan, P., Zhang, L., Liu, Z., Zhang, W., Cui, Q. & Wang, H. 2020. Analysis of trace and its

correlation with COD in condensate from natural gas to hydrogen production. *Water Science & Technology*: 843–850.

Feng, T., Sun, M., Song, S., Zhuang, H. & Yao, L. 2019. 12 - Gas chromatography for food quality evaluation. In *Evaluation Technologies for Food Quality*. Elsevier Inc.: 219–265. http://dx.doi.org/10.1016/B978-0-12-814217-2.00012-3.

Fennell, T.R., Mathews, J.M., Snyder, R.W., Hong, Y., Watson, S.L., Black, S.R., McIntyre, B.S. & Waidyanatha, S. 2017. Metabolism and Disposition of 2-Ethylhexyl-p-methoxycinnamate Following Oral Gavage and Dermal Exposure in Harlan Sprague Dawley Rats and B6C3F1/N Mice and in Hepatocytes in vitro. *Xenobiotica*. http://dx.doi.org/10.1080/00498254.2017.1400129.

Freyria, F.S., Geobaldo, F. & Bonelli, B. 2018. Nanomaterials for the Abatement of Pharmaceuticals and Personal Care Products from Wastewater. *Applied Sciences*, 8(170).

Gackowska, A. 2020. Effect of Activated Sludge on the Degradation of 2-Ethylhexyl 4-Methoxycinnamate and 2-Ethylhexyl 4- (Dimethylamino) Benzoate in Wastewater. *Water Air Soil & Pollution*, 231(158).

Gedam, V. V, Patil, J.L., Kagne, S., Sirsam, R.S. & Labhasetwar, P. 2012. Performance Evaluation of Polyamide Reverse Osmosis Membrane for Removal of Contaminants in Ground Water Collected from Chandrapur Performance Evaluation of Polyamide Reverse Osmosis Membrane for Removal of Contaminants in Ground Water Collected from Chandrapur District. , (January).

Guo, H., Yao, Z., Yang, Z., Ma, X., Wang, J. & Tang, C.Y. 2017. Article A one-step rapid assembly of thin film coating using green coordination complexes for enhanced removal of trace organic contaminants by membranes complexes for enhanced removal of trace organic contaminants by. *Environmental science & technology*.

Hansen, E., Rodrigues, M.A.S. & Aquim, P.M. de. 2016. Wastewater reuse in a cascade based system of a petrochemical industry for the replacement of losses in cooling towers. *Journal of environmental management*, 181: 157–162.

Heath, D., Krivec, M., Ko, J., Kosjek, T. & Heath, E. 2018. Seasonal and spatial variations in the occurrence , mass loadings and removal of compounds of emerging concern in the Slovene aqueous environment and environmental risk assessment *. , 242.

Heo, J., Boateng, L.K., Flora, J.R. V, Lee, H., Her, N., Park, Y. & Yoon, Y. 2013. Comparison

of fl ux behavior and synthetic organic compound removal by forward osmosis and reverse osmosis membranes. *Journal of Membrane Science*, 443: 69–82. http://dx.doi.org/10.1016/j.memsci.2013.04.063.

Houck, M.M. & Siegel, J.A. 2015. Separation Methods. In *Fundamentals of Forensic Science*. 121–151.

Idrees, M.F. 2020. Case Studies in Chemical and Environmental Engineering Performance Analysis and Treatment Technologies of Reverse Osmosis Plant – A case study. *Case Studies in Chemical and Environmental Engineering*, 2(April): 100007. https://doi.org/10.1016/j.cscee.2020.100007.

Jalilnejad, N., Can, M., Parlar, İ., Kabay, N. & Pek, T.Ö. 2018. Evaluation of MBR treated industrial wastewater quality before and after desalination by NF and RO processes for agricultural reuse. *Journal of Water Process Engineering*, 22(October 2017): 103–108.

Jin, X., Jawor, A., Kim, S. & Hoek, E.M. V. 2009. Effects of feed water temperature on separation performance and organic fouling of brackish water RO membranes. *Desalination*, 239(1–3): 346–359. http://dx.doi.org/10.1016/j.desal.2008.03.026.

Juliano, C. & Magrini, G.A. 2017. Cosmetic Ingredients as Emerging Pollutants of Environmental and Health Concern. A Mini-Review. *Cosmetics*.

Kalia, V.C. 2019. 2. Pharmaceutical and personal care product contamination: a global scenario. In *Pharmaceuticals and Personal Care Products: Waste Management and Treatment Technology*. Elsevier Inc.: 27–62. http://dx.doi.org/10.1016/B978-0-12-816189-0.00002-0.

Kaur, H., Hippargi, G., Pophali, G.R. & Bansiwal, A.K. 2019. *6. Treatment methods for removal of pharmaceuticals and personal care products from domestic wastewater*. Elsevier Inc. http://dx.doi.org/10.1016/B978-0-12-816189-0.00006-8.

Khanzada, N.K., Farid, M.U., Kharraz, J.A., Tang, C.Y., Nghiem, L.D., Jang, A. & An, A.K. 2019. Removal of organic micropollutants using advanced membrane-based water and wastewater treatment: A review. *Journal of Membrane Science*: 117672. https://doi.org/10.1016/j.memsci.2019.117672.

Khulbe, K., Feng, C. & Matsuura, T. Membrane Characterization. *Water and wastewater treatment technology*.

Kim, I., Kim, M., Yoon, Y., Im, J. & Zoh, K. 2013. Kinetics and degradation mechanism of

clofibric acid and diclofenac in UV photolysis and UV/H 2 O 2 reaction. *Desalination and Water Treatment*: 37–41.

Kim, S., Hoon, K., Al-hamadani, Y.A.J., Min, C. & Jang, M. 2018. Removal of contaminants of emerging concern by membranes in water and wastewater : A review. *Chemical Engineering Journal*, 335(November 2017): 896–914.

Kosutic, K. & Dolar, D. 2014. Treatment Treatment of landfill leachate by membrane processes of nanofiltration and reverse osmosis. *Desalination and Water Treatment*, (June).

Kowalik-klimczak, A. 2016. Scanning Electron Microscopy (SEM) in the analysis of the structure of polymeric nanofiltration membranes. , (January).

Krogh, J., Lyons, S., Lowe, C.J. & Lowe, C.J. 2017. Pharmaceuticals and Personal Care Products in Municipal Wastewater and the Marine Receiving Environment Near Victoria Canada. *Frontiers in marine science*, 4(415): 1–13.

Krzeminski, P., Schwermer, C., Wennberg, A., Langford, K. & Vogelsang, C. 2017. Occurrence of UV filters , fragrances and organophosphate flame retardants in municipal WWTP effluents and their removal during membrane post-treatment. *Journal of Hazardous Materials*, 323: 166–176. http://dx.doi.org/10.1016/j.jhazmat.2016.08.001.

Kucera, J. 2015. *Reverse Osmosis: Industrial Processes and Application*. 2nd ed. Canada: Wiley.

Lakhouit, A. 2019. Removal of Pharmaceutical and Personal Care Products PPCPs from Wastewater. *Journal of environmental and soil sciences*, 2(3): 224–226.

Lau, W., Lai, G., Li, J., Gray, S., Hu, Y. & Fauzi, A. 2019. Journal of Industrial and Engineering Chemistry Development of microporous substrates of polyamide thin fi lm composite membranes for pressure-driven and osmotically-driven membrane processes : A review. *Journal of Industrial and Engineering Chemistry*, 77: 25–59. https://doi.org/10.1016/j.jiec.2019.05.010.

Li, W., Ma, Y., Guo, C., Hu, W., Liu, K., Wang, Y. & Zhu, T. 2007. Occurrence and behavior of four of the most used sunscreen UV filters in a wastewater reclamation plant. *Water Research*, 41(2007): 3506–3512.

Lim, M.Z.Y., Chong, W.C., Lau, W.J. & Koo, C.H. 2021. Performance of thin film composite membranes for ammonium removal and reuse of ammonium-enriched solution for plant

growth Marcus Ze Yuan Lim, Woon Chan Chong, Woei Jye Lau and Chai Hoon Koo. *Water Supply*: 318–330.

Lin, Y., Chiou, J. & Lee, C. 2014. Effect of silica fouling on the removal of pharmaceuticals and personal care products by nanofiltration and reverse osmosis membranes. *Journal of Hazardous Materials*, 277: 102–109. http://dx.doi.org/10.1016/j.jhazmat.2014.01.023.

Lin, Y. & Lee, C. 2014. Elucidating the Rejection Mechanisms of PPCPs by Nanofi ltration and Reverse Osmosis Membranes. *Industrial & Engineering Chemistry Research*.

Liu, M., Lü, Z., Chen, Z., Yu, S. & Gao, C. 2011a. Comparison of reverse osmosis and nano fi ltration membranes in the treatment of biologically treated textile ef fl uent for water reuse. *Desalination*, 281: 372–378.

Liu, M., Lü, Z., Chen, Z., Yu, S. & Gao, C. 2011b. Comparison of reverse osmosis and nano filtration membranes in the treatment of biologically treated textile effluent for water reuse. *Desalination*, 281: 372–378. http://dx.doi.org/10.1016/j.desal.2011.08.023.

Lopera, A.E., Gutiérrez, S., María, J. & Alonso, Q. 2019. Journal of Water Process Engineering Removal of emerging contaminants from wastewater using reverse osmosis for its subsequent reuse : Pilot plant. *Journal of Water Process Engineering*, 29(March): 100800. https://doi.org/10.1016/j.jwpe.2019.100800.

Mamo, J., Santos-clotas, E., Salah, A. Ben, Khaled, W., Salvado, V., Monclus, H., Chtourou, M., Mallek, M. & Dalmau, M. 2018. Triclosan, carbamazepine and caffeine removal by activated sludge system focusing on membrane bioreactor. *Process Safety and Environmental Protection*. https://doi.org/10.1016/j.psep.2018.06.019.

Manová, E., Goetz, N. Von & Hungerbuehler, K. 2015. Aggregate consumer exposure to UV fi lter ethylhexyl methoxycinnamate via personal care products. *Environment International*, 74: 249–257. http://dx.doi.org/10.1016/j.envint.2014.09.008.

Mikhak, Y., Mohammad, M., Torabi, A. & Fouladitajar, A. 2019. Refinery and petrochemical wastewater treatment. In *Sustainable Water and Wastewater Processing*. Tehran, Iran: Elsevier Inc.: 55–91. http://dx.doi.org/10.1016/B978-0-12-816170-8.00003-X.

Mohammed, S.A., Abbas, A.D. & Sabry, L.S. 2014. Effect of Operating Conditions on Reverse Osmosis (RO) Membrane Performance. *Journal of Engineering*, 20(12): 61–70.

Moldoveanu, S. & David, V. 2015. The Role of Sample Preparation. In *Modern Sample*

Preparation for Chromatography. Elsevier: 33–49.

Morone, A., Mulay, P. & Kamble, S.P. 2019. Removal of pharmaceutical and personal care products from wastewater using advanced materials. In Majeti Narasimha Vara Prasad, M. Vithanage, & A. Kapley, eds. *Pharmaceuticals and Personal Care Products: Waste Management and Treatment Technology-Emerging Contaminants and Micro Pollutants*. Elsevier Inc.: 173–212. http://dx.doi.org/10.1016/B978-0-12-816189-0.00008-1.

Morris, B.G., Aziz, M. & Kasongo, G. 2022. REMEDIATION OF LAUNDRY WASTEWATER WITH A LOW-PRESSURE AROMATIC POLYAMIDE THIN-FILM COMPOSITE REVERSE OSMOSIS MEMBRANE FOR MEMBRANE. *Environment Protection Engineering*, 48(2).

Murakami, T. 2008. Membrane Bioreactors (MBR) for Wastewater Reuse Takao Murakami. *Water Science & Technology*.

Najmi, M., Reza, M., Reza, H., Iranpoury, A. & Alivand, M.S. 2020. Removal of personal care products (PCPs) from greywater using a submerged membrane bioreactor (SMBR): The effect of hydraulic retention time. *Journal of Environmental Chemical Engineering*, 8(5): 104432. https://doi.org/10.1016/j.jece.2020.104432.

Nanda, D., Tung, K., Li, Y., Lin, N. & Chuang, C. 2010. Effect of pH on membrane morphology , fouling potential , and filtration performance of nanofiltration membrane for water softening. *Journal of Membrane Science*, 349: 411–420.

National Center for Biotechnology Information. 2020a. PubChem Compound Summary for CID 21630, Octyl methoxycinnamate. PubChem Compound Summary for CID 21630, Octyl methoxycinnamate. 4 September 2020.

National Center for Biotechnology Information. 2020b. PubChem Compound Summary for CID 5564, Triclosan. *PubChem*. https://pubchem.ncbi.nlm.nih.gov/compound/Triclosan 4 September 2020.

National Center for Biotechnology Information. 2020c. PubChem Compound Summary for CID 7456, Methylparaben. *PubChem*: 1–50. PubChem Compound Summary for CID 7456, Methylparaben 4 September 2020.

Oatley-radcliffe, D. *Membrane Characterization*.

Ogutverici, A., Yilmaz, L., Yetis, U. & Dilek, F.B. 2016. Triclosan removal by NF from a real drinking water source – Effect of natural organic matter. *CHEMICAL ENGINEERING*

JOURNAL, 283: 330–337. http://dx.doi.org/10.1016/j.cej.2015.07.065.

Oluwole, A.O., Omotola, E.O. & Olatunji, O.S. 2020. Pharmaceuticals and personal care products in water and wastewater : a review of treatment processes and use of photocatalyst immobilized on functionalized carbon in AOP degradation. *BMC Chemistry*: 1–29. https://doi.org/10.1186/s13065-020-00714-1.

Omidi, M., Fatehinya, A., Farahani, M., Akbari, Z., Shahmoradi, S., Yazdian, F., Tahriri, M., Moharamzadeh, K., Tayebi, L. & Vashaee, D. 2017. 7. Characterization of biomaterials. In *Biomaterials for Oral and Dental Tissue Engineering*. Elsevier Ltd: 97–116. http://dx.doi.org/10.1016/B978-0-08-100961-1.00007-4.

Oota, S., Murakami, T., Takemura, K. & Noto, K. 2005. Evaluation of MBR effluent characteristics for reuse purposes. *Water Science & Technology*, 51(6): 441–446.

Osunmakinde, C.S., Tshabalala, O.S., Dube, S. & Nindi, M.M. 2013. *Verification and Validation of Analytical Methods for Testing the Levels of PPHCPs (Pharmaceutical & Personal Health Care Products) in treated drinking Water and Sewage by*.

Pang, B., Zhu, Y., Lu, L., Gu, F. & Chen, H. 2016. The Applications and Features of Liquid Chromatography-Mass Spectrometry in the Analysis of Traditional Chinese Medicine. *Evidence-Based Complementary and Alternative Medicine*.

Piechocka, J., Wieczorek, M. & Głowacki, R. 2020. Gas Chromatography – Mass Spectrometry Based Approach for the Determination of Methionine-Related Sulfur-Containing Compounds in Human Saliva. *International Journal of Molecular Sciences*, 21(9252).

Puretec water. Basics of Reverse Osmosis. : 1–16.

Racar, M., Dolar, D., Karadaki, K., Č, N., Glumac, N., A, D. & Ko, K. 2020. Challenges of municipal wastewater reclamation for irrigation by MBR and NF/RO :Physico-chemical and microbiological parameters , and emerging contaminants. *Science of the Total Environment*, 722.

Ramdani, A., Deratani, A., Taleb, S., Drouiche, N. & Lounici, H. 2021. Performance of NF90 and NF270 commercial nanofiltration membranes in the defluoridation of Algerian brackish water. *Desalination and Water Treatment*, 212: 286–296.

Ramos, S., Homem, V. & Santos, L. 2020. Chemosphere Analytical methodology to screen UV- fi lters and synthetic musk compounds in market tomatoes. *Chemosphere*, 238:

124605. https://doi.org/10.1016/j.chemosphere.2019.124605.

Redding, A.M., Cannon, F.S., Snyder, S.A. & Vanderford, B.J. 2009. A QSAR-like analysis of the adsorption of endocrine disrupting compounds , pharmaceuticals , and personal care products on modified activated carbons. *Water Research*, 43(15): 3849–3861. http://dx.doi.org/10.1016/j.watres.2009.05.026.

Reza, A. & Chen, L. 2021. Optimization and Modeling of Ammonia Nitrogen Removal from High Strength Synthetic Wastewater Using Vacuum. *Processes*, 9(2059).

Rienzie, R., Ramanayaka, S. & Adassooriya, N.M. 2019. *12. Nanotechnology applications for the removal of environmental contaminants from pharmaceuticals and personal care products*. Elsevier Inc. http://dx.doi.org/10.1016/B978-0-12-816189-0.00012-3.

Roberts, J., Kumar, A., Du, J., Hepplewhite, C., Ellis, D.J., Christy, A.G. & Beavis, S.G. 2016. Pharmaceuticals and personal care products (PPCPs) in Australia' s largest inland sewage treatment plant , and its contribution to a major Australian river during high and low fl ow. *Science of the Total Environment*, 541: 1625–1637. http://dx.doi.org/10.1016/j.scitotenv.2015.03.145.

Sachit, D.E. & Veenstra, J.N. 2017. Foulant Analysis of Three RO Membranes Used in Treating Simulated Brackish Water of the Iraqi Marshes. *Membranes*, 7(23): 7–9.

Shen, J., Ding, T. & Zhang, M. 2019. *Analytical techniques and challenges for removal of pharmaceuticals and personal care products in water*. Elsevier Inc. http://dx.doi.org/10.1016/B978-0-12-816189-0.00010-X.

Siew, Y., Jye, W., Yeow, Y., Karaman, M. & Gürsoy, M. 2022. Eco-friendly surface modification approach to develop thin film nanocomposite membrane with improved desalination and antifouling properties. *Journal of Advanced Research*, 36: 39–49. https://doi.org/10.1016/j.jare.2021.06.011.

Silva, C.P., Emídio, E.S. & Marchi, M.R.R. De. 2013. UV Filters in Water Samples: Experimental Design on the SPE Optimization followed by GC-MS/MS Analysis. , 24(9): 1433–1441.

Stavrianidi, A. 2020. A classification of liquid chromatography mass spectrometry techniques for evaluation of chemical composition and quality control of traditional medicines. *Journal of Chromatography A*, 1609: 460501. https://doi.org/10.1016/j.chroma.2019.460501.

Sterlitech Corporation. 2017. Sepa CF cell assembly & operation manual.

Stone, J. 2017. *Chapter 3 - Sample preparation techniques for mass spectrometry in the clinical laboratory*. Elsevier Inc. http://dx.doi.org/10.1016/B978-0-12-800871-3/00003-1.

Strmecky, T., Dolar, D. & Košutic, K. 2016. Hybrid processes for treatment of landfill leachate : Coagulation/UF/NF-RO and ardsorption/UF/NF-RO. *Separation and Purification Technology*, 168: 39–46.

Sun, Q., Lv, M., Hu, A., Yang, X. & Yu, C. 2014. Seasonal variation in the occurrence and removal of pharmaceuticals and personal care products in a wastewater treatment plant in. *Journal of Hazardous Materials*, 277: 69–75. http://dx.doi.org/10.1016/j.jhazmat.2013.11.056.

Ternes, T., Joss, A. & Oehlmann, J. 2015. Occurrence , fate , removal and assessment of emerging contaminants in water in the water cycle (from wastewater to drinking water). *Water Research*, 2(72): 1–2.

Titus, D., Samuel, E.J.J. & Roopan, S.M. 2019. *Chapter 12 - Nanoparticle characterization techniques*. Elsevier Inc. https://doi.org/10.1016/B978-0-08-102579-6.00012-5.

Torres-rivero, K., Bastos-arrieta, J. & Fiol, N. 2021. *Metal and metal oxide nanoparticles : An integrated perspective of the green synthesis methods by natural products and waste valorization : applications and challenges*. 1st ed. Elsevier B.V. http://dx.doi.org/10.1016/bs.coac.2020.12.001.

Üstün, G.E., Solmaz, S.K.A., Çiner, F. & Bažkaya, H.S. 2011. Tertiary treatment of a secondary effluent by the coupling of coagulation-flocculation-disinfection for irrigation reuse. *Desalination*, 277(1–3): 207–212.

Vrijenhoek, E.M., Hong, S. & Elimelech, M. 2001. Influence of membrane surface properties on initial rate of colloidal fouling of reverse osmosis and nanofiltration membranes. , 188: 115–128.

Wang, J. 2014. *Transport and Removal Mechanisms of Trace Organic Pollutants by Nanofiltration and Reverse Osmosis Membranes*. University of California.

Wang, J., Mo, Y., Mahendra, S. & Hoek, E.M. V. 2014. Effects of water chemistry on structure and performance of polyamide composite membranes. *Journal of Membrane Science*, 452: 415–425. http://dx.doi.org/10.1016/j.memsci.2013.09.022.

Wang, J. & Wang, S. 2016. Removal of pharmaceuticals and personal care products (

PPCPs) from wastewater : A review. *Journal of Environmental Management*, 182: 620–640. http://dx.doi.org/10.1016/j.jenvman.2016.07.049.

Wang, W., Qi, M., Jia, X., Jin, J., Zhou, Q., Zhang, M., Zhou, W. & Li, A. 2019. Differential adsorption of zwitterionic PPCPs by multifunctional resins: The influence of the hydrophobicity and electrostatic potential of PPCPs. *Chemosphere*: 125023. https://doi.org/10.1016/j.chemosphere.2019.125023.

Wang, Y., Liu, J., Kang, D., Wu, C. & Wu, Y. 2017. Removal of pharmaceuticals and personal care products from wastewater using algae-based technologies : a review. *Reviews in Environmental Science and Bio/Technology*, 16(4): 717–735.

Wang, Y., Wang, X., Li, M., Dong, J., Sun, C. & Chen, G. 2018. Removal of Pharmaceutical and Personal Care Products (PPCPs) from Municipal Waste Water with Integrated Membrane Systems, MBR-RO/NF. *Environmental research and public health*, 15(269).

Wei, X., Bao, X., Wu, J., Li, C., Shi, Y., Chen, J. & Zhu, B. 2018. Typical pharmaceutical molecule removal behavior from water by positively and negatively charged composite hollow fi ber nano fi ltration membranes. *Royal Society of Chemistry advances*, 8: 10396–10408.

Wei, X., Shi, Y., Fei, Y., Chen, J., Lv, B., Chen, Y., Zheng, H., Shen, J. & Zhu, L. 2016. Removal of trace phthalate esters from water by thin-film composite nanofiltration hollow fiber membranes. *CHEMICAL ENGINEERING JOURNAL*, 292: 382–388. http://dx.doi.org/10.1016/j.cej.2016.02.037.

Wei, X., Xu, X., Li, C., Wu, J., Chen, J., Lv, B. & Wang, J. 2020. *Removal of Pharmaceuticals and Personal Care Products in Aquatic Environment by Membrane Technology*.

Wenning, R.J. & Martello, L. 2014. POPs in Marine and Freshwater Environments. In *Environmental Forensics for Persistent Organic Pollutants*. Elsevier B.V.: 357–390. http://dx.doi.org/10.1016/B978-0-444-59424-2.00008-6.

Wenten, I.G. & Khoiruddin. 2015. Reverse osmosis applications : Prospect and challenges. *Desalination*. http://dx.doi.org/10.1016/j.desal.2015.12.011.

Xu, H., Lu, G. & Xue, C. 2020. Effects of Sulfamethoxazole and 2-Ethylhexyl-4-Methoxycinnamate on the Dissimilatory Nitrate Reduction Processes and N2O Release in Sediments in the Yarlung Zangbo River. *International journal of Environmental Research and Public Health*, 17(1822).

Xu, R., Qin, W., Tian, Z., He, Y., Wang, X. & Wen, X. 2020. Science of the Total Environment Enhanced micropollutants removal by nano fi ltration and their environmental risks in wastewater reclamation : A pilot-scale study. *Science of the Total Environment*, 744: 140954. https://doi.org/10.1016/j.scitotenv.2020.140954.

Xu, Y., Liu, T., Zhang, Y., Ge, F., Steel, R.M. & Sun, L. 2017. personal care products removal. *Journal of Materials Chemistry A: Materials for energy and sustainability*, 5: 12001–12014. http://dx.doi.org/10.1039/C7TA03698A.

Zahbi, M. 2022. Basic Overview on Gas Chromatography and its Mechanism. *Pharmaceutical Analytical Chemistry*, 7(1): 1–2.

Zeeman, G., Buisman, C.J.N., Vieno, N., Temmink, H. & Hernandez Leal, L. 2010. Occurrence of Xenobiotics in Gray Water and Removal in Three Biological Treatment Systems. , 44(17): 6835–6842.

APPENDICES

Appendix A XLE experimental run and duplicate at pH 3

Table A-1: Operating conditions for XLE run and duplicate at pH 3 at 15°C

Run	
Initial permeate flux (L/m^2 hr):	76,60
Feed P_0 (bar)	10
Piston P (bar)	13
Feed velocity (Hz)	12,98
Brine pressure (Kpa)	95
Dimensions	14.5 cm x 9.5 cm
Area (m^2)	0,013775
pH	3±0,3
Temperature	15
Concentration (µg/l)	
MeP	451.9
TCS	450
EHMC	450

Table A-2: Experimental run for XLE at pH 3 at 15°C

	FEED			Brine		Permeate			.				
Time (min)	**EC F (µS)**	**TDS F (mg/L)**	**Temperature (° C)**	**EC (µS)**	**TDS (mg/L)**	**EC P (µS)**	**TDS P (mg/L)**	**Temperature (°C)**	**Time (hr)**	**Volume (L)**	**Flow Rate (l/h)**	**Flux (L/h m²)**	**% rejection**
0	368	184	13,1	365	183	36	18	15,9	0,0041667	0,0024	0,576	41,82	90,22
45	349	174	15,4	365	182	50	25	16,5	0,0041667	0,0026	0,624	45,3	85,67
90	314	157	14,7	329	165	40	20	16,6	0,0041667	0,0022	0,528	38,33	87,26
135	308	154	11,9	318	159	31	16	16,5	0,0041667	0,002	0,48	34,85	89,94
180	303	151	14	315	157	26	13	15,8	0,0041667	0,0022	0,528	38,33	91,42
225	373	186	16,2	396	198	46	23	16,6	0,0041667	0,0026	0,624	45,30	87,67
270	426	213	16,3	393	196	48	24	17,4	0,0041667	0,0028	0,672	48,78	88,73
315	380	190	17,2	401	200	50	25	17,6	0,0041667	0,0024	0,576	41,82	86,84
360	355	177	14,8	383	191	43	22	17,5	0,0041667	0,0022	0,528	38,33	87,89
405	348	174	16,1	368	184	36	18	17,2	0,0041667	0,0026	0,624	45,30	89,66
450	425	212	14,5	457	229	63	51	15,9	0,0041667	0,0022	0,528	38,33	85,18
495	396	198	16	420	210	48	24	16,5	0,0041667	0,002	0,48	34,85	87,88

Table A-3: Experimental duplicate for XLE at pH 3 at 15°C

	Feed			Brine		Permeate							
Time (min)	**EC F (µS)**	**TDS F (mg/L)**	**Temperature (° C)**	**EC (µS)**	**TDS (mg/L)**	**EC P (µS)**	**TDS P (mg/L)**	**Temperature (°C)**	**Time (hr)**	**Volume (L)**	**Flow Rate (l/h)**	**Flux (L/h m²)**	**% rejection**
0	403	201	14,8	431	215	73	36	16,6	0,0041667	0,002	0,48	34,85	81,886
45	409	201	15,9	432	216	74	37	16,8	0,0041667	0,002	0,48	34,85	81,907
90	368	184	15,9	391	195	58	29	16,6	0,0041667	0,002	0,48	34,85	84,239
135	349	175	15,1	372	186	51	25	16,5	0,0041667	0,0018	0,432	31,36	85,387
180	336	168	15	349	174	44	22	16,1	0,0041667	0,0018	0,432	31,36	86,905
225	406	203	14,9	429	213	72	36	16,5	0,0041667	0,0018	0,432	31,36	82,266
270	365	187	15,6	386	193	54	27	16,7	0,0041667	0,0018	0,432	31,36	85,205
315	345	173	15	366	183	48	24	16,1	0,0041667	0,0018	0,432	31,36	86,087
360	332	164	14,6	358	179	42	22	16,6	0,0041667	0,002	0,48	34,85	87,349
405	517	259	14,7	456	226	35	17	16,8	0,0041667	0,002	0,48	34,85	93,230
450	474	237	15,3	486	443	78	39	16,8	0,0041667	0,0024	0,576	41,81	83,544
495	449	224	15,7	444	222	78	39	16,7	0,0041667	0,0018	0,432	31,36	82,628

Table A-4: Operating conditions for XLE run and duplicate at pH 3 at 25°C

Run	
Initial permeate flux (L/m^2 hr)	76,60
Feed P_0 (bar)	10
Piston P (bar)	13
Feed velocity (Hz)	12,98
Brine p (Kpa)	95
Dimensions	14.5 cm x 9.5 cm
Area (m^2)	0,013775
Nomination	XLE
pH	3±0,3
Temperature	25
Concentration (µg/L)	
MeP	450
TCS	450
EHMC	450

Table A-5: Experimental run for XLE at pH 3 at 25°C

	Feed			Brine		Permeate							
Time (min)	**EC F (µS)**	**TDS F (mg/L)**	**Temperature (° C)**	**EC (µS)**	**TDS (mg/L)**	**EC P (µS)**	**TDS P (mg/L)**	**Temperature (°C)**	**Time (hr)**	**Volume (L)**	**Flow Rate (l/h)**	**Flux (L/h m^2)**	**% rejection**
0	375	186	24,9	371	185	60	30	20,2	0,0041667	0,0032	0,77	55,75	84
45	368	184	25,1	373	187	58	29	22,5	0,0041667	0,0038	0,91	66,21	84,24
90	369	185	25	388	185	60	30	22,1	0,0041667	0,0032	0,768	55,75	83,74
135	373	186	25	379	190	61	30	22,5	0,0041667	0,003	0,72	52,29	83,65
180	375	189	25,1	381	190	64	32	22,7	0,0041667	0,0028	0,672	48,78	82,93
225	378	189	25,1	384	192	69	34	21,7	0,0041667	0,0034	0,816	59,24	81,75
270	381	191	25,1	387	194	72	34	21,2	0,0041667	0,003	0,72	52,27	81,10
315	385	193	25,1	391	196	76	36	21,3	0,0041667	0,0036	0,864	62,72	80,26
360	390	195	25,1	397	199	80	40	21,5	0,0041667	0,0032	0,768	55,75	79,49
405	396	198	25,1	403	201	88	44	21,4	0,0041667	0,0034	0,816	59,24	77,78
450	399	199	25,1	407	203	93	46	21,3	0,0041667	0,0032	0,768	55,75	76,69
495	412	206	25	421	210	85	42	21,4	0,0041667	0,003	0,72	52,27	79,37

Table A-6: Experimental duplicate for XLE at pH 3 at 25°C

	Feed			Brine		Permeate							
Time (min)	**EC F (µS)**	**TDS F (mg/L)**	**Temperature (° C)**	**EC (µS)**	**TDS (mg/L)**	**EC P (µS)**	**TDS P (mg/L)**	**Temperature (°C)**	**Time (hr)**	**Volume (L)**	**Flow Rate (l/h)**	**Flux (L/h m^2)**	**% rejection**
0	538	269	25,2	541	270	89	45	21,7	0,0041667	0,0032	0,768	55,75	83,46
45	530	265	25,1	538	269	91	46	19,7	0,0041667	0,003	0,72	52,27	82,83
90	544	272	25,1	552	276	91	46	21,6	0,0041667	0,0032	0,768	55,75	83,27
135	545	273	25,1	554	277	95	48	21,7	0,0041667	0,003	0,72	52,27	82,57
180	542	271	25,1	551	276	98	49	21,2	0,0041667	0,003	0,72	52,27	81,92
225	550	275	25,1	563	282	105	52	21	0,0041667	0,0032	0,768	55,75	80,91
270	557	279	25,1	570	285	105	53	20,4	0,0041667	0,003	0,72	52,27	81,15
315	560	280	25	569	285	94	47	16,8	0,0041667	0,003	0,72	52,27	83,21
360	564	282	25,5	577	286	96	48	17,6	0,004	0,0032	0,768	55,75	82,98

									1667				
405	564	282	25,4	578	288	97	49	18,2	0,0041667	0,0034	0,816	59,24	82,80
450	566	283	25,3	580	290	98	49	18	0,0041667	0,0032	0,768	55,75	82,69
495	569	285	25,2	284	292	99	49	19,6	0,0041667	0,0032	0,768	55,75	82,60

Table A-7: Operating conditions for XLE run and duplicate at pH 3 at 35°C

Run	
Initial permeate flux (L/m^2 hr):	76,60
Feed P_0 (bar)	10
Piston P (bar)	13
Feed velocity (Hz)	12,98
Brine p (Kpa)	95
Dimensions	14.5 cm x 9.5 cm
Area (m^2)	0,013775
Nomination	XLE
pH	3±0,3
Temperature	35°C
Concentration (µg/L)	
MeP	450
TCS	450
EHMC	450

Table A-8: Experimental run for XLE at pH 3 at 35°C

	FEED			Brine		Permeate			.				
Time (min)	**EC F (µS)**	**TDS F (mg/L)**	**Temperature (°C)**	**EC (µS)**	**TDS (mg/L)**	**EC P (µS)**	**TDS P (mg/L)**	**Temperature (°C)**	**Time (hr)**	**Volume (L)**	**Flow Rate (l/h)**	**Flux (L/h m^2)**	**% rejection**
0	382	191	35,5	378	189	57	29	25,6	0,0041667	0,0038	0,912	66,21	85,08
45	386	193	35,3	387	193	65	32	25,6	0,0041667	0,004	0,96	69,69	83,16
90	390	195	35,2	387	194	65	33	27,2	0,0041667	0,004	0,96	69,69	83,33
135	390	195	35,2	389	195	78	39	26,9	0,0041667	0,0044	1,056	76,66	80,00
180	391	195	35,2	389	195	84	42	27,6	0,0041667	0,0042	1,008	73,18	78,52
225	388	194	35,2	389	195	87	44	28,2	0,0041667	0,004	0,96	69,69	77,58
270	390	195	35,2	392	196	92	46	25,9	0,0041667	0,0042	1,008	73,18	76,41
315	399	199	35,2	401	200	145	73	26,8	0,004	0,004	0,96	69,69	63,66

									1667				
360	401	200	35,3	402	201	149	74	27,4	0,0041667	0,0038	0,912	66,21	62,84
405	403	202	35,2	404	202	165	83	25,5	0,0041667	0,0042	1,008	73,18	59,06
450	407	204	35,2	407	203	160	80	26,2	0,0041667	0,0038	0,912	66,21	60,69
495	407	204	35,3	407	203	153	76	26,5	0,0041667	0,0042	1,008	73,18	62,41

Table A-9: Experimental duplicate for XLE at pH 3 at 35°C

	Feed			Brine		Permeate							
Time (min)	**EC F (µS)**	**TDS F (mg/L)**	**Temperature (°C)**	**EC (µS)**	**TDS (mg/L)**	**EC P (µS)**	**TDS P (mg/L)**	**Temperature (°C)**	**Time (hr)**	**Volume (L)**	**Flow Rate (l/h)**	**Flux (L/h m^2)**	**% rejection**
0	415	207	35,3	412	206	82	41	26,1	0,0041667	0,0046	1,104	80,15	80,24
45	413	207	35,2	416	208	72	36	26,5	0,0041667	0,0036	0,864	62,72	82,57
90	416	208	35,2	419	210	72	36	26	0,0041667	0,0046	1,104	80,15	82,69
135	416	208	35,2	420	210	73	37	25,8	0,0041667	0,0038	0,912	66,21	82,45
180	420	210	35,2	422	211	75	37	26,2	0,0041667	0,004	0,96	69,69	82,14
225	422	211	35,2	424	212	77	39	25,2	0,0041667	0,0036	0,864	62,72	81,75
270	430	215	35,2	431	216	86	43	25	0,0041667	0,0048	1,152	83,63	80,00
315	428	214	35,2	432	216	85	43	24,9	0,0041667	0,0038	0,912	66,21	80,14
360	428	214	35,2	433	217	87	43	25,4	0,0041667	0,0036	0,864	62,72	79,67

405	436	218	35,2	440	220	88	44	27,2	0,0041667	0,0032	0,768	55,75	79,82
450	437	219	35,2	442	221	92	46	26,3	0,0041667	0,0036	0,864	62,72	78,95
495	439	220	35,3	445	223	91	46	24,5	0,0041667	0,0036	0,864	62,72	79,27

Appendix B XLE experimental run and duplicate at pH 6

Table B-1: Operating conditions for XLE run and duplicate at pH 6 at 15°C

Initial permeate flux (L/m² hr):	76,60
Feed P_0 (bar)	10
Piston P (bar)	13
Feed velocity (Hz)	12,98
Brine p (Kpa)	95
Dimensions	14.5 cm x 9.5 cm
Area (m²)	0,013775
Nomination	XLE
pH	6±0,3
Temperature	15°C
Concentration	
MeP	451,9
TCS	450
EHMC	450

Table B-2: Experimental run for XLE at pH 6 at 15°C

	FEED			Brine		Permeate			.				
Time (min)	**EC F (µS)**	**TDS F (mg/L)**	**Temperature (°C)**	**EC (µS)**	**TDS (mg/L)**	**EC P (µS)**	**TDS P (mg/L)**	**Temperature (°C)**	**Time (hr)**	**Volume (L)**	**Flow Rate (l/h)**	**Flux (L/h m^2)**	**% rejection**
0	193	97	15,9	195	97	33	17	17,4	0,0041667	0,0024	0,576	41,81	82,90
45	195	97	15,4	198	97	9	5	17,1	0,0041667	0,0022	0,528	38,33	95,38
90	194	97	14,8	196	98	29	14	17	0,0041667	0,0024	0,576	41,81	85,05
135	196	98	14,4	197	98	34	17	17,6	0,0041667	0,0024	0,576	41,81	82,65
180	201	100	15,6	203	101	40	20	17,4	0,0041667	0,0026	0,624	45,30	80,10
225	193	96	15,4	196	98	33	16	17,2	0,0041667	0,0028	0,672	48,78	82,90
270	191	95	14,9	194	97	38	19	17,4	0,0041667	0,0026	0,624	45,30	80,10
315	195	97	15,4	196	98	37	18	17,4	0,0041667	0,0024	0,576	41,81	81,03

360	196	98	15	197	98	31	16	17,4	0,004 1667	0,0024	0,576	41,81	84,18
405	195	97	15,1	196	98	27	14	17,3	0,004 1667	0,0022	0,528	38,33	86,15
450	195	98	15	198	99	22	11	17,2	0,004 1667	0,0024	0,576	41,81	88,72
495	196	98	15,6	198	99	23	12	17,2	0,004 1667	0,0022	0,528	38,33	88,27

Table B-3: Experimental duplicate for XLE at pH 6 at 15°C

	Feed			Brine		Permeate							
Time (min)	EC	TDS	Temp	EC	TDS	EC	TDS	Temperature (°C)	Time(hr)	Volume	Flow rate	Flux	Rejection
0	404	202	15,5	414	207	22	11	19,1	0,0041667	0,0022	0,528	38,33	94,55
45	411	205	15,2	413	206	7	3	18,5	0,0041667	0,0018	0,432	31,36	98,30
90	410	205	15,3	412	206	5	2	18,4	0,0041667	0,0022	0,528	38,33	98,78
135	409	204	14,9	413	206	9	4	18,3	0,0041667	0,0024	0,576	41,81	97,80
180	410	205	14,1	414	207	33	16	18,2	0,0041667	0,0022	0,528	38,33	91,95
225	415	207	14,6	417	208	50	25	18,1	0,0041667	0,0024	0,576	41,81	87,95
270	418	208	15,2	418	209	50	25	18,2	0,0041667	0,0024	0,576	41,81	88,04
315	415	207	15,7	418	209	44	22	18,1	0,0041667	0,0026	0,624	45,30	89,40
360	417	208	14,6	419	209	42	21	18	0,0041667	0,0026	0,624	45,30	89,93
405	419	209	15,5	422	211	50	25	17,9	0,0041667	0,0022	0,528	38,33	88,07
450	422	211	14,4	422	211	52	26	18	0,0041667	0,002	0,48	34,85	87,68
495	421	211	15,1	423	211	52	26	17,9	0,0041667	0,002	0,48	34,85	87,65

Table B-4: Operating conditions for XLE run and duplicate at pH 6 at 35°C

Run	
Initial permeate flux (L/m² hr):	76,60
Feed P_0 (bar)	10
Piston P (bar)	13
Feed velocity (Hz)	12,98
Brine p (Kpa)	95
Dimensions	14.5 cm x 9.5 cm
Area (m²)	0,013775
Nomination	XLE
pH	6±0,3
Temperature	35°C
Concentration(µg/L)	
MeP	459,62
TCS	457,5
EHMC	450

Table B-5: Experimental run for XLE at pH 6 at 35°C

	FEED			Brine		Permeate			.				
Time (min)	**EC F (µS)**	**TDS F (mg/L)**	**Temperature (°C)**	**EC (µS)**	**TDS (mg/L)**	**EC P (µS)**	**TDS P (mg/L)**	**Temperature (°C)**	**Time (hr)**	**Volume (L)**	**Flow Rate (l/h)**	**Flux (L/h m^2)**	**% rejection**
0	255	127	35,5	254	127	8	4	25,6	0,0041667	0,0048	1,152	83,63	96,86
45	261	130	35,1	258	129	6	3	27,5	0,0041667	0,0042	1,008	73,18	97,70
90	265	133	35,2	263	132	37	19	26,8	0,0041667	0,0058	1,392	101,05	86,04
135	273	137	35,2	272	137	46	23	29	0,0041667	0,0052	1,248	90,60	83,15
180	273	137	35,2	273	137	44	22	29,1	0,0041667	0,005	1,2	87,11	83,88
225	280	140	35,3	278	139	34	17	27,8	0,0041667	0,0052	1,248	90,60	87,86
270	285	142	35,4	283	142	28	14	27,1	0,0041667	0,0048	1,152	83,63	90,18
315	290	145	34,8	287	144	20	10	25,2	0,0041667	0,005	1,2	87,11	93,10

360	285	143	35,1	283	143	15	8	27	0,0041667	0,005	1,2	87,11	94,74
405	285	143	34,9	284	142	13	7	26	0,0041667	0,0046	1,104	80,15	95,44
450	284	142	35,5	280	140	12	6	28	0,0041667	0,0042	1,008	73,18	95,77
495	282	141	35,2	280	140	12	6	26	0,0041667	0,0046	1,104	80,15	95,74

Table B-6: Experimental duplicate for XLE at pH 6 at 35°C

	Feed			Brine		Permeate							
Time (min)	**EC**	**TDS**	**Temp**	**EC**	**TDS**	**EC**	**TDS**	**Temperature**	**Time (hr)**	**Volume (L)**	**Flow Rate (l/h)**	**Flux (L/h m^2)**	**% rejection**
0	251	125	35,3	248	124	14	17	24,6	0,0041667	0,0042	1,008	73,18	94,42
45	252	126	34,9	250	125	6	3	27,7	0,0041667	0,0038	0,912	66,21	97,62
90	257	128	35,3	254	127	8	4	25,6	0,0041667	0,0038	0,912	66,21	96,89
135	265	132	35	262	131	16	8	27	0,0041667	0,004	0,96	69,69	93,96
180	265	132	35,4	261	131	24	12	26,2	0,0041667	0,0036	0,864	62,72	90,94
225	257	129	35,2	253	127	21	11	27	0,0041667	0,0034	0,816	59,24	91,83
270	260	130	34,6	252	126	21	11	24,5	0,0041667	0,003	0,72	52,27	91,92
315	252	126	35,1	250	125	21	11	26,6	0,0041667	0,0034	0,816	59,24	91,67
360	247	123	35,2	244	122	20	10	26	0,0041667	0,0032	0,768	55,75	91,90
405	258	129	35,2	255	127	26	13	26,7	0,0041667	0,0032	0,768	55,75	89,92
450	252	126	35,2	245	123	32	16	27,5	0,0041667	0,0032	0,768	55,75	87,30
495	253	126	35,1	251	125	47	23	27	0,0041667	0,0034	0,816	59,24	81,42

Appendix C XLE experimental run and duplicate at pH 10

Table C-1: Operating conditions for XLE run and duplicate at pH 10 at 15°C

Initial permeate flux (L/m² hr)	76,60
Feed P_0 (bar)	10
Piston P (bar)	13
Feed velocity (Hz)	12,98
Brine p (Kpa)	95
Dimensions	14.5 cm x 9.5 cm
Area (m²)	0,013775
Nomination	XLE
pH	10±0,3
Temperature(°C)	15
Concentration (µg/L)	
MeP	453,85
TCS	451,92
EHMC	450

Table C-2: Experimental run for XLE at pH 10 at 15°C

	Feed			Brine		Permeate							
Time (min)	**EC**	**TDS**	**Temperature**	**EC**	**TDS**	**EC**	**TDS**	**Temperature**	**Time (hr)**	**Volume (L)**	**Flow Rate (l/h)**	**Flux (L/h m^2)**	**% rejection**
0	218	109	15,6	219	110	52	26	17,2	0,0041667	0,0024	0,576	41,81	76,15
45	214	107	11,7	215	108	49	24	17,2	0,0041667	0,0018	0,432	31,36	77,10
90	215	107	15	216	108	51	25	17,8	0,0041667	0,002	0,48	34,85	76,28
135	216	108	15	218	108	50	25	17,3	0,0041667	0,002	0,48	34,85	76,85
180	214	107	14,9	216	108	47	23	17,1	0,0041667	0,0022	0,528	38,33	78,04
225	215	107	15,1	218	108	50	25	17,2	0,0041667	0,0022	0,528	38,33	76,74
270	216	108	15,6	217	109	49	24	17,6	0,0041667	0,0022	0,528	38,33	77,31
315	215	108	15,9	217	109	48	24	17,9	0,0041667	0,002	0,48	34,85	77,67
360	217	108	15,1	219	109	48	24	18,7	0,0041667	0,0024	0,576	41,81	77,88
405	219	109	15,9	219	110	45	23	18,3	0,0041667	0,0022	0,528	38,33	79,45
450	219	109	17	220	110	45	22	18,5	0,0041667	0,0022	0,528	38,33	79,45
495	217	109	14,9	221	110	44	22	18,5	0,004166667	0,002	0,48	34,85	79,72

Table C-3: Experimental duplicate for XLE at pH 10 at 15°C

	FEED			Brine		Permeate			.				
Time (min)	**EC F (µS)**	**TDS F (mg/L)**	**Temperature (°C)**	**EC (µS)**	**TDS (mg/L)**	**EC P (µS)**	**TDS P (mg/L)**	**Temperature (°C)**	**Time (hr)**	**Volume (L)**	**Flow Rate (l/h)**	**Flux (L/h m^2)**	**% rejection**
0	301	151	15,4	302	151	39	19	18,1	0,0041667	0,0028	0,672	48,78	87,04
45	302	151	16	303	151	48	24	18,7	0,0041667	0,0026	0,624	45,30	84,11
90	301	150	16	305	153	50	25	18,5	0,0041667	0,003	0,72	52,27	83,39
135	316	158	16	319	160	41	20	17,8	0,0041667	0,0032	0,768	55,75	87,03
180	315	158	14,5	320	160	47	24	17,5	0,0041667	0,0026	0,624	45,30	85,08
225	318	159	14,9	320	160	49	25	17,5	0,0041667	0,0024	0,576	41,81	84,59
270	319	160	15,4	320	160	48	24	17,6	0,0041667	0,0028	0,672	48,78	84,95
315	320	160	14,4	321	160	47	24	17,5	0,0041667	0,0026	0,624	45,30	85,31

360	320	160	14,9	322	161	44	22	17,2	0,004 1667	0,003	0,72	52,27	86,25
405	321	160	15	323	161	45	22	17,5	0,004 1667	0,0028	0,672	48,78	85,98
450	320	160	13,9	321	161	44	22	17,1	0,004 1667	0,0024	0,576	41,81	86,25
495	322	161	14,8	323	162	43	22	17,7	0,004 1667	0,0022	0,528	38,33	86,65

Table C-4: Operating conditions for XLE run and duplicate at pH 10 at 25°C

Run	
Initial permeate flux (L/m² hr)	76,60
Feed P_0 (bar)	10
Piston P (bar)	13
Feed velocity (Hz)	12,98
Brine p (Kpa)	95
Dimensions	14.5 cm x 9.5 cm
Area (m²)	0,013775
Nomination	XLE
pH	10±0,3
Temperature(°C)	25
Concentration(µg/L)	
MeP	459,62
TCS	457,6
EHMC	450

Table C-5: Experimental run for XLE at pH 10 at 25°C

	FEED			Brine		Permeate			.				
Time (min)	**EC F (µS)**	**TDS F (mg/L)**	**Temperature (°C)**	**EC (µS)**	**TDS (mg/L)**	**EC P (µS)**	**TDS P (mg/L)**	**Temperature (°C)**	**Time (hr)**	**Volume (L)**	**Flow Rate (l/h)**	**Flux (L/h m^2)**	**% rejection**
0	302	151	25,5	293	147	35	17	21,3	0,0041667	0,0022	0,528	38,33	88,41
45	284	142	24,8	283	142	56	28	19,3	0,0041667	0,0022	0,528	38,33	80,28
90	283	142	25,2	285	143	74	37	22	0,0041667	0,003	0,72	52,27	73,85
135	340	170	25,6	337	169	73	37	21,4	0,0041667	0,0028	0,672	48,78	78,53
180	333	167	25,6	333	166	65	33	21,5	0,0041667	0,003	0,72	52,27	80,48
225	405	202	25,2	401	200	68	34	22	0,0041667	0,0028	0,672	48,78	83,21
270	399	199	25,2	399	199	62	31	20,3	0,0041667	0,0028	0,672	48,78	84,46
315	401	200	24,7	399	199	50	25	20,8	0,0041667	0,003	0,72	52,27	87,53

360	477	239	24,3	474	239	59	30	21,4	0,004 1667	0,0024	0,576	41,81	87,63
405	477	238	24,5	477	238	57	28	21,4	0,004 1667	0,0026	0,624	45,30	88,05
450	558	279	25,2	554	277	61	30	20,9	0,004 1667	0,0026	0,624	45,30	89,07
495	548	274	25,6	545	272	54	27	21,9	0,004 1667	0,0024	0,576	41,81	90,15

Table C-6: Experimental duplicate for XLE at pH 10 at 25°C

	Feed			Brine		Permeate							
Time (min)	**EC**	**TDS**	**Temperature (°C)**	**EC**	**TDS**	**EC**	**TDS**	**Temp**	**Time (hr)**	**Volume**	**Flow Rate (l/h)**	**Flux (L/h m²)**	**rejection**
0	384	192	24,9	378	189	56	33	21,3	0,0041667	0,0024	0,576	41,81	85,42
45	375	187	25,2	372	186	55	28	20,8	0,0041667	0,0026	0,624	45,30	85,33
90	375	187	24,8	376	188	42	21	20,5	0,0041667	0,0026	0,624	45,30	88,80
135	386	193	24,6	388	194	29	15	21,3	0,0041667	0,0028	0,672	48,78	92,49
180	484	242	24,6	483	242	46	23	21,1	0,0041667	0,0028	0,672	48,78	90,50
225	507	253	24,9	506	253	44	22	20,5	0,0041667	0,0026	0,624	45,30	91,32
270	507	253	25,2	507	254	45	22	20,9	0,0041667	0,0026	0,624	45,30	91,12
315	669	334	25	662	339	74	37	21,7	0,0041667	0,0026	0,624	45,30	88,94
360	643	321	24,9	641	320	73	37	20,7	0,0041667	0,0022	0,528	38,33	88,65
405	634	317	24,8	631	316	71	36	20,6	0,0041667	0,0026	0,624	45,30	88,80
450	621	311	25,1	619	309	61	30	21,1	0,0041667	0,0024	0,576	41,81	90,18
495	624	312	25,3	621	311	60	30	20,1	0,0041667	0,0032	0,768	55,75	90,38

Table C-7: Operating conditions for XLE run and duplicate at pH 10 at 35°C

Run	
Initial permeate flux (L/m^2 hr):	76,60
Feed P_0 (bar)	10
Piston P (bar)	13
Feed velocity (Hz)	12,98
Brine p (Kpa)	95
Dimensions	14.5 cm x 9.5 cm
Area (m^2)	0,013775
Nomination	XLE
pH	10±0,3
Temperature(°C)	35
Concentration(µg/L)	
MeP	478,85
TCS	453,85
EHMC	450

Table C-8: Experimental run for XLE at pH 10 at 35°C

	Feed			Brine		Permeate			.				
Time (min)	**EC F (µS)**	**TDS F (mg/L)**	**Temperature (°C)**	**EC (µS)**	**TDS (mg/L)**	**EC P (µS)**	**TDS P (mg/L)**	**Temperature (°C)**	**Time (hr)**	**Volume (L)**	**Flow Rate (l/h)**	**Flux (L/h m^2)**	**% rejection**
0	292	147	34,6	291	146	85	42	20,6	0,0041667	0,0048	1,152	83,63	70,89
45	280	140	35,5	276	138	53	27	24,9	0,0041667	0,0044	1,056	76,66	81,07
90	296	148	34,6	293	147	48	24	24,8	0,0041667	0,0044	1,056	76,66	83,78
135	325	163	35,4	321	160	50	25	27,7	0,0041667	0,0044	1,056	76,66	84,62
180	365	182	35,1	360	180	49	25	25,9	0,0041667	0,004	0,96	69,69	86,58
225	449	224	35,2	442	221	56	28	27,9	0,0041667	0,0038	0,912	66,21	87,53
270	433	217	35,2	427	213	55	28	23,1	0,0041667	0,0044	1,056	76,66	87,30
315	424	212	35,2	416	208	43	21	25,4	0,0041667	0,004	0,96	69,69	89,86

360	484	242	35,2	479	240	46	23	28	0,004 1667	0,0038	0,912	66,21	90,50
405	529	264	35,3	513	259	45	22	25,9	0,004 1667	0,004	0,96	69,69	91,49
450	557	278	35,3	551	276	40	20	28,7	0,004 1667	0,0038	0,912	66,21	92,82
495	555	277	35,3	546	273	35	17	27,5	0,004 1667	0,004	0,96	69,69	93,69

Table C-9: Experimental run for XLE at pH 10 at 35°C

	Feed			Brine		Permeate							
Time (min)	**EC F (µS)**	**TDS F (mg/L)**	**Temperature (°C)**	**EC (µS)**	**TDS (mg/L)**	**EC P (µS)**	**TDS P (mg/L)**	**Temperature (°C)**	**Time (hr)**	**Volume (L)**	**Flow Rate (l/h)**	**Flux (L/h m^2)**	**% rejection**
0	383	191	35,2	369	185	70	35	22,8	0,004 1667	0,0046	1,104	80,15	81,72
45	356	178	34,8	351	175	58	29	26,7	0,004 1667	0,0044	1,056	76,66	83,71
90	347	174	34,7	346	173	52	26	29,1	0,004 1667	0,004	0,96	69,69	85,01
135	353	176	34,9	350	175	45	23	29,2	0,004 1667	0,0045	1,08	78,40	87,25

180	369	184	34,7	365	183	56	28	27,7	0,004 1667	0,0038	0,912	66,21	84,82
225	517	259	34,7	505	252	72	36	27,8	0,004 1667	0,0036	0,864	62,72	86,07
270	499	250	35,1	492	246	61	31	26,4	0,004 1667	0,0034	0,816	59,24	87,78
315	481	290	35,1	469	284	64	32	27,5	0,004 1667	0,0034	0,816	59,24	86,69
360	568	282	35	557	279	54	27	28,4	0,004 1667	0,004	0,96	69,69	90,49
405	641	320	35,1	633	316	56	28	28,4	0,004 1667	0,0034	0,816	59,24	91,26
450	636	318	35,1	626	313	52	26	25,6	0,004 1667	0,0034	0,816	59,24	91,82
495	688	344	35,3	675	338	52	26	26,3	0,004 1667	0,0032	0,768	55,75	92,44
540	680	340	35,2	672	336	50	25	25,2	0,004 1667	0,0036	0,864	62,72	92,65

Appendix D NF270 experimental run and duplicate at pH 3

Table D-1: Operating conditions for NF270 run and duplicate at pH 3 at 15°C

Run	
Initial permeate flux (L/m^2 hr):	76,60
Feed P_0 (bar)	10
Piston P (bar)	13
Feed velocity (Hz)	12,98
Brine p (Kpa)	95
Dimensions	14.5 cm x 9.5 cm
Area (m^2)	0,013775
Nomination	NF70
pH	3±0,3
Temperature(°C)	15
Concentration(µg/L)	
MeP	453,85/450
TCS	451,92
EHMC	450

Table D-2: Experimental run for NF270 at pH 3 at 15°C

	FEED			Brine		Permeate			.				
Time (min)	**EC F (µS)**	**TDS F (mg/L)**	**Temperature (°C)**	**EC (µS)**	**TDS (mg/L)**	**EC P (µS)**	**TDS P (mg/L)**	**Temperature (°C)**	**Time (hr)**	**Volume (L)**	**Flow Rate (l/h)**	**Flux (L/h m^2)**	**% rejection**
0	1589	793	15,3	1571	786	1052	531	16,4	0,0041667	0,0078	1,872	135,898	33,79
45	1867	933	15,1	1852	926	779	389	16,8	0,0041667	0,006	1,44	104,537	58,28
90	2372	1186	15,3	2347	1174	1619	809	17,2	0,0041667	0,0076	1,824	132,414	31,75
135	2069	1033	15,3	2063	1032	1469	750	17,8	0,0041667	0,0074	1,776	128,929	29,00
180	1954	977	15,1	1935	968	1420	710	18,3	0,0041667	0,007	1,68	121,960	27,33
225	2877	1439	15,3	2840	1420	2232	1115	18,6	0,0041667	0,008	1,92	139,383	22,42
270	2720	1360	15,7	2711	1356	2077	1039	18,2	0,0041667	0,0066	1,584	114,991	23,64
315	2627	1314	14,3	2628	1314	1952	974	17,5	0,004	0,0068	1,632	118,475	25,69

									1667				
360	2545	1273	15,1	2536	1268	1925	961	18,1	0,004 1667	0,0056	1,344	97,568	24,36
405	2492	1246	14,9	2471	1236	1900	951	17,7	0,004 1667	0,0054	1,296	94,083	23,76
450	2426	1213	15,7	2411	1209	1809	905	17,9	0,004 1667	0,0058	1,392	101,053	25,43
495	2371	1189	15,1	2386	1193	1771	886	18,1	0,004 1667	0,0052	1,248	90,599	25,31

Table D-3: Experimental duplicate for NF270 at pH 3 at 15°C

	Feed			Brine		Permeate							
Time (min)	**EC**	**TDS**	**Temperature(°C)**	**EC**	**TDS**	**EC**	**TDS**	**Temperature(°C)**	**Time (hr)**	**Volume (L)**	**Flow Rate (l/h)**	**Flux (L/h m^2)**	**% rejection**
0	3883	1942	15,7	3866	1933	2609	1301	17,4	0,0041667	0,0068	1,632	118,48	32,81
45	3717	1863	14,8	3720	1860	2619	1310	17,2	0,0041667	0,0066	1,584	114,99	29,54
90	3606	1801	15,3	3605	1802	2491	1245	17,1	0,0041667	0,0066	1,584	114,99	30,92
135	3535	1765	14,7	3521	1761	2454	1227	17,3	0,0041667	0,0054	1,296	94,08	30,58
180	3436	1723	15,4	3442	1721	2245	1125	17,7	0,0041667	0,0056	1,344	97,57	34,66
225	3385	1695	15,3	3390	1695	2251	1126	17,7	0,0041667	0,0058	1,392	101,05	33,50
270	3356	1683	13,5	3359	1680	2189	1095	17,5	0,0041667	0,0052	1,248	90,60	34,77
315	335	167	14,8	336	168	218	109	17,6	0,00416	0,0052	1,248	90,60	34,90

	2	6		0	0	2	2		67				
360	3251	1628	16,2	3251	1626	2174	1087	18,1	0,0041667	0,0056	1,344	97,57	33,13
405	3204	1604	16,4	3196	1598	2112	1057	17,9	0,0041667	0,0062	1,488	108,02	34,08
450	3049	1526	14,1	3048	1525	1926	963	17,8	0,0041667	0,0056	1,344	97,57	36,83
495	3038	1524	15,2	2998	1499	1876	939	18	0,0041667	0,0066	1,584	114,99	38,25

Table D-4: Operating conditions for run and duplicate of NF270 at pH 3 at 25°C

Run	
Initial permeate flux (L/m^2 hr):	76,60
Feed P_0 (bar)	10
Piston P (bar)	13
Feed velocity (Hz)	12,98
Brine p (Kpa)	95
Dimensions	14.5 cm x 9.5 cm
Area (m^2)	0,013775
Nomination	NF270
pH	3±0,3
Temperature(°C)	
Concentration(µg/L)	
MeP	457,6
TCS	457,6
EHMC	450

Table D-5: Experimental run for NF270 at pH 3 at 25°C

	FEED			Brine		Permeate			.				
Time (min)	**EC F (µS)**	**TDS F (mg/L)**	**Temperature (°C)**	**EC (µS)**	**TDS (mg/L)**	**EC P (µS)**	**TDS P (mg/L)**	**Temperature (°C)**	**Time (hr)**	**Volume (L)**	**Flow Rate (l/h)**	**Flux (L/h m²)**	**Rejection(%)**
0	407	203	25,2	406	203	142	71	22,3	0,0041667	0,0076	1,824	132,41	65,11
45	404	202	25,4	407	203	150	75	22,7	0,0041667	0,008	1,92	139,38	62,87
90	404	202	25,2	409	204	156	78	22,6	0,0041667	0,0078	1,872	135,90	61,39
135	400	200	25	393	198	141	72	22,4	0,0041667	0,0092	2,208	160,29	64,75
180	403	201	25,2	412	206	156	78	22	0,0041667	0,008	1,92	139,38	61,29
225	405	203	25,3	414	207	170	85	22,2	0,0041667	0,0074	1,776	128,93	58,02
270	404	202	25,4	415	208	173	86	22,9	0,0041667	0,0076	1,824	132,41	57,18
315	407	203	25,4	417	209	171	86	23,1	0,0041667	0,0074	1,776	128,93	57,99
360	408	204	25,3	420	210	175	88	22,6	0,004	0,0072	1,728	125,44	57,11

									1667				
405	410	205	25,5	420	210	186	93	22,6	0,004 1667	0,007	1,68	121,96	54,63
450	417	208	25,2	423	212	192	96	22,8	0,004 1667	0,006	1,44	104,54	53,96
495	416	208	25,2	423	213	197	99	22,5	0,004 1667	0,0062	1,488	108,02	52,64

Table D-6: Experimental duplicate for NF270 at pH 3 at 25°C

	Feed			Brine		Permeate							
Time (min)	**EC F (µS)**	**TDS F (mg/L)**	**Temperature (°C)**	**EC (µS)**	**TDS (mg/L)**	**EC P (µS)**	**TDS P (mg/L)**	**Temperature (°C)**	**Time (hr)**	**Volume (L)**	**Flow Rate (l/h)**	**Flux (L/h m^2)**	**% rejection**
0	402	201	24,8	412	206	159	79	22,2	0,0041667	0,0094	2,256	163,77	60,45
45	402	201	24,8	412	206	157	79	22,8	0,0041667	0,008	1,92	139,38	60,95
90	409	204	25,1	419	209	161	81	22,5	0,0041667	0,0082	1,968	142,87	60,64
135	412	206	25	420	210	167	83	22,6	0,0041667	0,0072	1,728	125,44	59,47
180	415	208	25	424	212	173	86	22,3	0,0041667	0,0074	1,776	128,93	58,31
225	419	210	25	427	214	176	88	22,7	0,0041667	0,007	1,68	121,96	58,00
270	422	212	25	428	214	180	90	22,7	0,0041667	0,0068	1,632	118,48	57,35
315	426	214	25	432	216	183	93	22,6	0,004	0,007	1,68	121,96	57,04

									1667				
360	432	216	25	436	219	192	98	22,5	0,0041667	0,007	1,68	121,96	55,56
405	436	218	25	445	223	204	102	22,6	0,0041667	0,007	1,68	121,96	53,21
450	438	219	25	446	223	215	107	22,8	0,0041667	0,0062	1,488	108,02	50,91
495	446	223	25,1	454	227	227	113	21,8	0,0041667	0,006	1,44	104,54	49,10

Table D-7: Operating conditions for run and duplicate of NF270 at pH 3 and 35°C

Run	
Initial permeate flux (L/m^2 hr):	76,60
Feed P_0 (bar)	10
Piston P (bar)	13
Feed velocity (Hz)	12,98
Brine p (Kpa)	95
Dimensions	14.5 cm x 9.5 cm
Area (m^2)	0,013775
Nomination	NF270
pH	3±0,3
Temperature(°C)	35
Concentration(µg/L)	
MeP	457,6/ 451,9
TCS	457,6/450
EHMC	450

Table D-8: Experimental run for NF270 at pH 3 at 35°C

	FEED			**Brine**		**Permeate**			.				
Time (min)	**EC F (µS)**	**TDS F (mg/L)**	**Temperature (°C)**	**EC (µS)**	**TDS (mg/L)**	**EC P (µS)**	**TDS P (mg/L)**	**Temperature (°C)**	**Time (hr)**	**Volume (L)**	**Flow Rate (l/h)**	**Flux (L/h m^2)**	**% rejection**
0	427	213	34,9	442	221	220	110	28,9	0,0041667	0,012	2,88	209,07	48,48
45	436	218	34,7	443	221	229	114	28	0,0041667	0,014	3,36	243,92	47,48
90	440	220	35	447	223	242	121	27,2	0,0041667	0,01	2,4	174,23	45,00
135	443	221	35,3	449	224	244	122	27,5	0,0041667	0,0084	2,016	146,35	44,92
180	450	225	35,1	452	226	254	127	27,9	0,0041667	0,0088	2,112	153,32	43,56
225	458	229	35,1	462	231	260	130	28,2	0,0041667	0,0082	1,968	142,87	43,23
270	460	230	35,2	464	232	277	138	28,9	0,0041667	0,0088	2,112	153,32	39,78
315	467	233	35,1	473	236	291	146	27,1	0,004	0,0084	2,016	146,35	37,69

									1667				
360	470	235	35,1	472	236	288	144	27,6	0,0041667	0,008	1,92	139,38	38,72
405	475	238	35	475	238	293	146	27,6	0,0041667	0,0074	1,776	128,93	38,32
450	476	237	35	476	238	286	143	27,8	0,0041667	0,0076	1,824	132,41	39,92
495	475	238	35	477	238	292	146	27,6	0,0041667	0,0074	1,776	128,93	38,53

Table D-9: Experimental duplicate for NF270 at pH 3 at 35°C

	Feed			Brine		Permeate							
Time (min)	**EC (µS)**	**TDS (mg/L)**	**Temperature (°C)**	**EC (µS)**	**TDS (mg/L)**	**ECP (µS)**	**TDSP (mg/L)**	**Temperature (°C)**	**Time (hr)**	**Volume (L)**	**Flow Rate (l/h)**	**Flux (L/h m²)**	**% rejection**
0	390	195	35,2	396	198	180	90	25,9	0,0041667	0,013	3,12	226,50	53,85
45	389	195	35,3	395	197	196	98	28,1	0,0041667	0,013	3,12	226,50	49,61
90	390	195	35,2	396	198	197	99	27,9	0,0041667	0,01	2,4	174,23	49,49
135	394	197	35,2	396	198	200	100	28	0,0041667	0,0076	1,824	132,41	49,24
180	396	198	35,2	400	200	202	101	28	0,0041667	0,008	1,92	139,38	48,99
225	395	198	35,2	401	200	210	105	27,6	0,0041667	0,0074	1,776	128,93	46,84
270	401	200	35,1	402	201	221	110	27,9	0,0041667	0,007	1,68	121,96	44,89
315	408	204	35,2	410	205	224	112	25,2	0,0041667	0,0066	1,584	114,99	45,10

360	408	204	35,1	410	205	222	111	26,1	0,0041667	0,006	1,44	104,54	45,59
405	410	205	35	411	205	228	114	25,6	0,0041667	0,006	1,44	104,54	44,39
450	410	205	35,1	411	206	226	113	27	0,0041667	0,006	1,44	104,54	44,88
495	407	203	35,1	414	207	234	117	26,3	0,0041667	0,006	1,44	104,54	42,51

Appendix E NF270 experimental run and duplicate at pH 6

Table E-1: Operating conditions for run and duplicate of NF270 at pH 6 at 15°C

Run	
Initial permeate flux (L/m^2 hr):	76,60
Feed P_0 (bar)	10
Piston P (bar)	13
Feed velocity (Hz)	12,98
Brine p (Kpa)	95
Dimensions	14.5 cm x 9.5 cm
Area (m^2)	0,013775
Nomination	NF270
pH	6±0,3
Temperature (°C)	15
Concentration(µg/L)	
MeP	463,46/ 459,62
TCS	459,62/ 451,92
EHMC	450

Table E-2: Experimental run for NF270 at pH 6 at 15°C

	FEED			Brine		Permeate			.				
Time (min)	**EC F (µS)**	**TDS F (mg/L)**	**Temperature (°C)**	**EC (µS)**	**TDS (mg/L)**	**EC P (µS)**	**TDS P (mg/L)**	**Temperature (°C)**	**Time (hr)**	**Volume (L)**	**Flow Rate (l/h)**	**Flux (L/h m²)**	**Rejection(%)**
0	220	110	15,7	221	110	27	13	17,7	0,0041667	0,0062	1,488	108,022	87,73
45	224	112	15,3	224	112	25	13	17,3	0,0041667	0,0066	1,584	114,991	88,84
90	229	115	15	230	115	25	12	17,2	0,0041667	0,0064	1,536	111,506	89,08
135	235	118	15,5	236	118	27	14	17,3	0,0041667	0,006	1,44	104,537	88,51
180	239	119	15	239	120	27	13	17,1	0,0041667	0,0062	1,488	108,022	88,70
225	251	126	14,5	250	125	29	14	17,4	0,0041667	0,0064	1,536	111,506	88,45
270	251	126	15,6	254	127	29	14	17	0,0041667	0,0064	1,536	111,506	88,45
315	251	126	15	253	126	29	15	16,8	0,0041667	0,0056	1,344	97,568	88,45

360	255	127	15	255	127	28	14	16,8	0,004 1667	0,006	1,44	104,537	89,02
405	254	127	15,3	255	128	28	14	16,5	0,004 1667	0,006	1,44	104,537	88,98
450	255	127	15,7	256	128	28	14	17,1	0,004 1667	0,0062	1,488	108,022	89,02
495	256	128	14,8	257	128	28	14	17	0,004 1667	0,0052	1,248	90,599	89,06

Table E-3: Experimental duplicate for NF270 at pH 6 at 15°C

	Feed			Brine		Permeate							
Time (min)	**EC (µS)**	**TDS (mg/L)**	**Temperature (°C)**	**EC (µS)**	**TDS (mg/L)**	**EC (µS)**	**TDS (mg/L)**	**Temperature (°C)**	**Time (hr)**	**Volume (L)**	**Flow Rate (l/h)**	**Flux (L/h m^2)**	**% rejection**
0	207	104	15,8	213	107	26	13	18,8	0,0041667	0,0064	1,536	111,51	87,44
45	211	106	15	216	108	21	11	18	0,0041667	0,006	1,44	104,54	90,05
90	212	106	15,3	215	107	22	11	17,8	0,0041667	0,0064	1,536	111,51	89,62
135	213	107	14,7	215	107	21	10	17,9	0,0041667	0,006	1,44	104,54	90,14
180	215	108	14,9	218	109	21	10	17,6	0,0041667	0,0056	1,344	97,57	90,23
225	216	108	15,3	218	109	21	10	17,7	0,0041667	0,0058	1,392	101,05	90,28
270	217	109	15,3	219	109	21	10	17,6	0,0041667	0,0064	1,536	111,51	90,32
315	219	110	16,3	221	111	23	11	17,4	0,0041667	0,006	1,44	104,54	89,50

360	223	111	14,8	222	111	23	12	17,8	0,0041667	0,006	1,44	104,54	89,69
405	224	112	15,8	227	114	23	12	17,7	0,0041667	0,006	1,44	104,54	89,73
450	224	112	15,2	227	114	24	12	17,2	0,0041667	0,0062	1,488	108,02	89,29
495	236	118	15,1	237	118	25	12	17,3	0,0041667	0,006	1,44	104,54	89,41

Table E-4: Operating conditions for run and duplicate of NF270 at pH 6 at 35°C

Run	
Initial permeate flux (L/m^2 hr)	76,60
Feed P_0 (bar)	10
Piston P (bar)	13
Feed velocity (Hz)	12,98
Brine p (Kpa)	95
Dimensions	14.5 cm x 9.5 cm
Area (m^2)	0,013775
Nomination	NF270
pH	6±0,3
Temperature(°C)	35
Concentration (µg/L)	
MeP	457,6/ 451,9
TCS	457,6/ 450
EHMC	450

Table E-5: Experimental run for NF270 at pH 6 at 35°C

	FEED			Brine		Permeate			.				
Time (min)	**EC F (µS)**	**TDS F (mg/L)**	**Temperature (°C)**	**EC (µS)**	**TDS (mg/L)**	**EC P (µS)**	**TDS P (mg/L)**	**Temperature (°C)**	**Time (hr)**	**Volume (L)**	**Flow Rate (l/h)**	**Flux (L/h m^2)**	**% rejection**
0	325	163	35,4	320	160	34	17	24,5	0,0041667	0,014	3,36	243,92	89,54
45	337	168	35	340	170	32	16	24,6	0,0041667	0,014	3,36	243,92	90,50
90	333	166	34,9	334	167	35	17	24,7	0,0041667	0,014	3,36	243,92	89,49
135	335	168	34,8	337	168	36	18	24,4	0,0041667	0,012	2,88	209,07	89,25
180	338	169	35,2	341	171	39	19	23	0,0041667	0,01	2,4	174,23	88,46
225	341	171	35,1	343	172	40	20	23,9	0,0041667	0,012	2,88	209,07	88,27
270	341	170	35,1	341	171	43	21	22,6	0,0041667	0,012	2,88	209,07	87,39
315	346	173	34,9	348	176	50	25	24,2	0,0041667	0,012	2,88	209,07	85,55

360	350	175	34,9	349	172	53	26	23,3	0,0041667	0,0088	2,112	153,32	84,86
405	348	174	34,9	351	175	58	29	22,8	0,0041667	0,0086	2,064	149,84	83,33
450	363	181	34,9	361	181	59	30	22,7	0,0041667	0,0076	1,824	132,41	83,75
495	368	184	34,9	365	183	63	32	22,3	0,0041667	0,0058	1,392	101,05	82,88

Table E-6: Experimental duplicate for NF270 at pH 6 at 35°C

	Feed			Brine		Permeate							
Time (min)	EC	TDS	Temperature (°C)	EC	TDS	EC	TDS	Temperature (°C)		volume			
0	205	103	36	207	104	24	12	24,5	0,0041667	0,016	3,84	278,77	88,29
45	208	104	34,6	209	104	26	13	25	0,0041667	0,014	3,36	243,92	87,50
90	209	105	35	210	105	33	16	24,3	0,0041667	0,01	2,4	174,23	84,21
135	218	109	35,1	219	109	43	21	24	0,0041667	0,01	2,4	174,23	80,28
180	215	107	35,1	216	107	42	20	23,9	0,0041667	0,0098	2,352	170,74	80,47
225	212	106	35,1	213	107	42	21	23,5	0,0041667	0,0078	1,872	135,90	80,19
270	208	104	35,1	206	103	45	22	22,6	0,0041667	0,006	1,44	104,54	78,37
315	210	105	35	205	103	49	24	21,4	0,0041667	0,0078	1,872	135,90	76,67
360	200	100	35	199	98	49	24	20,9	0,0041667	0,0068	1,632	118,48	75,50
405	198	99	35	199	98	55	28	20,9	0,0041667	0,0042	1,008	73,18	72,22
450	207	104	35,1	205	102	69	34	21	0,0041667	0,0042	1,008	73,18	66,67
495	204	102	35,1	202	101	73	37	22,4	0,0041667	0,004	0,96	69,69	64,22

Appendix F NF270 experimental run and duplicate at pH 10

Table F-1: Operating conditions for run and duplicate of NF270 at pH 10 and 15

Run	
Initial permeate flux (L/m^2 hr)	76,60
Feed P_0 (bar)	10
Piston P (bar)	13
Feed velocity (Hz)	12,98
Brine p (Kpa)	95
Dimensions	14.5 cm x 9.5 cm
Area (m^2)	0,013775
Nomination	NF270
pH	10±0,3
Temperature(°C)	15
Concentration(µg/L)	
MeP	453,85
TCS	451,91
EHMC	450

Table F-2: Experimental run for NF270 at pH 10 at 15°C

	FEED			Brine		Permeate			.				
Time (min)	**EC F (µS)**	**TDS F (mg/L)**	**Temperature (°C)**	**EC (µS)**	**TDS (mg/L)**	**EC P (µS)**	**TDS P (mg/L)**	**Temperature (°C)**	**Time (hr)**	**Volume (L)**	**Flow Rate (l/h)**	**Flux (L/h m^2)**	**% rejection**
0	220	110	16	221	111	94	47	21,1	0,0041667	0,0074	1,776	128,93	57,27
45	217	109	15,9	218	109	92	46	21,2	0,0041667	0,0072	1,728	125,44	57,60
90	216	108	16,7	217	109	88	44	21	0,0041667	0,0072	1,728	125,44	59,26
135	217	109	14,8	218	109	83	42	20,2	0,0041667	0,0066	1,584	114,99	61,75
180	217	109	15,4	217	109	81	41	20,8	0,0041667	0,0062	1,488	108,02	62,67
225	220	110	13,8	218	109	77	39	21	0,0041667	0,0054	1,296	94,08	65,00
270	219	110	15	220	110	80	40	20,4	0,0041667	0,0056	1,344	97,57	63,47
315	229	115	15,4	231	115	73	37	20,9	0,004	0,0058	1,392	101,05	68,12

									1667				
360	231	116	14,9	232	116	69	34	21,4	0,0041667	0,0052	1,248	90,60	70,13
405	234	117	14,9	235	117	67	34	20,5	0,0041667	0,005	1,2	87,11	71,37
450	237	118	14,9	236	118	70	35	20,5	0,0041667	0,0054	1,296	94,08	70,46
495	244	122	15,5	250	125	73	36	21,2	0,0041667	0,005	1,2	87,11	70,08

Table F-3: Experimental duplicate for NF270 at pH 10 at 15°C

	Feed			Brine		Permeate							
Time (min)	**EC (µS)**	**TDS (mg/L)**	**Temperature (°C)**	**EC (µS)**	**TDS (mg/L)**	**EC (µS)**	**TDS (mg/L)**	**Temperature (°C)**	**Time (hr)**	**Volume (L)**	**Flow Rate (l/h)**	**Flux (L/h m^2)**	**% rejection**
0	193	97	15,2	194	97	65	33	16	0,0041667	0,0064	1,536	111,51	66,32
45	193	97	15,4	195	97	66	33	15,9	0,0041667	0,0056	1,344	97,57	65,80
90	195	97	15,1	195	98	64	32	15,9	0,0041667	0,0058	1,392	101,05	67,18
135	208	104	15,8	208	104	65	32	16	0,0041667	0,0072	1,728	125,44	68,75
180	210	105	14,2	210	105	63	32	16,2	0,0041667	0,0062	1,488	108,02	70,00
225	211	106	15,7	211	106	60	30	16,5	0,0041667	0,0072	1,728	125,44	71,56
270	212	106	14,8	212	106	59	30	17	0,0041667	0,006	1,44	104,54	72,17
315	226	113	14,9	227	113	59	29	17,2	0,0041667	0,0074	1,776	128,93	73,89
360	225	112	15,3	229	114	76	33	17,1	0,0041667	0,006	1,44	104,54	66,22

405	230	115	15,9	231	115	71	35	17,4	0,0041667	0,0068	1,632	118,48	69,13
450	248	124	15,2	256	128	69	34	16,8	0,0041667	0,0064	1,536	111,51	72,18
495	248	124	14,8	248	124	85	42	17,1	0,0041667	0,0062	1,488	108,02	65,73

Table F-4: Operating conditions for run and duplicate of NF270 at pH 10 and 25°C

Run	
Initial permeate flux (L/m^2 hr)	76,60
Feed P_0 (bar)	10
Piston P (bar)	13
Feed velocity (Hz)	12,98
Brine p (Kpa)	95
Dimensions	14.5 cm x 9.5 cm
Area (m^2)	0,013775
Nomination	NF270
pH	10±0,3
Temperature(°C)	25
Concentration(µg/L)	
MeP	450
TCS	451,92
EHMC	450

Table F-5: Experimental run for NF270 at pH 10 at 25°C

	FEED			Brine		Permeate			.				
Time (min)	**EC (µS)**	**TDS (mg/L)**	**Temperature (°C)**	**EC (µS)**	**TDS (mg/L)**	**EC(µS)**	**TDS(mg/L)**	**Temperature (°C)**	**Time (hr)**	**Volume (L)**	**Flow Rate (l/h)**	**Flux (L/h m^2)**	**% rejection**
0	199	99	26,2	233	116	56	28	21,1	0,0041667	0,0098	2,352	170,74	71,86
45	209	104	25,9	209	104	70	35	22,3	0,0041667	0,0096	2,304	167,26	66,51
90	224	112	25,9	224	112	85	42	21,8	0,0041667	0,0096	2,304	167,26	62,05
135	254	127	25	253	126	120	60	19,9	0,0041667	0,008	1,92	139,38	52,76
180	251	125	25	253	127	97	48	19,8	0,0041667	0,0084	2,016	146,35	61,35
225	250	124	25	247	123	88	44	21,5	0,0041667	0,0092	2,208	160,29	64,80
270	260	130	25	257	129	80	40	20	0,0041667	0,0074	1,776	128,93	69,23
315	289	145	25,2	290	145	118	59	20,4	0,0041	0,007	1,68	121,96	59,17

									667				
360	288	144	25,5	287	143	104	52	20,1	0,0041667	0,007	1,68	121,96	63,89
405	285	142	25,3	285	143	90	45	20,1	0,0041667	0,0066	1,584	114,99	68,42
450	283	141	25	284	142	78	39	19,5	0,0041667	0,0062	1,488	108,02	72,44
495	345	172	25,1	346	173	127	64	19,7	0,0041667	0,0064	1,536	111,51	63,19

Table F-6: Experimental duplicate for NF270 at pH 10 at 25°C

	FEED			BRINE		PERMEATE							
Time (min)	**EC (µS)**	**TDS (mg/L)**	**Temperature (°C)**	**EC (µS)**	**TDS (mg/L)**	**EC (µS)**	**TDS (mg/L)**	**Temperature (°C)**	**Time (hr)**	**Volume (L)**	**Flow Rate (l/h)**	**Flux (L/h m^2)**	**% rejection**
0	226	113	25,3	227	115	98	49	20,4	0,0041667	0,0094	2,256	163,77	56,64
45	226	113	25,6	231	115	79	40	20,3	0,0041667	0,0086	2,064	149,84	65,04
90	241	120	25,1	243	122	94	47	19,9	0,0041667	0,0092	2,208	160,29	61,00
135	242	121	25,1	240	120	90	45	20,5	0,0041667	0,0094	2,256	163,77	62,81
180	280	140	25,1	281	141	138	69	20,9	0,0041667	0,0098	2,352	170,74	50,71
225	277	139	25,1	278	139	123	62	20,4	0,0041667	0,0098	2,352	170,74	55,60
270	291	145	25,1	292	146	133	66	19,7	0,0041667	0,01	2,4	174,23	54,30
315	285	143	25,2	289	145	90	46	21	0,0041667	0,009	2,16	156,81	68,42
360	310	155	24,6	312	156	129	64	21,2	0,0041667	0,0086	2,064	149,84	58,39

405	307	153	25,3	308	154	97	49	20,9	0,0041667	0,0078	1,872	135,90	68,40
450	346	174	25,3	347	174	125	62	21,2	0,0041667	0,0078	1,872	135,90	63,87
495	346	173	25,1	347	173	105	53	20,5	0,0041667	0,0074	1,776	128,93	69,65

Table F-7: Operating conditions for run and duplicate of NF270 at pH 10 and 35°C

Run	
Initial permeate flux (L/m^2 hr)	76,60
Feed P_0 (bar)	10
Piston P (bar)	13
Feed velocity (Hz)	12,98
Brine p (Kpa)	95
Dimensions	14.5 cm x 9.5 cm
Area (m^2)	0,013775
Nomination	NF270
pH	10±0,3
Temperature (°C)	35
Concentration(µg/L)	
MeP	471,15
TCS	451,92
EHMC	450

Table F-8: Experimental run for NF270 at pH 10 at 35°C

	FEED			Brine		Permeate			.				
Time (min)	**EC F (µS)**	**TDS F (mg/L)**	**Temperature (°C)**	**EC (µS)**	**TDS (mg/L)**	**EC P (µS)**	**TDS P (mg/L)**	**Temperature (°C)**	**Time (hr)**	**Volume (L)**	**Flow Rate (l/h)**	**Flux (L/h m^2)**	**% rejection**
0	315	157	35,7	322	161	152	76	24	0,0041667	0,014	3,36	243,92	51,75
45	307	153	34,7	309	154	128	64	24	0,0041667	0,012	2,88	209,07	58,31
90	308	154	34,9	311	155	112	56	23,6	0,0041667	0,01	2,4	174,23	63,64
135	325	162	34,9	330	165	130	65	23,2	0,0041667	0,01	2,4	174,23	60,00
180	326	163	35	325	162	120	60	24	0,0041667	0,0084	2,016	146,35	63,19
225	368	184	35	364	182	149	74	23	0,0041667	0,0068	1,632	118,48	59,51
270	361	180	35	361	180	137	69	21,8	0,0041667	0,007	1,68	121,96	62,05
315	390	195	35,1	390	195	154	77	22,7	0,0041667	0,0062	1,488	108,02	60,51

360	386	193	35	380	190	135	68	23,9	0,0041667	0,0064	1,536	111,51	65,03
405	397	198	35,1	394	197	135	67	23,9	0,0041667	0,0062	1,488	108,02	65,99
450	428	214	35	426	213	159	79	23,4	0,0041667	0,0062	1,488	108,02	62,85
495	427	213	35	417	209	138	69	25,4	0,0041667	0,0056	1,344	97,57	67,68

Table F-9: Experimental duplicate for NF270 at pH 10 at 35°C

	Feed			Brine		Permeate							
Time (min)	**EC F (µS)**	**TDS F (mg/L)**	**Temperature (°C)**	**EC (µS)**	**TDS (mg/L)**	**EC P (µS)**	**TDS P (mg/L)**	**Temperature (°C)**	**Volume (L)**	**Volume**	**Flow rate**	**Flux**	**Rejection**
0	268	134	36,1	263	131	116	58	23,5	0,0041667	0,014	3,36	243,92	56,72
45	268	134	34,8	266	133	99	49	24,4	0,0041667	0,014	3,36	243,92	63,06
90	268	134	34,9	266	133	95	47	24,4	0,0041667	0,018	4,32	313,61	64,55
135	350	175	35,2	342	171	185	92	24,7	0,0041667	0,012	2,88	209,07	47,14
180	337	168	35,2	331	165	160	80	21,5	0,0041667	0,009	2,16	156,81	52,52
225	330	165	35,3	326	163	145	72	19,9	0,0041667	0,0084	2,016	146,35	56,06
270	414	207	35,1	407	203	219	109	19,7	0,0041667	0,007	1,68	121,96	47,10
315	403	201	35,2	388	194	180	90	20,3	0,0041667	0,0054	1,296	94,08	55,33
360	391	196	35	385	192	164	82	19,5	0,0041667	0,0048	1,152	83,63	58,06
405	385	193	35	378	189	138	69	19,5	0,00416	0,00	1,104	80,1	64,16

									67	46		5	
450	389	195	34,9	384	192	134	67	19,3	0,0041667	0,0046	1,104	80,15	65,55
495	412	206	34,9	403	202	150	75	20,2	0,0041667	0,0044	1,056	76,66	63,59

Appendix G 24-hour Long run and duplicate for XLE

Table G-1: Operating conditions for XLE 24-hour run and duplicate at pH 6 and 35 °C

Run	
Initial permeate flux (L/m^2 hr)	76,60
Feed P_0 (bar)	10
Piston P (bar)	13
Feed velocity (Hz)	12,98
Brine p (Kpa)	95
Dimensions	14.5 cm x 9.5 cm
Area (m^2)	0,013775
Nomination	XLE
pH	6±0,3
Temperature(°C)	35
Concentration(µg/L)	
MeP	455,77
TCS	451,92
EHMC	450

Table G-2: Experimental 24-hour run for XLE at pH 6 at 35°C

	Feed			Brine		Permeate							
Time (hours)	**EC (µS)**	**TDS (mg/L)**	**Temperature (°C)**	**EC (µS)**	**TDS (mg/L)**	**EC P (µS)**	**TDS (mg/L)**	**Temperature (°C)**	**Time (hr)**	**Volume (L)**	**Flow Rate (l/h)**	**Flux (L/h m^2)**	**% rejection**
0	230	115	35,5	227	114	17	8	28,2	0,0041667	0,0042	1,008	73,18	92,61
2	227	114	35,4	228	114	23	11	26,9	0,0041667	0,0044	1,056	76,66	89,87
4	226	113	35,4	225	113	15	7	27,1	0,0041667	0,0048	1,152	83,63	93,36
6	227	114	36	224	112	12	6	26,1	0,0041667	0,0034	0,816	59,24	94,71
8	229	114	35,6	231	116	10	5	24,9	0,0041667	0,0034	0,816	59,24	95,63
10	229	115	35,6	229	114	9	4	27,8	0,0041667	0,0032	0,768	55,75	96,07
12	230	115	35,1	228	114	11	5	27,1	0,0041667	0,0028	0,672	48,78	95,22
14	304	152	35,1	303	152	14	7	23,5	0,0041667	0,003	0,72	52,27	95,39

16	308	154	35,1	306	153	15	7	25,3	0,0041667	0,0028	0,672	48,78	95,13
18	308	154	35,1	304	152	18	9	27,1	0,0041667	0,0028	0,672	48,78	94,16
20	316	158	35	314	157	22	11	27	0,0041667	0,0028	0,672	48,78	93,04
22	357	178	35	355	178	20	10	25,7	0,0041667	0,0022	0,528	38,33	94,40
24	369	185	34,7	366	183	16	8	25,3	0,0041667	0,002	0,48	34,85	95,66

Table G-3: Experimental 24-hour duplicate for XLE at pH 6 at 35°C

	Feed			Brine		Permeate							
Time (hours)	**EC (µS)**	**TDS (mg/L)**	**Temperature (°C)**	**EC (µS)**	**TDS (mg/L)**	**ECP (µS)**	**TDS (mg/L)**	**Temperature (°C)**	**Time (hr)**	**Volume (L)**	**Flow Rate (l/h)**	**Flux (L/h m^2)**	**% rejection**
0	206	103	35,4	205	103	10	5	27,8	0,0041667	0,0056	1,344	97,57	95,15
2	211	106	35	210	105	6	3	26,7	0,0041667	0,0048	1,152	83,63	97,16
4	203	101	34,6	202	101	11	5	27,7	0,0041667	0,0024	0,576	41,81	94,58
6	204	102	35,8	203	101	6	3	27,8	0,0041667	0,003	0,72	52,27	97,06
8	206	103	35,1	205	103	4	2	24,9	0,0041667	0,003	0,72	52,27	98,06
10	208	104	34,8	206	103	2	1	23,7	0,0041667	0,0028	0,672	48,78	99,04
12	330	165	34,9	332	166	6	3	27	0,0041667	0,0032	0,768	55,75	98,18
14	337	169	35	334	167	5	3	25,3	0,0041667	0,0032	0,768	55,75	98,52
16	342	171	35	338	169	5	2	23,8	0,004166	0,003	0,72	52,27	98,54

									7				
18	341	170	35	338	169	3	2	27,1	0,0041667	0,003	0,72	52,27	99,12
20	346	173	35	342	171	5	2	25,8	0,0041667	0,0026	0,624	45,30	98,55
22	355	177	35	350	175	8	4	27,1	0,0041667	0,0024	0,576	41,81	97,75
24	362	181	35	360	180	4	2	23,2	0,0041667	0,0026	0,624	45,30	98,90

Appendix H 24-hour Long run and duplicate for NF270

Table H-1: Operating conditions for 24-hour run and duplicate of NF270 at pH 6 and 35°C

Run	
Initial permeate flux (L/m^2 hr)	76,60
Feed P_0 (bar)	10
Piston P (bar)	13
Feed velocity (Hz)	12,98
Brine p (kPa)	95
Dimensions	14.5 cm x 9.5 cm
Area (m^2)	0,013775
Nomination	NF270
pH	6±0,3
Temperature(°C)	35
Concentration(µg/L)	
MeP	455,77
TCS	451,92
EHMC	450

Table H-2: Experimental 24-hour run for NF270 at pH 6 at 35°C

	Feed			Brine		Permeate							
Time (hours)	**EC (µS)**	**TDS (mg/L)**	**Temperature (°C)**	**EC (µS)**	**TDS (mg/L)**	**ECP (µS)**	**TDS (mg/L)**	**Temperature (°C)**	**Time (hr)**	**Volume (L)**	**Flow Rate (l/h)**	**Flux (L/h m^2)**	**% rejection**
0	253	127	35,4	258	129	45	23	27,4	0,004167	0,018	4,32	313,61	82,21
2	283	142	35,8	283	142	45	22	29,6	0,004167	0,01	2,4	174,23	84,10
4	310	155	35,4	310	155	54	27	28,4	0,004167	0,0068	1,632	118,48	82,58
6	302	151	35,3	301	151	59	30	28,8	0,004167	0,006	1,44	104,54	80,46
8	292	146	35,2	291	146	64	32	28,3	0,004167	0,0054	1,296	94,08	78,08
10	281	140	35	278	139	64	32	27,1	0,004167	0,0048	1,152	83,63	77,22
12	270	130	35	269	135	59	29	25,8	0,004167	0,0036	0,864	62,72	78,15
14	264	132	35,1	261	131	60	30	25,3	0,004167	0,0038	0,912	66,21	77,27
16	261	130	35,1	259	130	64	32	27,4	0,00416	0,0038	0,912	66,21	75,48

									7				
18	264	132	35,1	262	132	69	34	27,4	0,004167	0,0036	0,864	62,72	73,86
20	269	135	35,1	267	133	70	35	27,9	0,004167	0,0036	0,864	62,72	73,98
22	281	141	35,1	279	139	87	43	27,9	0,004167	0,0032	0,768	55,75	69,04
24	307	153	35,1	303	152	94	47	26,7	0,004167	0,003	0,72	52,27	69,38

Table H-3: Experimental 24-hour duplicate for NF270 at pH 6 at 35°C

	Feed			Brine		Permeate							
Time (hours)	**EC (µS)**	**TDS (mg/L)**	**Temperature (°C)**	**EC (µS)**	**TDS (mg/L)**	**ECP (µS)**	**TDS (mg/L)**	**Temperature (°C)**	**Time (hr)**	**Volume (L)**	**Flow Rate (l/h)**	**Flux (L/h m^2)**	**% rejection**
0	163	81	34,3	166	83	43	22	24,5	0,004167	0,0068	1,632	118,48	73,62
2	177	89	35,1	176	88	35	17	27,5	0,004167	0,005	1,2	87,11	80,23
4	176	88	35,1	174	87	37	19	26,9	0,004167	0,004	0,96	69,69	78,98
6	180	89	35,1	179	89	40	20	26,3	0,004167	0,0036	0,864	62,72	77,78
8	177	88	35,1	175	88	35	16	26,5	0,004167	0,0032	0,768	55,75	80,23
10	174	87	35,1	172	86	36	18	26,4	0,004167	0,0034	0,816	59,24	79,31
12	171	86	35	170	85	38	19	26,2	0,004167	0,003	0,72	52,27	77,78
14	169	85	35	169	85	36	18	26	0,004167	0,0028	0,672	48,78	78,70

16	168	84	35	167	84	35	18	26,1	0,004167	0,0024	0,576	41,81	79,17
18	236	118	34,6	232	116	43	22	25	0,004167	0,0026	0,624	45,30	81,78
20	244	122	35	242	121	39	19	26,2	0,004167	0,0028	0,672	48,78	84,02
22	251	125	35,2	249	124	39	20	24,2	0,004167	0,003	0,72	52,27	84,46
24	256	128	35,2	254	127	38	19	26,5	0,004167	0,003	0,72	52,27	85,16

Appendix I Sample Calculation

Flux

$$Flux = J_v = \frac{V}{Ax\Delta t} = \frac{0.013L}{0.013775m^2 * 0.016667hr} = 56.62\frac{L}{m^2.hr}$$

Salt rejection

Salt rejection for XLE at pH 3 and temperature 15°C after 45 minutes

$$Rejection = \left(1 - \frac{EC_{Permeate}}{EC_{Feed}}\right) * 100\% = \left(1 - \frac{50}{349}\right) * 100 = 85{,}67\%$$

Appendix J COD and turbidity

Table J-1: COD raw data for XLE and NF270 at varying pH and temperature

pH	3			6		10		
Temp	15	25	35	15	35	15	25	35
XLE								
Run	2984	2542	2598	5258	4544	2464	3325	4372
Permeate	345	370	420	60	380	752	270	20
Removal	88,44	85,44	83,83	98,86	91,64	69,48	91,88	99,54
Duplicate	2894	2761	2491	3963	4956	2182	2352	4609
Permeate	250	520	380	170	320	543	230	370
Removal	91,36	81,17	84,75	95,71	93,54	75,11	90,22	91,97
% removal	89,90	83,31	84,29	97,28	92,59	72,30	91,05	95,76
NF270								
Run	4258	2164	2491	2200	4272	2211	1852	2911
Permeate	2782	560	500	132	350	800	190	260
Removal	34,66	74,12	79,93	94,00	91,81	63,82	89,74	91,07
Duplicate	4271	2009	2686	2642	4238	2213	4004	4657
Permeate	2747	340	650	127	300	700	260	400
Removal	35,68	83,08	75,80	95,19	92,92	68,37	93,51	91,41
%removal	35,17	78,60	77,86	94,60	92,36	66,09	91,62	91,24

Table J-2: Turbidity raw data for XLE and NF270 at varying pH and temperature

pH	**3**			**6**		**10**		
Temp	15	25	35	15	35	15	25	35
XLE								
Run	3,02	9,93	3,5	2,42	3,83	3,5	8,47	3,02
	0,33	0,18	0,04	0,01	0,49	0,13	1,06	0,23
	89,07	*98,19*	*98,86*	*99,59*	*87,21*	*96,29*	*87,49*	*92,38*
Duplicate	7,65	11,24	4	3,66	7,9	2,46	20,47	5,13
	0,78	0,14	0,08	0,33	0,96	0,22	0,19	0,22
	89,80	*98,75*	*98,00*	*90,98*	*87,85*	*91,06*	*99,07*	*95,71*
Average	**89,44**	**98,47**	**98,43**	**95,29**	**87,53**	**93,67**	**93,28**	**94,05**
NF270								
Run	2,07	39,32	19,61	2,75	2,14	2,24	3,5	3,52
	0,06	0,71	0,02	0,01	0,23	0,21	0,22	0,23
%removal	*97,10*	*98,19*	*99,90*	*99,64*	*89,25*	*90,63*	*93,71*	*93,47*
Duplicate	2,95	54,88	14,04	3,2	3,06	1,83	2,12	2,09
	0,11	0,01	0,01	0,19	0,49	0,39	0,01	0,4
%removal	*96,27*	*99,98*	*99,93*	*94,06*	*83,99*	*78,69*	*99,53*	*80,86*
Average	**96,69**	**99,09**	**99,91**	**96,85**	**86,62**	**84,66**	**96,62**	**87,16**

Appendix K Inorganics

Table K-1: Raw XLE data for ammonia removal

XLE													
		NH_3				NH4+				NH_3-N			
pH	Temp	Initial (mg/L)	Final (mg/L)	Removal (%)	Standard Deviation	Initial	Final	Removal (%)	Standard Deviation	Initial	Final	Removal (%)	Standard Deviation
	15	6,1	0,2	96,72		6,4	0,22	96,56		5	0,16	96,80	
		8,7	0,3	96,55	0,12	9,2	0,3	96,74	0,12	7,1	0,2	97,18	0,27
	25	6,1	0,7	88,52		6,5	0,7	89,23		5	0,57	88,60	
		5,8	0,56	90,34	1,29	6,1	0,6	90,16	0,66	4,8	0,48	90,00	0,99
	35	7,4	0,43	94,19		7,9	0,4	94,94		6,1	0,33	94,59	
3		9,8	0,6	93,88	0,22	10,4	0,72	93,08	1,32	8,1	0,54	93,33	0,89
6	15	13,4	2,92	78,21	14,30	14,1	3,09	78,09	13,91	11	2,4	78,18	14,07

		12,7	0,2	98,43		13,4	0,3	97,76		10,4	0,2	98,08	
		11,6	0,6	94,83		12,3	0,64	94,80		9,5	0,49	94,84	
	35	41,6	0,79	98,10	2,31	44,1	0,65	98,53	2,64	34,2	0,84	97,54	1,91
		23	7,94	65,48		24	8,41	64,96		19	6,53	65,63	
	15	17	6,63	61,00	3,17	18	7,02	61,00	2,80	14	5,45	61,07	3,22
		10,1	4,3	57,43		10,7	4,6	57,01		8,3	3,5	57,83	
	25	6,3	2,6	58,73	0,92	6,7	2,8	58,21	0,85	5,2	2,1	59,62	1,26
		14,7	5,2	64,63		15,5	5,5	64,52		12,1	4,3	64,46	
10	**35**	13,8	4,6	66,67	1,44	14,6	4,9	66,44	1,36	11,4	3,8	66,67	1,56

Table K-2: Raw NF270 data for ammonia removal

pH	Temp	NH3				NH4+				NH3-4			
		Initial (mg/L)	Final (mg/L)	Removal (%)	Standard Deviation	Initial	Final	Removal (%)	Standard Deviation	Initial	Final	Removal	Standard Deviation
3	15	21	2,6	87,62	5,86	22	2,4	89,09	6,87	17	2	88,24	7,00
		15	3,1	79,33		16	3,3	79,38		12	2,6	78,33	
	25	4	2,1	47,50	17,95	4,3	2,2	48,84	17,10	3,3	1,7	48,48	17,67
		5,9	1,6	72,88		6,3	1,7	73,02		4,9	1,3	73,47	
	35	9	2,4	73,33	5,30	9,5	2,6	72,63	5,58	7,4	2	72,97	4,97
		7,3	1,4	80,82		7,7	1,5	80,52		6	1,2	80,00	
6	15	25	2,09	91,64	1,64	26	2,22	91,46	1,82	20	1,72	91,40	1,81
		28	1,69	93,96		30	1,79	94,03		23	1,39	93,96	
	35	13,8	2,2	84,06	4,64	14,6	2,3	84,25	3,81	11,4	1,8	84,21	1,06
		12,8	1,2	90,63		13,5	1,4	89,63		10,5	1,5	85,71	
10	15	16	3,66	77,13	23,36	17	3,88	77,18	22,53	13	3,01	76,85	22,66

		12	6,71	44,08		13	7,11	45,31		10	5,52	44,80	
	25	16,2	5,5	66,05		17,2	5,8	66,28		13,3	4,5	66,17	
		12,2	5,7	53,28	9,03	12,9	6,1	52,71	9,59	10	4,7	53,00	9,31
	35	17,1	10,1	40,94		18,1	10,7	40,88		14	8,3	40,71	
		15,3	9	41,18	0,17	16,2	9,5	41,36	0,34	12,6	7,4	41,27	0,39

Table K-3: Ammonia effluent concentration at 35 °C

pH	Membrane	NH3	NH4+	NH3-4
3	XLE	0,43	0,4	0,33
	XLE	0,6	0,72	0,54
	NF270	2,4	2,6	2
	NF270	1,4	1,5	1,2
6	XLE	0,6	0,64	0,49
	XLE	0,79	0,65	0,84
	NF270	2,2	2,6	2
	NF270	1,2	1,5	1,2
10	XLE	5,2	5,5	4,3
	XLE	4,6	4,9	3,8
	NF270	10,1	10,7	8,3
	NF270	9	9,5	7,4

Table K-4: Anova: Two-Factor With Replication for pH 3

SUMMARY	NH3	NH4+	NH3-4	Total
XLE				
Count	2	2	2	6
Sum	1,03	1,12	0,87	3,02
Average	0,515	0,56	0,435	0,503333
Variance	0,01445	0,0512	0,02205	0,020747
NF270				
Count	2	2	2	6
Sum	3,8	4,1	3,2	11,1
Average	1,9	2,05	1,6	1,85
Variance	0,5	0,605	0,32	0,327
Total				
Count	4	4	4	
Sum	4,83	5,22	4,07	
Average	1,2075	1,305	1,0175	
Variance	0,810892	0,958766667	0,566425	

ANOVA

Source of Variation	*SS*	*df*	*MS*	*F*	*P-value*	*F crit*
Sample	5,440533	1	5,440533333	21,57943	0,003521	5,987377607
Columns	0,171017	2	0,085508333	0,339162	0,725189	5,14325285
Interaction	0,055017	2	0,027508333	0,10911	0,898371	5,14325285
Within	1,5127	6	0,252116667			
Total	7,179267	11				

Table K-5: Anova: Two-Factor With Replication for pH 6

SUMMARY	NH3	NH4+	NH3-4	Total
XLE				
Count	2	2	2	6
Sum	1,39	1,29	1,33	4,01
Average	0,695	0,645	0,665	0,668333
Variance	0,01805	5E-05	0,06125	0,016377
NF270				
Count	2	2	2	6
Sum	3,4	4,1	3,2	10,7
Average	1,7	2,05	1,6	1,783333
Variance	0,5	0,605	0,32	0,329667
Total				
Count	4	4	4	
Sum	4,79	5,39	4,53	
Average	1,1975	1,3475	1,1325	
Variance	0,509358	0,859692	0,418492	

ANOVA

Source of Variation	*SS*	*df*	*MS*	*F*	*P-value*	*F crit*
Sample	3,729675	1	3,729675	14,87556	0,008393	5,987378
Columns	0,097267	2	0,048633	0,193971	0,82865	5,143253
Interaction	0,1286	2	0,0643	0,256456	0,781858	5,143253
Within	1,50435	6	0,250725			
Total	5,459892	11				

Table K-6: Anova: Two-Factor With Replication for pH 10

SUMMARY	1,2	1,5	1,2	Total
XLE				
Count	2	2	2	6
Sum	9,8	10,4	8,1	28,3
Average	4,9	5,2	4,05	4,7166667
Variance	0,18	0,18	0,125	0,3816667
NF270				
Count	2	2	2	6
Sum	19,1	20,2	15,7	55
Average	9,55	10,1	7,85	9,1666667
Variance	0,605	0,72	0,405	1,4466667
Total				
Count	4	4	4	
Sum	28,9	30,6	23,8	
Average	7,225	7,65	5,95	
Variance	7,469167	8,303333	4,99	

ANOVA

Source of Variation	*SS*	*df*	*MS*	*F*	*P-value*	*F crit*
Sample	59,4075	1	59,4075	160,92325	1,47E-05	5,987378
Columns	6,261667	2	3,130833	8,4808126	0,017842	5,143253
Interaction	0,665	2	0,3325	0,9006772	0,454929	5,143253
Within	2,215	6	0,369167			
Total	68,54917	11				

Table K-7: raw phosphate data for XLE and NF270 at varying pH and temperature

XLE													
		P				PO4-3+				P205			
pH	Temp	Initial	Final	Removal		Initial	Final	Removal		Initial	Final	Removal	
3	15	3,3	0,02	99,39	0,99	10	0,07	99,30	1,15	7,5	0,05	99,33	1,14
		1	0,02	98,00		3	0,07	97,67		2,2	0,05	97,73	
	25	1,3	0,01	99,23	1,09	3,9	0,04	98,97	1,04	2,9	0,03	98,97	0,92
		1,3	0,03	97,69		4	0,1	97,50		3	0,07	97,67	
	35	2,1	0,08	96,19	1,28	6,5	0,25	96,15	1,35	4,9	0,19	96,12	1,51
		1	0,02	98,00		3,1	0,06	98,06		2,3	0,04	98,26	
6	15	1,5	0,08	94,67	0,39	4,7	0,24	94,89	0,55	3,5	0,18	94,86	0,09
		1,7	0,1	94,12		5,1	0,3	94,12		3,8	0,2	94,74	
	35	1,7	0	100,00	0,52	5,1	0	100,00	0,42	3,8	0,01	99,74	0,26
		2,7	0,02	99,26		8,4	0,05	99,40		6,3	0,04	99,37	
10	15	1	0,05	95,00	1,41	5	0,17	96,60	0,14	3	0,12	96,00	0,35
		2	0,06	97,00		5	0,18	96,40		4	0,14	96,50	

		4,9	0,19	96,12		15,1	0,57	96,23		11,3	0,42	96,28	
	25	1,7	0,03	98,24	1,49	5,3	0,1	98,11	1,34	3,9	0,07	98,21	1,36
		2	0,11	94,50		6,1	0,35	94,26		4,6	0,26	94,35	
	35	1,9	0,12	93,68	0,58	5,7	0,36	93,68	0,41	4,3	0,27	93,72	0,44
NF270													
pH	Temp	P				PO4-3+				P205			
		Initial	Final	Removal		Initial	Final	Removal		Initial	Final	Removal	
	15	4	1,2	70,00		11	3,8	65,45		8	2,9	63,75	
		1,5	0,9	40,00	21,21	4,7	2	57,45	5,66	3,5	2,7	22,86	28,92
	25	4	0,46	88,50		12	1,42	88,17		9	1,06	88,22	
		8	0,44	94,50	4,24	24	1	95,83	5,42	18	1,34	92,56	3,06
	35	3	0,68	77,33		9	2,1	76,67		6	1,57	73,83	
3		4	0,6	85,00	5,42	12	1,7	85,83	6,48	9	1,3	85,56	8,29
	15	7	0,05	99,29		20	0,15	99,25		15	0,11	99,27	
		2	0,01	99,50	0,15	7	0,04	99,43	0,13	6	0,03	99,50	0,16
	35	1,5	0,05	96,67		4,5	0,16	96,44		3,4	0,12	96,47	
6		2,2	0,02	99,09	1,71	6,8	0,06	99,12	1,89	5,1	0,04	99,22	1,94

	15	14	0,005	99,96		42	0,16	99,62		31	0,12	99,61	
		2	0,06	97,00	2,10	5	0,18	96,40	2,28	4	0,13	96,75	2,02
	25	2,2	0,1	95,45		6,8	0,3	95,59		5,1	0,2	96,08	
		1,4	0,6	57,14	27,09	4,4	2	54,55	29,02	3,3	1,5	54,55	29,37
	35	3,3	0,1	96,97		10,2	0,4	96,08		7,6	0,3	96,05	
10		1,8	0,4	77,78	13,57	5,5	1,2	78,18	12,65	4,1	0,9	78,05	12,73

Table K-8: Phosphate final concentration at 35 °C

pH	Membrane	P	PO4-3+	P2O5
3	XLE	0,08	0,25	0,19
	XLE	0,02	0,06	0,04
	NF270	0,68	2,1	1,57
	NF270	0,6	1,7	1,3
6	XLE	0	0	0,01
	XLE	0,02	0,05	0,04
	NF270	0,05	2,1	1,57
	NF270	0,02	1,7	1,3
10	XLE	0,11	0,35	0,26
	XLE	0,12	0,36	0,27
	NF270	0,1	0,4	0,3
	NF270	0,4	1,2	0,9

Table K-9: Anova: Two-Factor With Replication for pH 3

SUMMARY	P	PO4-3+	P2O5	Total
XLE				
Count	2	2	2	6
Sum	0,1	0,31	0,23	0,64
Average	0,05	0,155	0,115	0,106667
Variance	0,0018	0,01805	0,01125	0,008467
NF270				
Count	2	2	2	6
Sum	1,28	3,8	2,87	7,95
Average	0,64	1,9	1,435	1,325
Variance	0,0032	0,08	0,03645	0,34871
Total				
Count	4	4	4	
Sum	1,38	4,11	3,1	
Average	0,345	1,0275	0,775	
Variance	0,1177	1,047692	0,5967	

ANOVA

Source of Variation	*SS*	*df*	*MS*	*F*	*P-value*	*F crit*
Sample	4,453008	1	4,453008	177,2342	1,11E-05	5,987378
Columns	0,952617	2	0,476308	18,95755	0,00255	5,143253
Interaction	0,682517	2	0,341258	13,58242	0,005921	5,143253
Within	0,15075	6	0,025125			
Total	6,238892	11				

Table K-10: Anova: Two-Factor With Replication for pH 6

SUMMARY	P	PO4-3+	P2O5	Total
XLE				
Count	2	2	2	6
Sum	0,02	0,05	0,05	0,12
Average	0,01	0,025	0,025	0,02
Variance	0,0002	0,00125	0,00045	0,00044
NF270				
Count	2	2	2	6
Sum	0,07	3,8	2,87	6,74
Average	0,035	1,9	1,435	1,123333
Variance	0,00045	0,08	0,03645	0,777307
Total				
Count	4	4	4	
Sum	0,09	3,85	2,92	
Average	0,0225	0,9625	0,73	
Variance	0,000425	1,198958	0,675	

ANOVA

Source of Variation	*SS*	*df*	*MS*	*F*	*P-value*	*F crit*
Sample	3,652033	1	3,652033	184,4461	9,89E-06	5,987378
Columns	1,917617	2	0,958808	48,42466	0,000199	5,143253
Interaction	1,852317	2	0,926158	46,77567	0,000219	5,143253
Within	0,1188	6	0,0198			
Total	7,540767	11				

Table K-11: Anova: Two-Factor With Replication for pH 10

SUMMARY	P	PO4-3+	P2O5	Total
XLE				
Count	2	2	2	6
Sum	0,23	0,71	0,53	1,47
Average	0,115	0,355	0,265	0,245
Variance	0,00005	5E-05	5E-05	0,01179
NF270				
Count	2	2	2	6
Sum	0,5	1,6	1,2	3,3
Average	0,25	0,8	0,6	0,55
Variance	0,045	0,32	0,18	0,171
Total				
Count	4	4	4	
Sum	0,73	2,31	1,73	
Average	0,1825	0,5775	0,4325	
Variance	0,021092	0,172692	0,097425	

ANOVA

Source of Variation	*SS*	*df*	*MS*	*F*	*P-value*	*F crit*
Sample	0,279075	1	0,279075	3,07154	0,130225	5,987378
Columns	0,3194	2	0,1597	1,757681	0,250713	5,143253
Interaction	0,0494	2	0,0247	0,271852	0,770873	5,143253
Within	0,54515	6	0,090858			
Total	1,193025	11				

Appendix L PCP concentration

Table L-1: PCP removal at varying pH and temperature

XLE						NF270					
Run	**PCP**	**Initial concentration**	**Final**	**% Removal**	**Average**	**Run**	**PCP**	**Initial concentration**	**Final**	**% Removal**	**Average**
XLE 3-15(1)	MeP	451,9	0,3	99,93	99,94	NF270 3-15(1)	MeP	453,85	2,89	99,36	99,31
	TCS	450	0,35	99,92			TCS	451,92	0,53	99,88	
	EHMC	450	0,03	99,99			EHMC	450	0,65	99,86	
XLE 3-15 (2)	MeP	451,9	0,25	99,94	99,90	NF270 3-15(2)	MeP	450	3,37	99,25	99,89
	TCS	450	0,52	99,88	99,66		TCS	451,92	0,42	99,91	99,86
	EHMC	450	3,06	99,32			EHMC	450	0,64	99,86	
XLE 3-25 (1)	MeP	450	2,72	99,40	99,53	NF270 3-25(1)	MeP	457,6	13,38	97,08	62,12
	TCS	450	1,36	99,70			TCS	457,6	1,77	99,61	
	EHMC	450	0,38	99,92	99,78		EHMC	450	0,27	99,94	89,86
XLE 3-25(2)	MeP	450	1,5	99,67		NF270 3-25(2)	MeP	457,6	333,31	27,16	

	TCS	450	0,66	99,85			TCS	457,6	91	80,11	
	EHMC	450	0,08	99,98	99,95		EHMC	450	0,53	99,88	99,91
	MeP	450	0,51	99,89			MeP	457,6	1,57	99,66	
	TCS	450	0,57	99,87	99,91		TCS	457,6	3,29	99,28	99,61
XLE 3-35 (1)	EHMC	450	0,25	99,94		NF270 3-35(1)	EHMC	450	0,3	99,93	
	MeP	450	0,33	99,93	99,90		MeP	451,9	1,99	99,56	99,32
	TCS	450	0,29	99,94			TCS	450	2,88	99,36	
XLE 3-35(2)	EHMC	450	0,21	99,95	99,95	NF270 3-35(2)	EHMC	450	0,32	99,93	99,93
	MeP	451,9	0,25	99,94			MeP	463,46	1,07	99,77	
	TCS	450	2,53	99,44	99,94		TCS	459,62	0,22	99,95	99,80
XLE 6-15(1)	EHMC	450	0,49	99,89		NF270 6-15(1)	EHMC	450	0,14	99,97	
	MeP	451,9	0,29	99,94	99,06		MeP	459,62	0,82	99,82	99,92
	TCS	450	5,95	98,68			TCS	451,92	0,49	99,89	
XLE 6-15(2)	EHMC	450	12,6	97,20	98,55	NF270 6-15(2)	EHMC	450	0,12	99,97	99,97

	MeP	459,62	15,98	96,52	98,21		MeP	471,15	2,03	99,57	99,67
	TCS	457,5	2,28	99,50			TCS	451,92	0,52	99,88	
XLE 6-35(1)	EHMC	450	0,15	99,97	99,70	NF270 6-35(1)	EHMC	450	0,05	99,99	99,90
	MeP	459,62	0,44	99,90			MeP	459,62	1,07	99,77	
	TCS	457,5	0,46	99,90	99,48		TCS	453,85	0,38	99,92	99,92
XLE 6-35(2)	EHMC	450	4,57	98,98		NF270 6-35(2)	EHMC	450	0,64	99,86	
	MeP	453,85	0,42	99,91			MeP	451,92	2,27	99,50	
	TCS	451,92	1,07	99,76	99,91		TCS	451,92	2,26	99,50	99,67
XLE 10-15(1)	EHMC	450	1,61	99,64		NF270 10-15(1)	EHMC	450	2,39	99,47	
	MeP	453,85	0,43	99,91	99,80		MeP	453,85	0,69	99,85	99,69
	TCS	451,92	0,7	99,85			TCS	451,92	0,57	99,87	
XLE 10-15(2)	EHMC	450	0,8	99,82	99,73	NF270 10-15(2)	EHMC	450	0,07	99,98	99,73
	MeP	459,62	0,22	99,95			MeP	450	0,82	99,82	
	TCS	457,5	1,32	99,71	99,94		TCS	451,92	3,51	99,22	99,80
XLE 10-25(1)	EHM	450	0,17	99,96	99,75	NF270 10-25(1)	EHM	450	0,13	99,97	99,39

	C						C				
	MeP	459,62	0,29	99,94			MeP	471,15	1,03	99,78	
	TCS	457,5	1	99,78			TCS	451,92	1,99	99,56	
XLE 10-25(2)	EHMC	450	0,2	99,96	99,96	NF270 10-25(2)	EHMC	450	0,08	99,98	99,98
	MeP	478,85	0,33	99,93			MeP	471,15	4,51	99,04	
	TCS	453,85	0,79	99,83	95,74		TCS	451,92	3,94	99,13	99,40
XLE 10-35(1)	EHMC	450	0,03	99,99		NF270 10-35(1)	EHMC	450	0,06	99,99	
	MeP	478,85	40,45	91,55	87,17		MeP	471,15	1,15	99,76	99,43
	TCS	453,85	115,66	74,52			TCS	451,92	1,21	99,73	
XLE 10-35(2)	EHMC	450	38,35	91,48	95,74	NF270 10-35(2)	EHMC	450	0,02	100,00	99,99

Table L-2: PCP final concentration at 35°C

pH	Membrane	MeP	TCS	EHMC
3	XLE	0,51	0,57	0,25
	XLE	0,33	0,29	0,21
	NF270	1,57	3,29	0,3
	NF270	1,99	2,88	0,32
6	XLE	15,98	2,28	0,15
	XLE	0,44	0,46	4,57
	NF270	2,03	0,52	0,05
	NF270	1,07	0,38	0,64
10	XLE	0,33	0,79	0,03
	XLE	40,45	115,66	38,35
	NF270	4,51	3,94	0,06
	NF270	1,15	1,21	0,02

Table L-3: Anova: Two-Factor With Replication for pH-3

SUMMARY	MeP	TCS	EHMC	Total
XLE				
Count	2	2	2	6
Sum	0,84	0,86	0,46	2,16
Average	0,42	0,43	0,23	0,36
Variance	0,0162	0,0392	0,0008	0,0214
NF270				
Count	2	2	2	6
Sum	3,56	6,17	0,62	10,35
Average	1,78	3,085	0,31	1,725
Variance	0,0882	0,08405	0,0002	1,57643
Total				
Count	4	4	4	
Sum	4,4	7,03	1,08	
Average	1,1	1,7575	0,27	
Variance	0,651333	2,390758	0,002467	

ANOVA

Source of Variation	*SS*	*df*	*MS*	*F*	*P-value*	*F crit*
Sample	5,589675	1	5,589675	146,6785	1,93E-05	5,987378
Columns	4,44515	2	2,222575	58,32255	0,000117	5,143253
Interaction	3,31535	2	1,657675	43,49902	0,000269	5,143253
Within	0,22865	6	0,038108			
Total	13,57883	11				

Table L-4: Anova: Two-Factor With Replication for pH 6

SUMMARY	MeP	TCS	EHMC	Total
XLE				
Count	2	2	2	6
Sum	16,42	2,74	4,72	23,88
Average	8,21	1,37	2,36	3,98
Variance	120,7458	1,6562	9,7682	37,3658
NF270				
Count	2	2	2	6
Sum	3,1	0,9	0,69	4,69
Average	1,55	0,45	0,345	0,781667
Variance	0,4608	0,0098	0,17405	0,485337
Total				
Count	4	4	4	
Sum	19,52	3,64	5,41	
Average	4,88	0,91	1,3525	
Variance	55,1874	0,837467	4,667492	

ANOVA

Source of Variation	*SS*	*df*	*MS*	*F*	*P-value*	*F crit*
Sample	30,68801	1	30,68801	1,386351	0,283607	5,987378
Columns	37,86662	2	18,93331	0,855325	0,471173	5,143253
Interaction	18,57422	2	9,287108	0,419551	0,675237	5,143253
Within	132,8149	6	22,13581			
Total	219,9437	11				

Table L-5: Anova: Two-Factor With Replication for pH-10

SUMMARY	MeP	TCS	EHMC	Total
XLE				
Count	2	2	2	6
Sum	40,78	116,45	38,38	195,61
Average	20,39	58,225	19,19	32,60167
Variance	804,8072	6597,558	734,2112	2021,536
NF270				
Count	2	2	2	6
Sum	5,66	5,15	0,08	10,89
Average	2,83	2,575	0,04	1,815
Variance	5,6448	3,72645	0,0008	3,77779
Total				
Count	4	4	4	
Sum	46,44	121,6	38,46	
Average	11,61	30,4	9,615	
Variance	372,9352	3232,736	366,9782	

ANOVA

Source of Variation	***SS***	***df***	***MS***	***F***	***P-value***	***F crit***
Sample	2843,457	1	2843,457	2,094383	0,19799	5,987378
Columns	1052,08	2	526,0402	0,387461	0,694609	5,143253
Interaction	928,5421	2	464,271	0,341965	0,723366	5,143253
Within	8145,949	6	1357,658			
Total	12970,03	11				

Appendix M Chromatographs

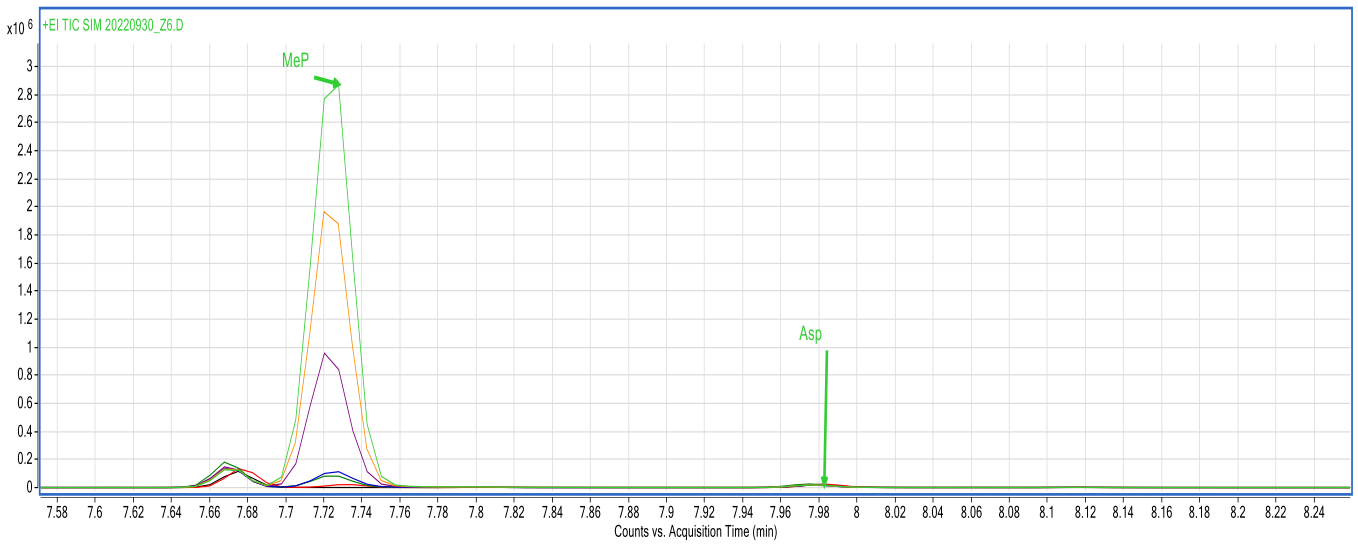

Figure M-1: MeP chromatograph

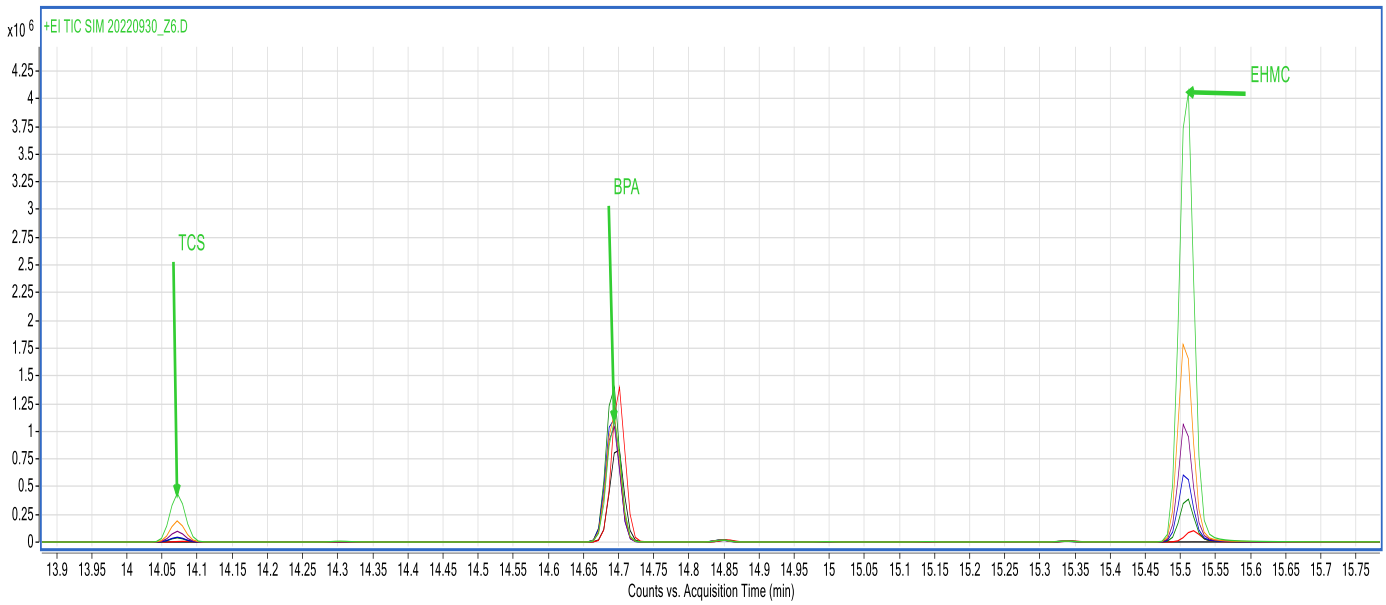

Figure M-2: EHMC and TCS chromatographs

Appendix N Standard Curves

Table N-1: Normalized peak ratio and concentration for standard curve using BPA

	0,1	0,5	1	5	10	15
MeP N. BPA	0,016	0,062	0,100	0,900	1,769	2,721
	0,1	0,5	0,75	1,5	3	6
TCS N. BPA	0,0052	0,03	0,0410	0,0975	0,1750	0,4338
	0,1	0,25	0,5	1	2	4
EHMC N. BPA	0,0853	0,3046	0,5797	1,0799	1,7220	3,9691

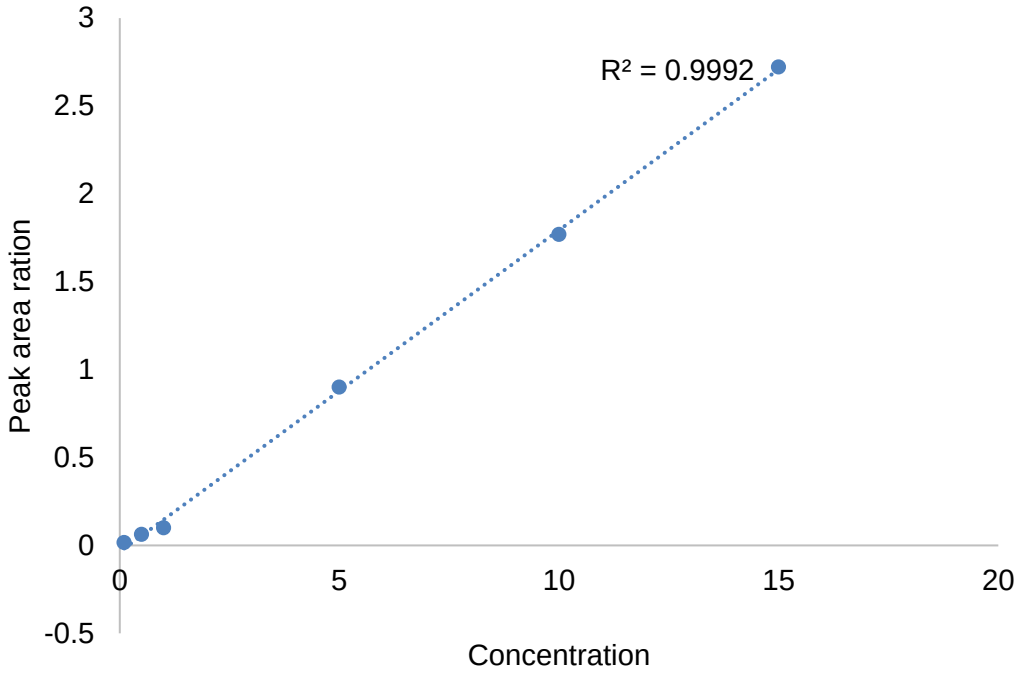

Figure N-1: MeP standard curve

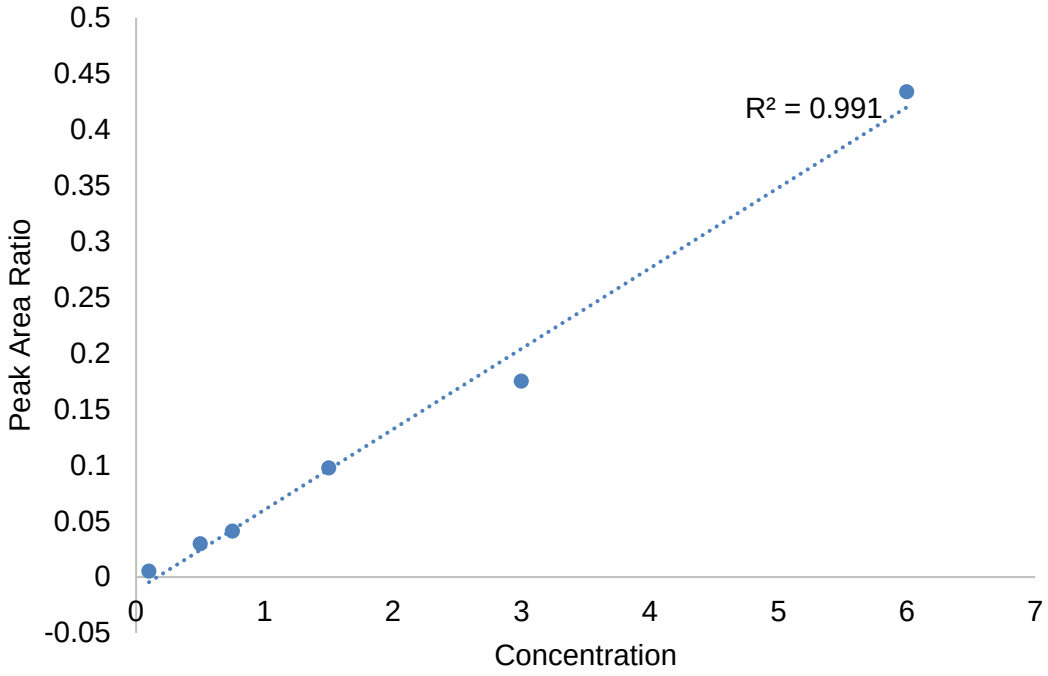

Figure N-2: TCS standard curve

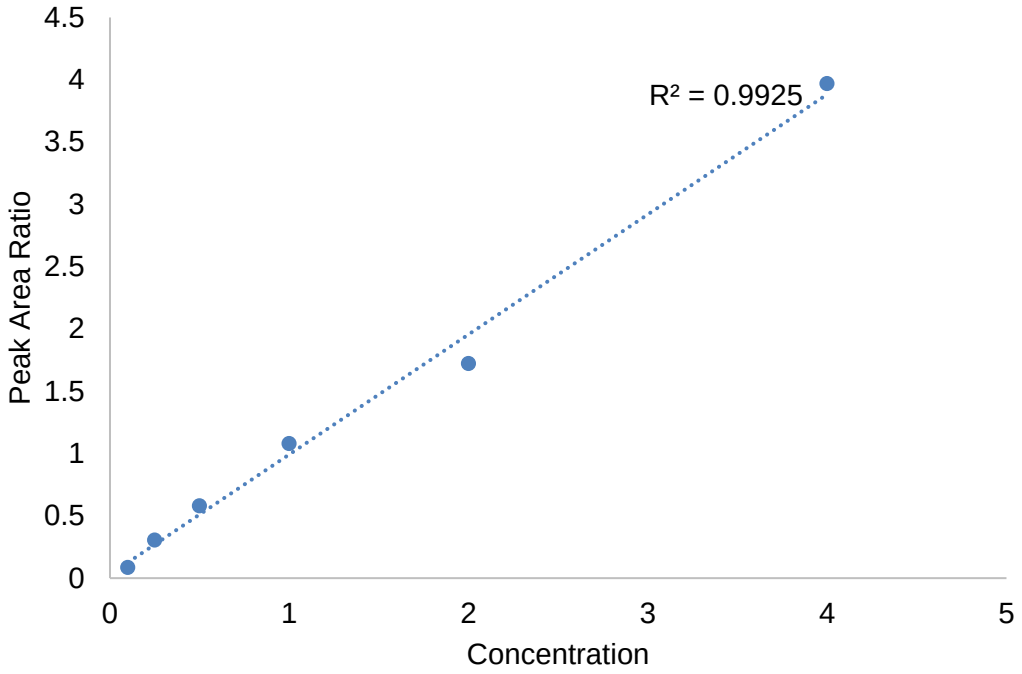

Figure N-3: EHMC standard curve

Appendix O EDX

Table O-1: Element analysis for XLE at varying pH at 35

Spectrum	N	O	Al	S	Cl	P	Mg	Mn	Na
3-35	20,79	44,98	2,33	8,3	23,61	0	0	0	0
6-35	18,07	47,8	2,92	8,37	19,64	1,06	0	2,14	0
10-35	0	46,06	1,63	0,67	17,6	5,91	3,67	20,5	1,44

Table O-2: Element analysis for NF270 at varying pH at 35

Spectrum	N	O	Na	Al	Si	S	Cl	K	Ca	Mn	Mg
3-35	31,62	7,96	4,55	0,75	0,24	1,7	52,87	0,3	0	0	0
6-35	28,41	20,64	0	4,52	0	0,8	40,35	0	0	3,04	0
10-35	0	50,79	1,22	13,9	0	0,99	14,34	0	6,14	15,44	1,64